UTILITY OF THE FLOW SUBSTITUTION PRINCIPLE FOR HIGH SPEED PROPULSION APPLICATIONS

by

Gregory Scott Stanislaw

B.S. Aeronautical and Astronautical Engineering, The Ohio State University (1994)

Submitted to the Department of Aeronautics and Astronautics
in partial fulfillment of the requirements for the degree of

Master of Science

at the

MASSACHUSETTS INSTITUTE OF TECHNOLOGY

February 1997

Author .....
Department of Aeronautics and Astronautics
October 12, 1996

Certified by .....
Dr. Choon S. Tan
Principal Research Engineer
Thesis Supervisor

Certified by .....
Professor Edward M. Greitzer
H. N. Slater Professor
Thesis Supervisor

Accepted by .....
Professor Jaime Peraire
Chairman, Department Graduate Committee

Acknowledgments

This work could not have been competed without the help, support, and friendship of many individuals. Foremost, I would like to thank Prof. **Edward M. Greitzer** and **Dr. Choon S. Tan** for giving me the opportunity to attend MIT and for their advice, assistance, and supervision throughout the course of this investigation. I would also like to thank Prof. **Ian A. Waitz** for allowing me to become part of the Aero-Environmental Research Laboratory and for the insights that he brought to my work. The research was supported by NASA Grant NAG3-1591 through the NASA Lewis Research Center. The assistance provided by the technical monitors, Mr. **Colin Drummond**, Mr. **Masashi Mizukami** and Mr. **Jim Debonis**, is greatly appreciated. There are many others I would like to thank:

To the members of the HSR Program whom I have had the pleasure of working with, Mr. **Ed Kawecki**, Mr. **Eric Gamble**, Mr. **Gary Lidstone**, Mr. **Dwight Arney**, Dr. **Muni Majjigi**, and Dr. **Hyoun-Woo Shin**, for their advice, assistance, and especially their patience in dealing with a new graduate student who wanted "all of their data."

To Mr. **Keisuke Asai** for providing me with data from his work with variable temperature, variable composition flows.

To my present and former officemates, **Luc Fréchette**, **Dave Tew**, **Yang-Sheng "the Yang-inator" Tzeng**, **Fouzi Al-Essa**, and **John Kerwin**, for their friendship, help, and patience and for weathering my sometimes brutal sarcasm.

To **Brian Teeple** for letting me bounce ideas off of him and for getting me the ball when I was open and had room to run.

To **Brian Corn** for being a dependable friend (but not for his puns).

To my close friend and confidant, **Sonia Ensenant**, for providing much appreciated distractions, conversations, and mischief.

To the many other friends that I have found at the GTL who have made leaving such a bittersweet occasion.

To my friends **Mark**, **Scott** and **Jeff** who always welcomed me home.

To my mother who has supported all of my endeavors, my sister who has supported a couple of my endeavors, and the rest of the Stanislaw family who were always behind me.

This thesis is dedicated to my father, **Benjamin A. Stanislaw** (1940-1984).

Contents

List of Figures

Nomenclature

Roman

a	Speed of sound
A	Cross-sectional area
CER	Chute expansion ratio, $(A_p/A_{p,throat})$
Cm_A	Area corrected mass flow ratio, $(\frac{A_p}{A_s})\frac{\dot{m}_s}{\dot{m}_p})$
$Cm_{A,\mathcal{U}}$	Area and similarity parameter corrected mass flow ratio, $(\frac{A_p}{A_s})\sqrt{\frac{\mathcal{U}_s}{\mathcal{U}_p}}\frac{\dot{m}_s}{\dot{m}_p}$
Cm_T	Similarity parameter corrected mass flow ratio, $\sqrt{\frac{T_{t,s}}{T_{t,p}}}\frac{\dot{m}_s}{\dot{m}_p}$
$Cm_{\mathcal{U}}$	Similarity parameter corrected mass flow ratio, $\sqrt{\frac{\mathcal{U}_s}{\mathcal{U}_p}}\frac{\dot{m}_s}{\dot{m}_p}$
D	Hydraulic diameter
D_j	Jet diameter
$\frac{d_1}{d_e}$	Ratio of maximum plume diameter to nozzle exit diameter
$EPNLdB$	Estimated Perceived Noise Level in decibels
$f_{viscous}$	Forces due to shear stresses
$HSCT$	High Speed Civil Transport
h	Lobe peak to peak height
$L_{interface}$	Stream interface length
$\dot{m}$	Mass flow
M	Mach number
MAR	Mixing duct area ratio, (A_{exit}/A_{inlet})
NPR	Primary stream mixing duct nozzle pressure ratio, $(P_{t,p}/P_{amb})$
P	Pressure

PEN	Penetration, (h/h_{inlet})
r	Secondary to primary velocity ratio
R	Gas constant
$\Re$	Universal gas constant
s	Secondary to primary density ratio
SAR	Suppressor area ratio, $(A_{inlet}/A_{p,throat})$
$SNPR$	Secondary stream mixing duct nozzle pressure ratio, $(P_{t,s}/P_{amb})$
T	Temperature
$\mathcal{U}$	Internal energy parameter
u, V	Axial velocity
x^*	Nondimensional axial position, (x/λ)
Y^*	Nondimensional duct height, (y/λ)

Greek

α	Lobe half angle
γ	Ratio of specific heats
δ	Shear layer thickness
Θ	Scaling error correlation parameter, $(\sqrt{T_{t,p}/T_{t,s}} + 1/\sqrt{T_{t,s}/T_{t,p}})$
λ	Lobe wavelength
μ_M	Molecular Weight
ρ	Density
ω	Vorticity

Subscripts

e	Exit quantity
j	Jet quantity

mix	Fully mixed out quantity
o	Freestream quantity
p	Primary stream quantity
pit	Pitot quantity
s	Secondary stream quantity
t	Stagnation quantity

Subscripts

$*$	Quantity normalized by a random number

Chapter 1

Introduction

1.1 Background and Motivation

NASA and the American aerospace industry are jointly engaged in the High Speed Research (HSR) Program to develop enabling technologies for a High Speed Civil Transport (HSCT) to service the growing trans-Pacific passenger market. This supersonic aircraft will have to be economically competive with existing subsonic aircraft while meeting current environmental regulations. An aircraft of this type powered by engines developed using current technology would exceed the allowable take-off noise levels as determined by the Federal Aviation Adminstration's FAR36 Stage 3 community noise regulations by over 20 EPNdB [22]. A key enabling technology is thus noise suppression.

For a noise suppression technology to be viable for the HSCT, it must have minimal impact on thrust. The current goal of the HSR program is to reduce noise by 4 EPNdB per percent of thrust loss [22]. One method that has shown considerable promise is an acoustically treated lobed mixer-ejector [1, 11].

An ejector, as illustrated in Figure 1-1, entrains cool relatively slow moving ambient air (secondary flow) which then mixes with the hot faster moving engine exhaust (primary flow). This results in a reduction in the velocity of the jet exiting the engine nozzle. The noise produced by the exiting flow is reduced because jet noise intensity is proportional to a high power of jet velocity (see Figure 1-2). Further, the high

frequency noise associated with the mixing that takes place in the ejector can be absorbed by acoustic treatment lining the inside of the ejector shroud [11].

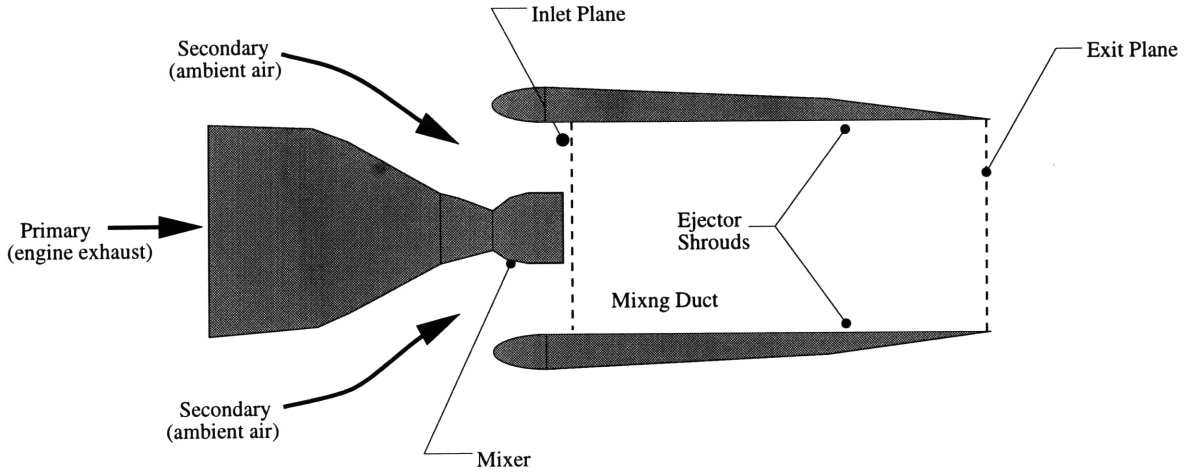

Figure 1-1: Schematic of an ejector

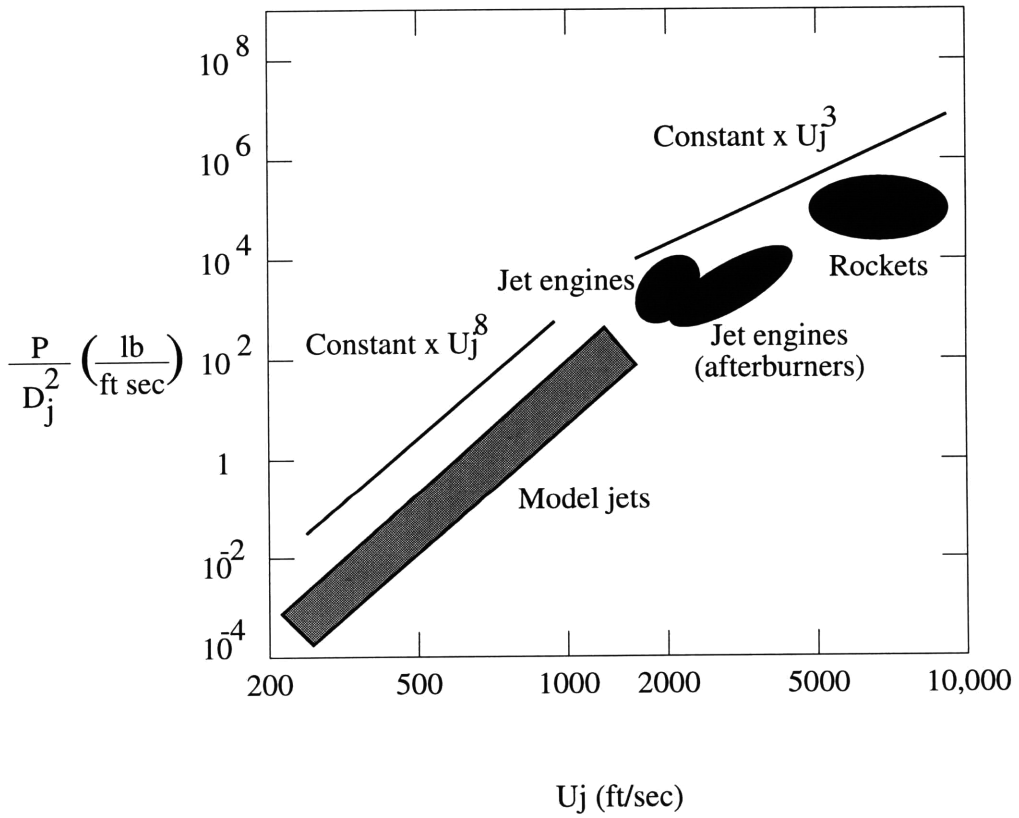

Figure 1-2: Noise power vs. jet speed, showing the transition from $\sim U_j^8$ to $\sim U_j^3$, approximately, when convection speed $U_j/2$ exceeds the speed of sound. [18]

The disadvantage of using an ejector for jet noise reduction is that considerable

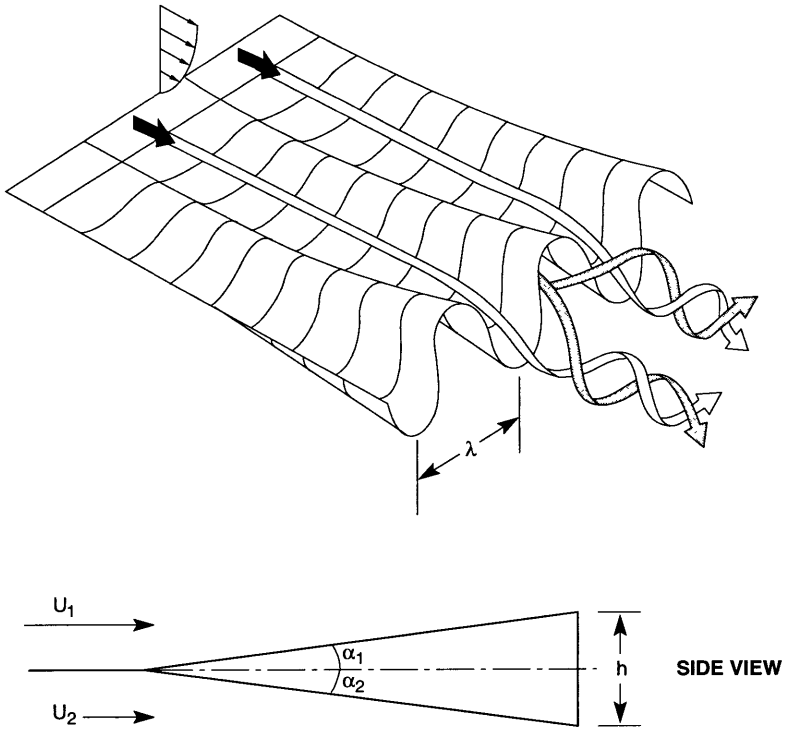

Figure 1-3: Schematic of a lobed mixer [19]

weight is added to the aircraft. So, it is of primary importance to reduce the size of the ejectors without infringing upon their noise suppressing capability. Optimal noise reduction is attained when the primary and secondary flows are uniformly mixed at the ejector exit. The required length of the mixing duct (i.e. the distance over which the streams become fully mixed) is thus inversely proportional to the rate at which the flows mix and to reduce the length of the ejector (i.e. reduce the weight of the ejector), the rate at which the flows mix must be increased. This mixing enhancement can be accomplished by using a lobed mixer as shown schematically in Figure 1-3.

There are two mechanisms by which a lobed mixer increases the mixing rate. First, the initial interface length between the mixing streams is increased due to the convoluted shape of the mixer's trailing edge [12]. Second, the mean cross-flow interface is stretched by the circulatory motion associated with shed streamwise vorticity [21, 25].

Some lobed mixer shapes, which bracket the range of potential configurations,

are shown in Figure 1-4. The top figure shows a mixer which will have substantial shed streamwise vorticity. The bottom configuration (referred to as a convoluted plate), from which the flows emerge essentially parallel, has very little shed streamwise vorticity.

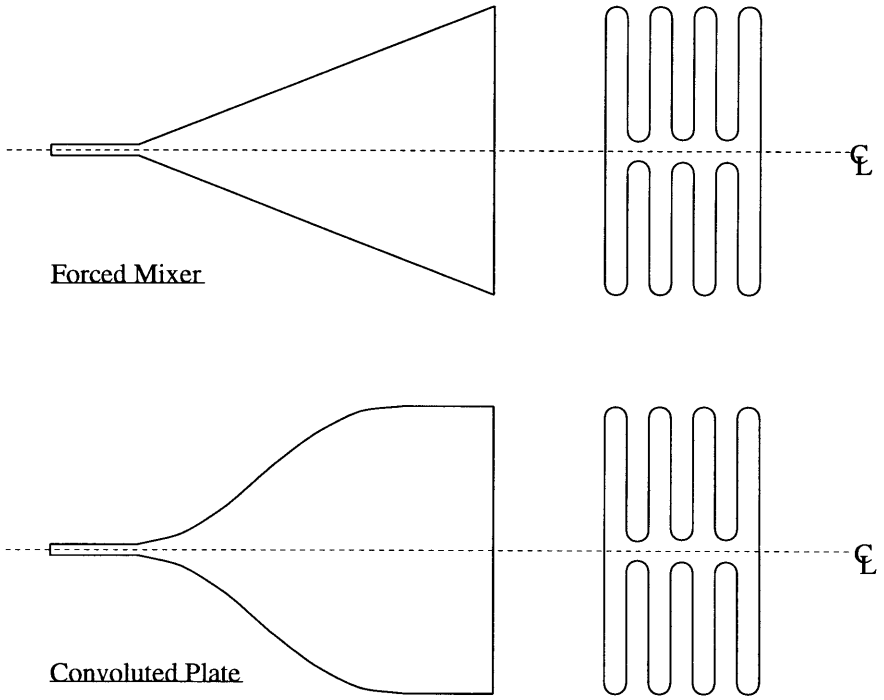

Figure 1-4: Types of lobed mixers

Lobed mixers have not yet been installed in supersonic mixer ejectors for the purpose of noise suppression, although, they have been used in subsonic engines for this purpose. Integration of these devices with possible engine cycles is currently being investigated through parametric test programs addressing their aerodynamic and acoustic performance of the mixer-ejectors.

The parametric tests are performed at temperatures representative of HSCT operating conditions which implies primary to secondary stagnation temperature ratios of up to 3.5. Costs of such testing is high due to facility and the associated hardware requirements, and significant savings in time and money could be realized if aerodynamic performance data could be gathered from tests at or near ambient temperatures. This thesis presents a quantitative assessment of the feasibility of doing this.

1.1.1 Similarity Principles and Experimental Results

A way to use cold (i.e. uniform temperature) tests results to predict the aerodynamic performance of hot tests is through utilization of similarity principles. A similarity principle allows one to employ results from one set of conditions to infer the behavior at another; an example is the use of the Prandtl-Glauert transformation to relate flows at different Mach numbers. Similarity principles are used when it is difficult or expensive to simulate experimentally the actual device operating conditions and computational procedures do not give the required accuracy.

1.1.1.1 Ideal and Approximate Munk and Prim Similarity Principles

For steady isentropic flow of a perfect gas one can apply the "Munk and Prim substitution principle" [14]:

> For a given geometry all flows with the same stagnation pressure distribution have the same streamline and Mach number pattern, regardless of the distribution in stagnation temperatures

In mixer-ejector flows, however, there is substantial heat transfer and momentum exchange between the primary and secondary streams, and the Munk and Prim Principle does not strictly apply. An approximate similarity principle, however, has been developed by Greitzer, Paterson, and Tan [9] for these flows. The approximate similarity principle can be stated as follows:

> For steady flows in which heat transfer and momentum transfer are important, stagnation pressure and Mach number distributions will be approximately similar regardless of the stagnation temperature variations

The central idea behind this principle is that there are two competing effects on the stagnation pressure, exchange of momentum and transfer of heat. Figure 1-5 illustrates the situation for the case of equal stagnation pressures at the inlet. A hot, fast moving, stream is bounded on one side by a cooler slower moving stream with the two streams becoming completely mixed at station 3.Greitzer, Paterson, and Tan

[9] showed that in this type of flow heat transfer from the hot stream to the cold stream tends to decrease the stagnation pressure of the latter. However, because the hot stream has a higher velocity than the cold stream, there is a net amount of work done on the latter, which tends to increase the stagnation pressure, counteracting the effect of heat transfer.

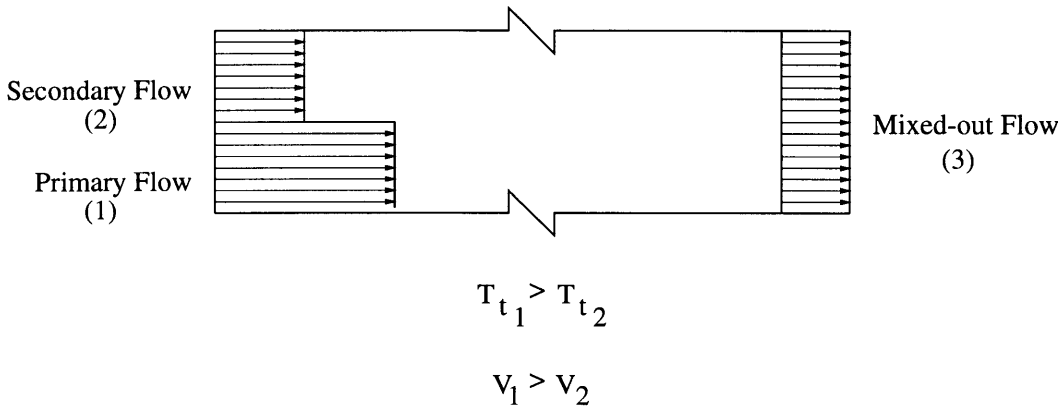

Figure 1-5: Mixing of two streams with equal stagnation pressures at the inlet [9]

The approximate Munk and Prim similarity principle has been shown to be useful in the aerodynamic performance prediction of subsonic mixing devices. Presz and Greitzer [20] and Barankiewicz, Perusek, and Ibrahim [4] applied the principle to thrust augmenting subsonic ejectors. Despite the large variations in primary stream stagnation temperature, the temperature corrected mass flow ratio and the gross thrust coefficient displayed similarity as can be seen in Figures 1-6,1-7,1-8, and 1-9. The temperature corrected mass flow ratio is defined as

$$\sqrt{\frac{T_{t,s}}{T_{t,p}}}\frac{\dot{m}_s}{\dot{m}_p}$$

and the gross thrust coefficient is defined as

$$C_{fg} = \frac{F_{measured}}{F_{ideal}}$$

The ideal thrust is defined as the thrust produced by the primary nozzle if it is perfectly expanded to ambient conditions.

The issue here concerns the application of the approximate similarity principle to supersonic mixer ejectors. If this concept can be used in supersonic flows in the same manner as it has been used in subsonic flows, it would be possible to infer the aerodynamic performance (e.g. mass flow ratios and gross thrust coefficients) of these devices from cold tests.

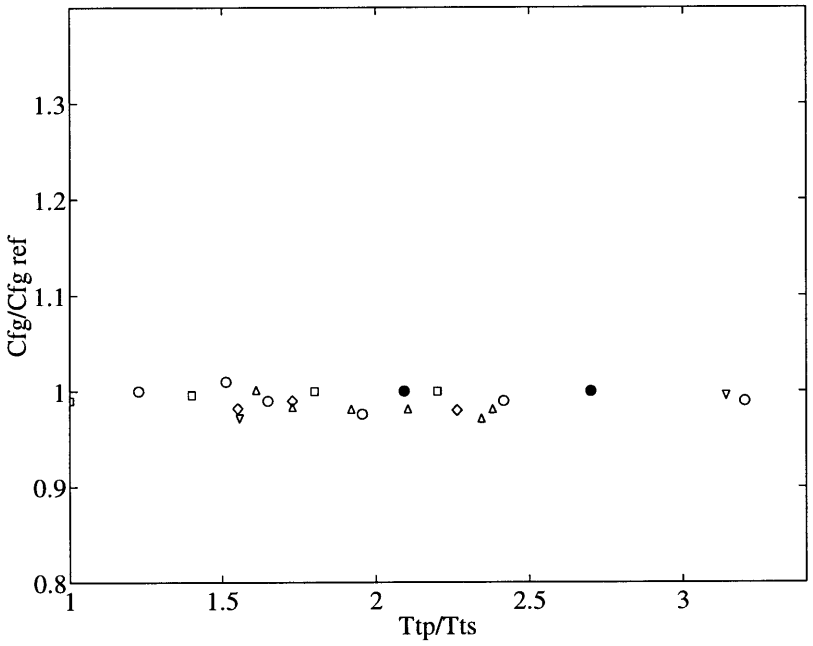

Figure 1-6: Gross thrust coefficient ratio from eight different ejector tests plotted against stagnation temperature ratio, (Cfg ref=Cfg at 294^oK, NPR=1.01 to 3.0, Cfg=1.05 to 1.55, various geometries); ○ Wood; ◊ Rockwell(1); □ Quinn(1); △ Rockwell(2); • Quinn(2); ▽ Hiller; ○ Lockheed; [20].

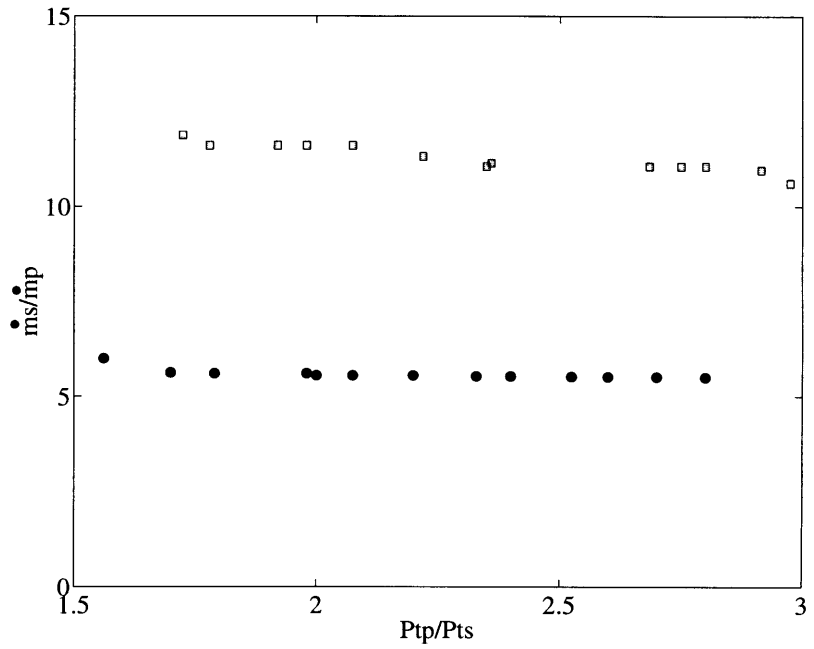

Figure 1-7: Mass flow ratio versus stagnation pressure ratio, $\bullet \frac{T_{t,p}}{T_{t,s}} = 1.06$; $\blacksquare \frac{T_{t,p}}{T_{t,s}} = 3.18$ [4].

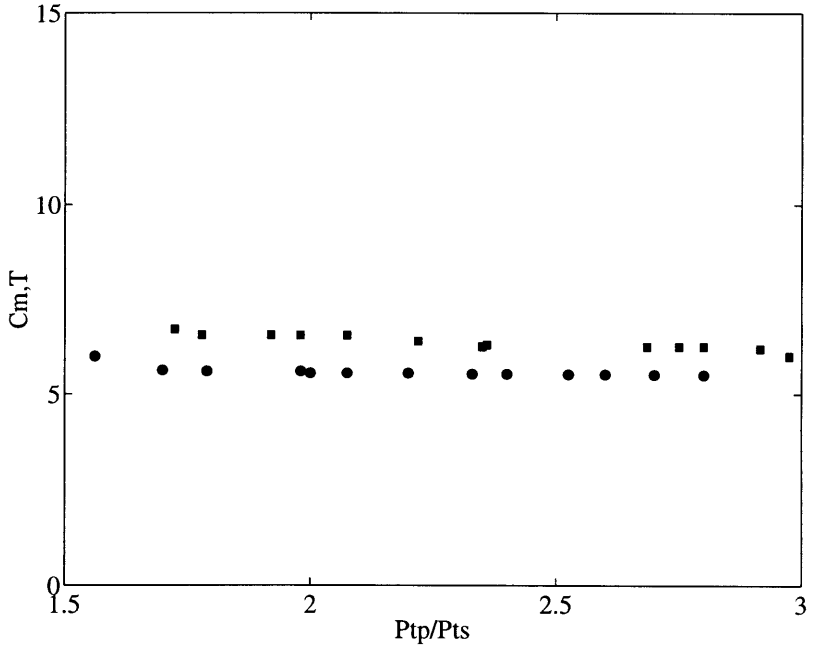

Figure 1-8: Temperature corrected mass flow ratio versus stagnation pressure ratio, $\bullet \frac{T_{t,p}}{T_{t,s}} = 1.06$; $\blacksquare \frac{T_{t,p}}{T_{t,s}} = 3.18$ [4].

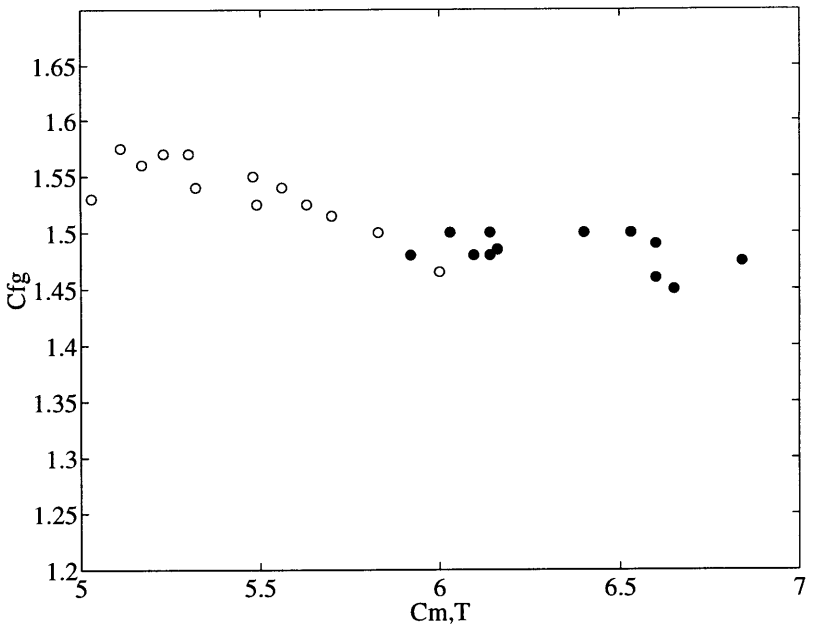

Figure 1-9: Gross thrust coefficient versus temperature corrected mass flow ratio, $\bigcirc \frac{T_{t,p}}{T_{t,s}} = 1.06$; $\bullet \frac{T_{t,p}}{T_{t,s}} = 3.18$ [4].

1.1.1.2 Additional Experimental Observations

Several investigators have found that varying the compositions of the mixing gases has the same effect on entrainment as varying the stagnation temperatures [3, 20, 16, 17]. In reference [3], mixtures of nitrogen and either methane, argon, or helium at varying temperatures were employed in a cryogenic wind tunnel to determine separate effects of jet temperature, specific heat ratio, and gas constant on the base pressure of a cylindrical afterbody model at transonic speeds. Figure 1-10 shows a schematic of the model that was used in this experiment.

Jet temperature affects afterbody flow in two ways. The first is entrainment through turbulent mixing [3]. It has been demonstrated that the approximate similarity principle is applicable to jets different temperatures. The second effect is referred to as plume shape efffect and is a result of the jet exhaust acting like a solid body and blocking the external flow during expansion to freestream pressure [16]. This effect can be correlated with the maximum plume diameter to nozzle exit diameter ratio which is solely a function of NPR and the ratio of specific heats of the

jet [16, 17].

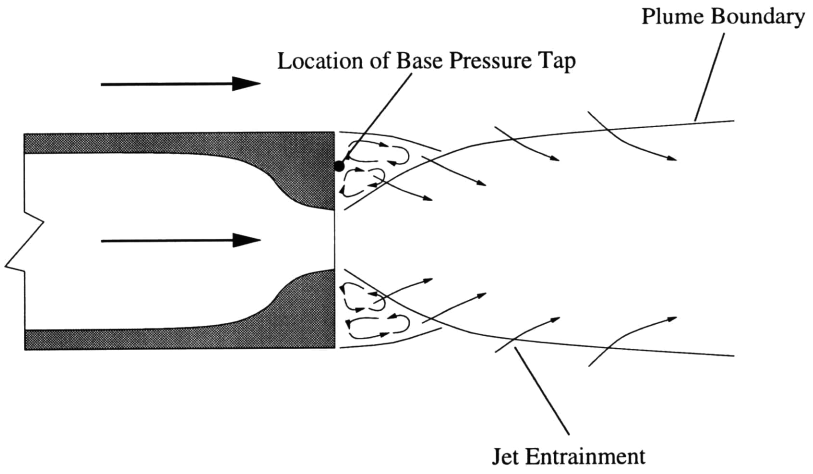

Figure 1-10: Schematic model of jet interaction with after body flow

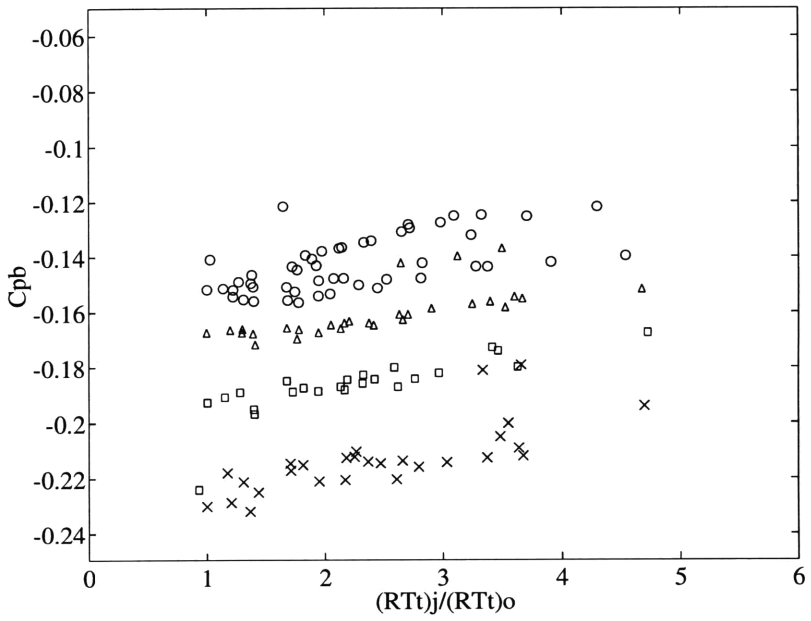

Figure 1-11: Correlation of data with d_1/d_e and RT ratio, $\bigcirc d_1/d_e = 1.0$; $\triangle$ $d_1/d_e = 1.1$; $\square d_1/d_e = 1.15$; $\times d_1/d_e = 1.2$ [3].

Figure 1-11 gives base pressure measurements for four values of the maximum plume diameter to nozzle exit diameter ratios (i.e. four cases of constant pressure and Mach number) plotted against the jet to freestream ratio of the product of gas constant and stagnation temperature (i.e. $(RT)_j/(RT)_o$) [3]. The conclusion was drawn that base pressure, for constant plume effect, is a function of the product of

gas constant and jet temperature. This implies that the stagnation temperature and the molecular weight of a jet have a similar effect on entrainment. The approximate similarity principle has been used to understand the effects of temperature on entrainment when the stagnation pressure and Mach numbers are constant [20, 4], but it is unclear as to why changing the composition of the jet would have the same effect as changing the temperature. Thus, it may be possible to extend the applicability of the approximate similarity principle to include the mixing of different gases.

1.2 Technical Objectives

The primary objective of this research was to determine the applicability and limitations of the approximate similarity principle to flow conditions representative of HSCT supersonic noise suppressing mixer-ejectors. This involved determining which cold flow test measurements could be used to predict hot flow performance parameters and what errors were inherent in the scaling.

A secondary objective was to extend the range of application of the approximate similarity principle to include mixing of different gases. This includes understanding the effect of variations in composition on entrainment.

1.3 Approach

There are two main strands in the present work. First, control volume models of mixer-ejector flows were used to examine the influence of flow parameters (e.g. M_p, NPR, $\frac{T_{t,p}}{T_{t,s}}$, and $\frac{\mu_{M,s}}{\mu_{M,p}}$) on similarity and to define the regions of applicability. A description of a incompressible control volume is presented in Section 2.2 and a compressible control volume is derived and explained in Appendix A. Second, the available mixer data was evaluated in light of the approximate similarity principle. The data was obtained from the HSR program [2, 8, 13] and published literature [15, 7, 26]. The data includes stagnation pressure, Mach number, and stagnation temperature profiles from the exit of a model HSCT mixer-ejector, mass flows, and thrust measurements.

Complete descriptions of the tests from which the HSR data originated can be found in Appendix B.

1.4 Contributions

The main contributions of this work are:

- The approximate similarity principle was determined to be applicable to the supersonic mixing regime encountered in HSCT mixer-ejectors. Previous applications have been limited to subsonic devices.
- A methodology for the prediction of supersonic mixer-ejector performance parameters at elevated temperatures from near ambient tests was developed.
- The range of application of the approximate similarity principle was extended to include the mixing of different gases. It was shown that exchanges of gases of diffferent molecular weight is analogous to changes associated with heat transfer and can counteract the effects of momentum exchange on stagnation pressure and result in flow similarity.

1.5 Overview of Thesis

In Chapter 2, the similarity principle is extended to mixing flows with nonuniform molecular weights and the mechanisms that lead to similarity are demonstrated for supersonic mixing flows. The similarity principle is applied to supersonic mixer-ejectors in Chapter 3. Summary and conclusions are presented in Chapter 4.

Chapter 2

Extension of the Approximate Similarity Principle

2.1 Introduction

The extension of the approximate similarity principle is broken into two parts. We first examine the extension to viscous flows with nonuniform molecular weight distributions. Experiments have shown that varying the composition of two mixing flows has an effect on stagnation pressure and Mach number similarity; while this is analogous to the effect of varying the stagnation temperature ratio [3, 16, 17, 20], there has been no explanation of this phenomenon. It will be shown that exhange of fluid of different molecular weights can act to counteract the effect of momentum transfer on stagnation pressure. In the flows considered here, exhange of fluid of different molecular weights and heat transfer produce opposite and nearly equal changes in the stagnation pressure that are opposite and nearly equal to those due to shear stresses. This results in stagnation pressure and Mach number profiles that closely resemble profiles produced without the presence of these effects. A new similarity parameter will be introduced that embodies the effects of both heat transfer and changes in mass averaged molecular weight.

The second part of the chapter is an analytical examination of the similarity principle in the supersonic mixing regime for conditions typical of HSCT mixer-ejectors.

It will be shown that the balance between changes in molecular weight, heat transfer and momentum transfer exists regardless of the Mach numbers of the mixing flows.

2.2 Application to Mixing Flows of Different Compositions: Low Speed Flow

2.2.1 Equations for Mixing Flows with Nonuniform Total Temperature and Molecular Weight Distributions

The equations of motion for a steady flow of a perfect gas at low Mach numbers (i.e. $M^2 \ll 1$) will now be examined to show that the similarity principle can be extended to mixing flows of variable composition. This type of investigation was performed by Greitzer et al [9] on mixing flows of variable stagnation temperature but constant composition. To account for varying composition, the gas constant of the flow is not assumed to be uniform, although, the ratio of specific heats is taken as uniform. Justification for this assumption will be presented post priori at the end of this chapter.

The equations for mass and momentum conservation [9] are

$$\vec{\nabla} \cdot (\rho \vec{V}) = 0 \tag{2.1}$$

$$\vec{\omega} \times \vec{V} = -\frac{1}{\rho}\vec{\nabla}P - \vec{\nabla}\frac{V^2}{2} + \frac{\vec{f}_{viscous}}{\rho} \tag{2.2}$$

where $\vec{\omega}$ is the vorticity vector ($\vec{\omega} = \vec{\nabla} \times \vec{V}$). The Reynolds number is taken to be sufficiently high that $\vec{f}_{viscous}$ (the force due to shear stresses), heat transfer, and the exchange of mass are primarily associated with turbulent rather than molecular diffusion.

The similarity of the Mach number and stagnation pressure in mixing flows regardless of the stagnation temperature distributions of those flows was demonstrated

in Reference [9]. Since this same similarity has been shown to exist when different gases are mixed, it is useful to cast the equations of motion in terms of these quantities. To do this, the definition of the Mach number vector, $\vec{M} = \vec{V}/a$, where a is the local speed of sound, is substituted into Equations 2.1 and 2.2. Also, the equation of state for low Mach numbers can be approximated as

$$\bar{\rho}\bar{R}\bar{T} = \rho RT + O(M^2) \tag{2.3}$$

where $\bar{\rho}$, $\bar{T}$, and $\bar{R}$ are reference values of density, temperature, and gas constant [5]. This approximation for the equation of state can be justified through an order of magnitude analysis. The equation of state

$$P = \rho RT \tag{2.4}$$

in logarithmic differential form is

$$\frac{d\rho}{\rho} = \frac{dP}{P} - \frac{dT}{T} - \frac{dR}{R} \tag{2.5}$$

Both $\Delta T/T$ and $\Delta R/R$ are of order one because both the temperature and the gas constant can experience changes of the same magnitude as their respective ambient values. From the momentum equation, it can be shown that changes in pressure are of the order M^2 so that from Equation 2.5,

$$\frac{\Delta\rho}{\rho} \sim \frac{\Delta T}{T} - \frac{\Delta R}{R} + O(M^2) \tag{2.6}$$

Thus, for low Mach numbers (i.e. $M^2 \ll 1$) the equation of state can be approximated as

$$\rho RT = constant + O(M^2) \tag{2.7}$$

The static temperature and the stagnation temperature also differ by $O(M^2)$. Hence, it does not matter whether the local Mach number vector is defined with static or

stagnation temperature.

Upon substitution of the definition of the Mach number vector and Equation 2.3 into Equations 2.1 and refeqn2:momentum, we have

$$\vec{\nabla} \cdot \vec{M} = \vec{M} \cdot \frac{\vec{\nabla}\mu_M}{2\mu_M} + \vec{M} \cdot \frac{\vec{\nabla}T}{2T} \tag{2.8}$$

$$\vec{\omega}_m \times \vec{M} = -\vec{M}\left(-\vec{M} \cdot \frac{\vec{\nabla}\mu_M}{2\mu_M} + \vec{M} \cdot \frac{\vec{\nabla}T}{2T}\right) - \frac{\vec{\nabla}P_t}{\bar{\rho}\bar{a}^2} + \frac{\vec{f}_{viscous}}{\bar{\rho}\bar{a}^2} + O(M^4) \tag{2.9}$$

where the quantity $\vec{\omega}_m$ is defined as [10]

$$\vec{\omega}_m = \vec{\nabla} \times \vec{M} \tag{2.10}$$

The vector field, $\vec{M}$, is determined through its curl, its divergence, and the boundary conditions imposed by geometry. Exact Mach number field equivalence is not possible between flows without heat transfer ($\vec{\nabla} \cdot \vec{M} = 0$) and those with heat transfer (for which the divergence of the Mach number was non-zero). Likewise, this is the case for flows with non-uniform molecular weight compared to flows with uniform molecular mass. However, in the flows that will be considered, it will be shown that the Mach numbers remain closely similar. Equations 2.8 and 2.9 also suggest that the Mach number field of a flow with heat transfer can be duplicated by a flow that experiences a change in molecular mass. The implication of the above statement will be explored further in the following sections.

In addition to Mach number similarity , the stagnation pressures of these various mixing cases also exhibit only a weak dependence on heat transfer and changes in molecular weight. To illustrate this, equation 2.9 can be rewritten as

$$\vec{M} \times \vec{\omega}_m = \frac{\vec{\nabla}P_t}{\bar{\rho}\bar{a}^2} + \frac{aM}{\bar{\rho}\bar{a}^2}\left[\frac{\vec{M}}{M}\frac{\bar{\rho}\bar{a}^2}{a}\left(-\vec{M} \cdot \frac{\vec{\nabla}\mu_M}{2\mu_M} + \vec{M} \cdot \frac{\vec{\nabla}T}{2T}\right) - \frac{\vec{f}_{viscous}}{V}\right] + O(M^4) \tag{2.11}$$

It can be seen from this equation that there will be no stagnation pressure change along a streamline if

$$\left(\frac{\vec{M}}{M}\right)\left(\frac{\bar{\rho}\bar{a}^2}{a}\right)\left(-\vec{M}\cdot\frac{\vec{\nabla}\mu_M}{2\mu_M}+\vec{M}\cdot\frac{\vec{\nabla}T}{2T}\right)=\frac{\vec{f}_{viscous}}{V} \tag{2.12}$$

Equations 2.11 and 2.12 reveal the possibility that there are situations in which the stagnation pressure change due to viscous effects is offset by a combination of the effects of heat transfer and molecular weight change. This suggests that the similarity principle described by Greitzer et al [9] (in which only the effects of heat transfer and shear stresses were considered) is actually a special case of a more general statement. It also explains the results of references [3], [20], [16], and [17], which showed that nonuniform molecular weight distributions have a similar impact on entrainment as nonuniform stagnation temperature.

This generalized similarity principle states that there are three competing effects which must be considered. Both the heat transfer, from a hot stream to a cold stream, and exchange of fluid, from a stream with low molecular weight to a stream with high molecular weight, tend to decrease the stagnation pressure of the latter. In the situations of interest, however, the hot stream and the stream with low molecular weight will have a higher velocity than the cold stream and the stream with higher molecular weight. This causes work to be done on the slower stream, increasing the stagnation pressure and countering the effect of heat transfer and entrainment of low molecular weight fluid.

The effects of heat transfer and molecular weight change can be encapsulated into a single similarity parameter, $\mathcal{U}$, ($\mathcal{U} = T_t/\mu_M$). It is of interest to note the similar changes in stagnation pressure occur as heat is transferred from a hotter stream to a cooler stream or as mass is transferred from a stream of lower molecular weight to a stream of higher molecular weight (e.g. the heat gradient is opposite of that of the molecular weight gradient). This reflects the opposite signs of the heat transfer and molecular weight change terms in the momentum equation and in the logarithmic

differential form of the similarity parameter definition.

$$\frac{d\mathcal{U}}{\mathcal{U}} = \frac{dT}{T} - \frac{d\mu_M}{\mu_M} \tag{2.13}$$

Using the similarity parameter, we can express the equations of motion as

$$\vec{\nabla} \cdot \vec{M} = \vec{M} \cdot \frac{\vec{\nabla}\mathcal{U}}{2\mathcal{U}} \tag{2.14}$$

$$\vec{\omega}_m \times \vec{M} = -\vec{M}\left(\vec{M} \cdot \frac{\vec{\nabla}\mathcal{U}}{2\mathcal{U}}\right) - \frac{\vec{\nabla}P_t}{\bar{\rho}\bar{a}^2} + \frac{\vec{f}_{viscous}}{\bar{\rho}\bar{a}^2} + O(M^4) \tag{2.15}$$

Equation 2.11 now assumes the form

$$\vec{M} \times \vec{\omega}_m = \frac{\vec{\nabla}P_t}{\bar{\rho}\bar{a}^2} + \frac{aM}{\bar{\rho}\bar{a}^2}\left[\frac{\vec{M}}{M}\frac{\bar{\rho}\bar{a}^2}{a}\left(\vec{M} \cdot \frac{\vec{\nabla}\mathcal{U}}{2\mathcal{U}}\right) - \frac{\vec{f}_{viscous}}{V}\right] + O(M^4) \tag{2.16}$$

It can be seen that there will be no change in stagnation pressure if

$$\left(\frac{\vec{M}}{M}\right)\left(\frac{\bar{\rho}\bar{a}^2}{a}\right)\left(\vec{M} \cdot \frac{\vec{\nabla}\mathcal{U}}{2\mathcal{U}}\right) = \frac{\vec{f}_{viscous}}{V} \tag{2.17}$$

In summary, we have identified exchange of gases with different molecular weights as a third mechanism that can affect the stagnation pressure and Mach numbers in low Mach number mixing experiments in addition to the effects of heat transfer and shear forces. A new scaling parameter, $\mathcal{U}$, has also been introduced. The next section will examine the competing effects in low speed flows qualitatively.

2.2.2 Incompressible Control Volume Results

We examine the mixing of two flows using a control volume approach, to illustrate the effects on ejector performance. The primary and the secondary streams are assumed to flow isentropically from known upstream conditions to the start of the mixing duct, where each stream is considered to be uniform. As shown in [19], the equations for

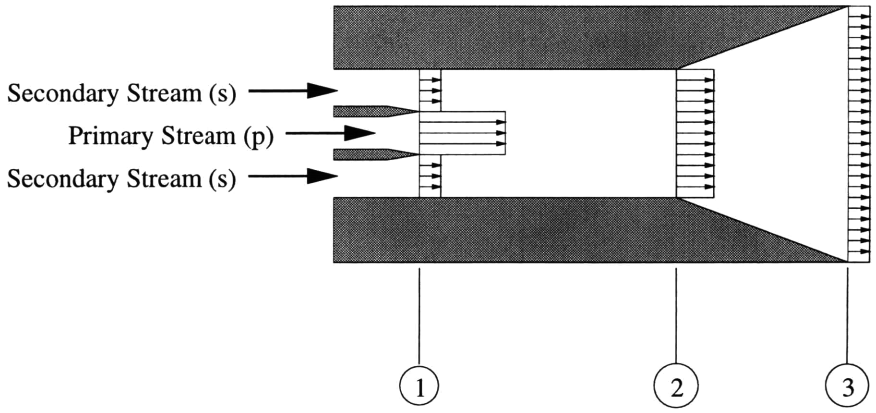

Figure 2-1: Incompressible control volume schematic

conservation of mass, momentum, and energy can be combined into a simple quadratic equation for the secondary to primary mass flow ratio, $\frac{\dot{m}_s}{\dot{m}_p}$.

$$\frac{\rho_s}{\rho_p}\left(\frac{\dot{m}_s}{\dot{m}_p}\right)^2\left[\left(\frac{A_p}{A_s}\right)^2+\left(\frac{A_2}{A_3}\right)^2\right]+\sqrt{\frac{\rho_p}{\rho_s}}\left(\frac{\dot{m}_s}{\dot{m}_p}\right)\left[1+\left(\frac{A_2}{A_3}\right)^2\right]\left[\sqrt{\frac{\rho_p}{\rho_s}}+\sqrt{\frac{\rho_s}{\rho_p}}\right] + \left[\left(\frac{A_2}{A_3}\right)^2-1-2\left(\frac{A_s}{A_p}\right)\right]=0 \quad (2.18)$$

The quantity, A_2/A_3, is the inlet-to-exit area ratio of a diffuser adjoining the constant area ejector (see Figure 2-1. A_2/A_3 was equal to one for all of the calculations done with this control volume.

The secondary to primary mass flow ratio ,$\frac{\dot{m}_s}{\dot{m}_p}$, is an ejector performance parameter known as the pumping characteristic. The quantity

$$\sqrt{\rho_p/\rho_s}\dot{m}_s/\dot{m}_p \quad (2.19)$$

can be written in terms of the temperature and molecular weight ratios since (with $P_s = P_p$)

$$\frac{\rho_p}{\rho_s}\frac{T_p}{T_s}\frac{\mu_{M,s}}{\mu_{M,p}}=1 \quad (2.20)$$

To order M^2, the temperatures and densities can be either stagnation or static and the static quantities in Equation 2.20 can be replaced by stagnation quantities allowing

Equation 2.19 to be expressed as

$$\sqrt{\frac{T_{t,s}}{T_{t,p}}}\sqrt{\frac{\mu_{M,p}}{\mu_{M,s}}}\left(\frac{\dot{m}_s}{\dot{m}_p}\right)$$

or, terms of the similarity parameter

$$\sqrt{\frac{\mathcal{U}_s}{\mathcal{U}_p}}\left(\frac{\dot{m}_s}{\dot{m}_p}\right)$$

The quantity, $\sqrt{\mathcal{U}_s/\mathcal{U}_p}(\dot{m}_s/\dot{m}_p)$, will be referred to as the corrected mass flow ratio. Similarly, the quantity

$$\sqrt{\frac{\rho_p}{\rho_s}}+\sqrt{\frac{\rho_s}{\rho_p}} \tag{2.21}$$

can be expressed as

$$\sqrt{\frac{\mathcal{U}_p}{\mathcal{U}_s}}+\sqrt{\frac{\mathcal{U}_s}{\mathcal{U}_p}} \tag{2.22}$$

The above discussion leads to the conclusion that ejector performance will be the same for a specified similarity parameter ratio regardless of what combinations of stagnation temperature and molecular weight ratios are used to acheive it. Figures 2-2 and 2-3 illustrate this point. In the figures, the mass flow ratio is plotted against the secondary to primary area ratio. The curves that are plotted correspond to similarity paramter ratios of 1.0, 2.0, 3.0, and 4.0. In Figure 2-2, the similarity parameter ratios are achieved by keeping the molecular weights equal and varying only the stagnation temperatures of the flows. This situation is reversed in Figure 2-3. In spite of the different quantities that were varied, these figures are identical.

Figure 2-4 shows the corrected mass flow ratios for the second situation. This figure shows that the corrected mass flow exhibits approximate similarity. This was observed by Presz and Greitzer in reference [20] for changes in stagnation temperature only. The results thus suggest that to account for both heat transfer and exchnge of

fluid with different molecular weights the similarity parameter ratio should be used to scale ejector performance.

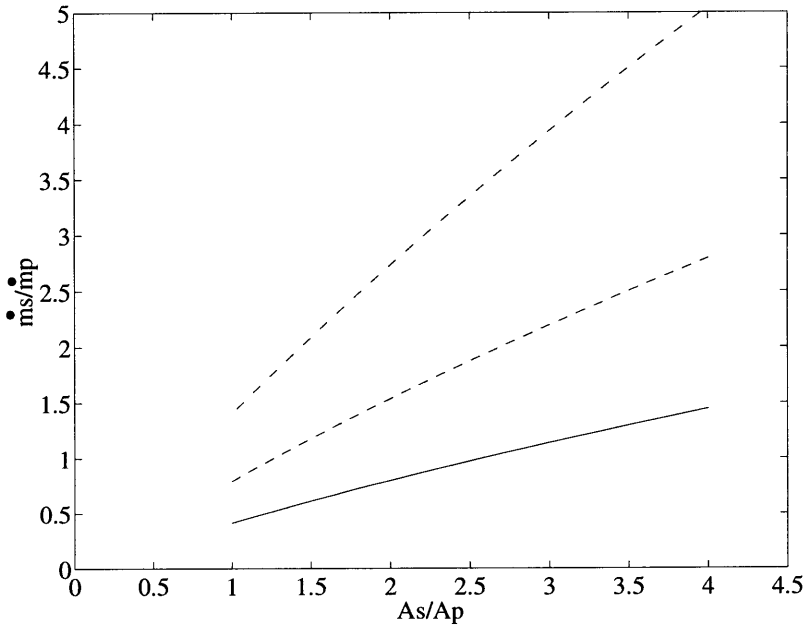

Figure 2-2: Mass flow ratios for flows of variable stagnation temperature as calculated from incompressible control volume analysis: —— $\frac{T_{t,p}}{T_{t,s}} = 1.0, \frac{\mu_{M,s}}{\mu_{M,p}} = 1.0, \frac{\mathcal{U}_s}{\mathcal{U}_p} = 1.0$; – – – $\frac{T_{t,p}}{T_{t,s}} = 2.0, \frac{\mu_{M,s}}{\mu_{M,p}} = 1.0, \frac{\mathcal{U}_s}{\mathcal{U}_p} = 0.5$; · · · · $\frac{T_{t,p}}{T_{t,s}} = 2.0, \frac{\mu_{M,s}}{\mu_{M,p}} = 1.0, \frac{\mathcal{U}_s}{\mathcal{U}_p} = 0.333$; – · – · $\frac{T_{t,p}}{T_{t,s}} = 4.0, \frac{\mu_{M,s}}{\mu_{M,p}} = 1.0, \frac{\mathcal{U}_s}{\mathcal{U}_p} = 0.25$

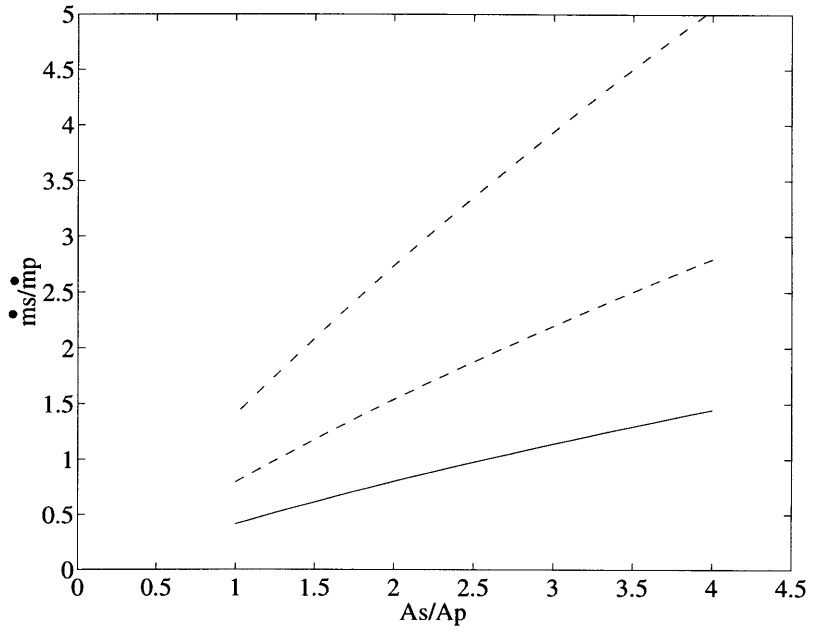

Figure 2-3: Mass flow ratios for flows of variable molecular weight as calculated from incompressible control volume analysis: —— $\frac{T_{t,p}}{T_{t,s}} = 1.0, \frac{\mu_{M,s}}{\mu_{M,p}} = 1.0, \frac{\mathcal{U}_s}{\mathcal{U}_p} = 1.0$; – – – $\frac{T_{t,p}}{T_{t,s}} = 1.0, \frac{\mu_{M,s}}{\mu_{M,p}} = 2.0, \frac{\mathcal{U}_s}{\mathcal{U}_p} = 0.5$; · · · · $\frac{T_{t,p}}{T_{t,s}} = 1.0, \frac{\mu_{M,s}}{\mu_{M,p}} = 3.0, \frac{\mathcal{U}_s}{\mathcal{U}_p} = 0.333$; – · – · $\frac{T_{t,p}}{T_{t,s}} = 1.0, \frac{\mu_{M,s}}{\mu_{M,p}} = 4.0, \frac{\mathcal{U}_s}{\mathcal{U}_p} = 0.25$

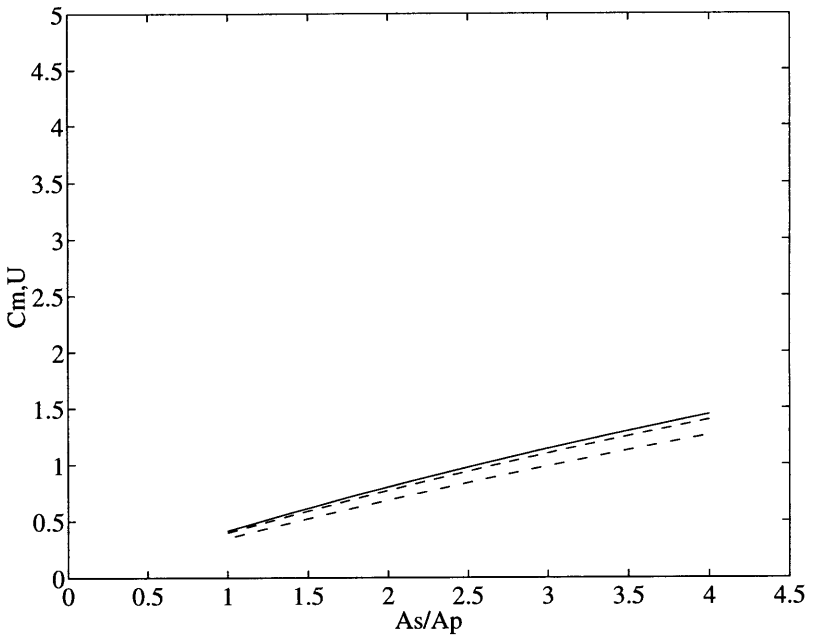

Figure 2-4: Corrected mass flow ratios for flows of variable molecular weight as calculated from incompressible control volume analysis: —— $\frac{T_{t,p}}{T_{t,s}} = 1.0, \frac{\mu_{M,s}}{\mu_{M,p}} = 1.0, \frac{U_s}{U_p} = 1.0$; – – – – $\frac{T_{t,p}}{T_{t,s}} = 1.0, \frac{\mu_{M,s}}{\mu_{M,p}} = 2.0, \frac{U_s}{U_p} = 0.5$; $\cdots$ $\frac{T_{t,p}}{T_{t,s}} = 1.0, \frac{\mu_{M,s}}{\mu_{M,p}} = 3.0, \frac{U_s}{U_p} = 0.333$; – · – · $\frac{T_{t,p}}{T_{t,s}} = 1.0, \frac{\mu_{M,s}}{\mu_{M,p}} = 4.0, \frac{U_s}{U_p} = 0.25$

2.3 Effects of Mach Number

The above derivations for the approximate similarity principle have been done for low Mach number flows ($M^2 \ll 1$). The HSCT mixer-ejectors have Mach number that ranges from 0.3 to 2.0. To apply the similarity principle to these devices, it is necessary to show that the effects of heat transfer, molecular weight change, and momentum transfer upon stagnation pressure still approximately balance one another over the presented range of Mach numbers.

Greitzer et al [9] examined the effect of Mach number on the stagnation pressure and Mach number similarity in mixing flows of unequal stagnation temperature. They found that the competing stagnation pressure effects were still present but that similarity degraded with increasing inlet Mach number (e.g. the error between the stagnation pressure in the homenthalpic case ($T_{t,p}/T_{t,s} = 1$) and in the nonhomenthatlpic case, $T_{t,p}/T_{t,s} = 4.0$, was 1.3% at $M = 0.05$ and 5.5% at $M = 0.7$). Presz

and Greitzer [20] investigated the effect of Mach number on the similarity of ejector performance and found that for the range of conditions that they investigated the corrected mass flow was insensitive to temperature differences in the compressible regime. The results of these earlier works suggest that the general similarity principle should be applicable to the flows present in supersonic mixer-ejectors, although, the results did not extend to the conditions experienced by HSCT mixer-ejectors. We thus examine the effects of heat transfer, exchange of fluid with different molecular weights, and momentum transfer on stagnation pressure and Mach number in the regime of interest.

2.3.1 Influence Coefficients

Shapiro[23] presents the equations of one dimensional flow as eight simultaneous linear differential equations. Each equation defines a dependent differential parameter as a function of six independent variables. He calls the coefficients of the independent variables influence coefficients since they indicate the influence of the independent variables on each of the dependent parameters.

Use of the First and Second Laws of Thermodynamics, together with the expression for the ratio of stagnation to static temperature in terms of Mach number (i.e. $\frac{T_t}{T} = 1 + \frac{(\gamma-1)}{2}M^2$), allows one to relate a change in P_t to a change in $\mathcal{U}$ as

$$\frac{dP_t}{P_t} = -\frac{\gamma M^2}{2}\frac{d\mathcal{U}}{\mathcal{U}} \tag{2.23}$$

The full derivation of this influence coeficient can be found in Appendix D. It is useful to separate the similarity parameter into its two components so that both the stagnation temperature and the molecular weight influence coefficients are brought out.

$$\frac{dP_t}{P_t} = -\frac{\gamma M^2}{2}\frac{dT_t}{T_t} + \frac{\gamma M^2}{2}\frac{d\mu_M}{\mu_M} \tag{2.24}$$

The opposite signs of the two influence coefficients reflect that the stagnation temper-

ature must increase and the molecular weight must decrease so as to have the same effect on the stagnation pressure.

The influence of the shear forces on the stagnation pressure will now be determined. The wall friction influence coefficient for the situations of constant molecular weight and constant specific heats is [23]

$$\frac{dP_t}{P_t} = -\frac{\gamma M^2}{2}\left(4f_{wall}\frac{dx}{D}\right) \tag{2.25}$$

In this equation, f_{wall} is the wall friction coefficient, x is the axial position, and D is the hydraulic diameter. By replacing the wall friction coefficient, f_{wall}, with the interstream friction coefficient, $f_{interstream}$, and including a term for the stream interface length, this becomes the interstream shear force influence coefficient.

$$\frac{dP_t}{P_t} = \pm\frac{\gamma M^2}{2}\left(4f_{interface}\frac{L_{interstream}}{A}dx\right) \tag{2.26}$$

The stream interface length is defined as the length of the stream interface in the cross-flow direction (see Figure 2-5). The interstream friction coefficients were defined by Clark [6] as,

$$\text{(Primary stream)} \quad f_{interstream,p} = (\frac{\rho_{avg}}{\rho_p})(\frac{1}{2\sqrt{\pi}\sigma}(1+\frac{u_s}{u_p})(\frac{u_s}{u_p}-1) \tag{2.27}$$

$$\text{(Secondary stream)} \quad f_{interstream,s} = (\frac{\rho_{avg}}{\rho_s})(\frac{1}{2\sqrt{\pi}\sigma}(1+\frac{u_p}{u_s})(\frac{u_p}{u_s}-1) \tag{2.28}$$

where ρ_{avg} is the mean density and σ is the spread rate constant. The spread rate constant is a parameter that must be obtained by employing correlations with experimental data.

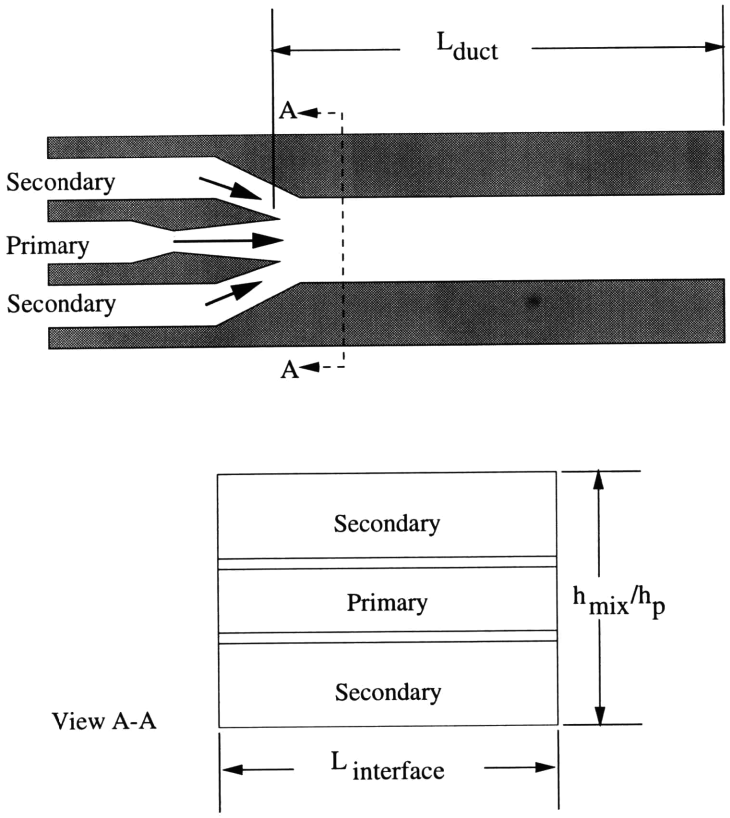

Figure 2-5: Boeing Single Lobe model schematic

Because the molecular weight does not enter the derivation, the shear stress influence coefficient for the case of flows of variable molecular mass but constant specific heats is the same as the case in which both are constant. The sign of the influence coefficient changes according to which flow is being considered. The high velocity flow will transfer momentum to the low velocity flow and the stagnation pressure of the high velocity flow will decrease so the negative sign is appropriate. Conversely, for the low velocity flow, the sign of the influence coefficient must be positive because the momentum transfered to it (from the high velocity flow) will result in a stagnation pressure rise.

Having determined the influence coefficients for heat transfer, variable molecular weight, and interstream shear forces, the changes in stagnation pressure due to these effects can be expressed as

$$\frac{dP_t}{P_t} = -\frac{\gamma M^2}{2}\frac{d\mathcal{U}}{\mathcal{U}} \pm \frac{\gamma M^2}{2}\left(4 f_{interface}\frac{L_{interstream}}{A}dx\right) \tag{2.29}$$

From this expression, it can be observed that molecular weight change and heat transfer (through the similarity parameter) can counteract the effect of interstream shear forces (i.e. momentum transfer) on stagnation pressure. Because incompressibility (i.e. $M^2 \ll 1$) was not assumed, it can now be said that flows well-approximated as one dimensional flow will have the balance of stagnation pressure effects that results in the approximate similarity principle can hold regardless of their Mach number. We now need to examine quantitatively how this balance holds.

2.3.2 Compressible Flow Results

We model the mixing of two streams in a supersonic mixer-ejector using a control volume. A complete description of the control volume and its application to mixer-ejectors is presented in Appendix A, but the key assumptions are that the duct area is constant and that the two flows are completely mixed at the exit of the duct. These assumptions are not strictly representative of HSCT mixer-ejectors because most configurations include a slightly converging mixing duct and the mixing duct lengths are not long enough to assure complete mixing of the streams. However, the analysis can be used to elucidate the trends found in mixer-ejector performance.

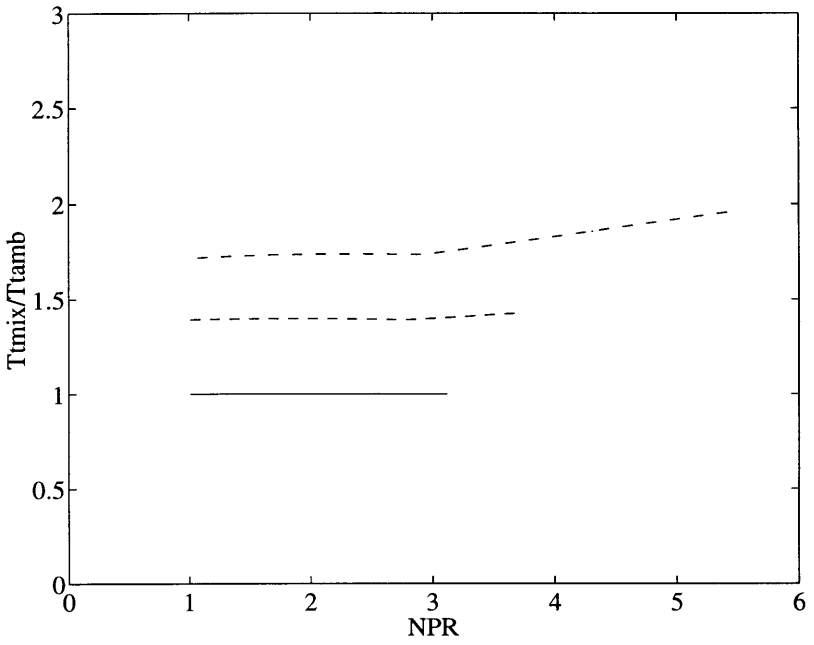

Figure 2-6: Mixed out exit stagnation temperatures as calculated from compressible control volume analysis, SNPR=1.0, Mp=supersonic, $\frac{A_s}{A_p} = 3.0$, —— $\frac{T_{t,p}}{T_{t,s}} = 1.0$; – – – – $\frac{T_{t,p}}{T_{t,s}} = 2.0$; – · – · $\frac{T_{t,p}}{T_{t,s}} = 3.0$; · · · · $\frac{T_{t,p}}{T_{t,s}} = 4.0$

With the exception of the stagnation temperature ratio (see Appendix B), the conditions used in this analysis were the same as those of the Boeing Single Lobe Tests. The results are shown in Figures 2-6, 2-7, and 2-8. Figure 2-6 shows the exit stagnation temperature plotted against the primary nozzle pressure ratio, NPR. The four curves represent stagnation temperature ratios of 1.0, 2.0, 3.0, and 4.0. The mixed-out stagnation temperature increases by a factor of two as the ratio of initial stagnation temperatures is increased to 4.0. The curves for $T_{t,p}/T_{t,s} = 1.0$ and 2.0 end abruptly because in each case choking of the secondary flow has occurred at the mixing duct inlet with the result that a completely mixed-out solution with the required exit static pressure is not attainable. Figure 2-7 illustrates that stagnation temperature ratio has little effect on exit stagnation pressure.

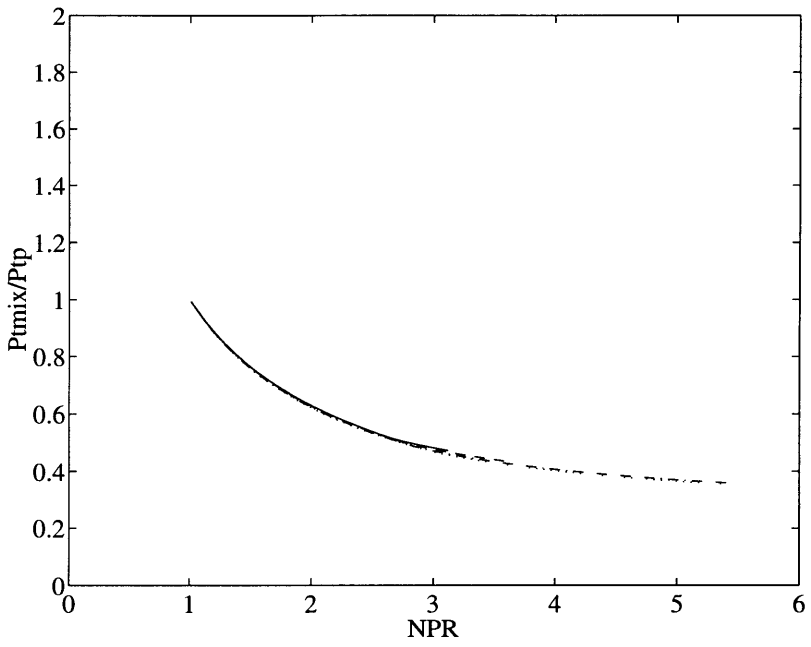

Figure 2-7: Mixed out exit stagnation pressures as calculated from compressible control volume analysis, SNPR=1.0, Mp=supersonic, $\frac{A_s}{A_p} = 3.0$, —— $\frac{T_{t,p}}{T_{t,s}} = 1.0$; – – – – $\frac{T_{t,p}}{T_{t,s}} = 2.0$; – · – · $\frac{T_{t,p}}{T_{t,s}} = 3.0$; · · · · $\frac{T_{t,p}}{T_{t,s}} = 4.0$

Figure 2-8 shows that over the same range of NPR and stagnation temperature ratio the exit Mach number is also nearly invariant with stagnation temperature ratio. The difference between the the Mach number at $T_{t,p}/T_{t,s} = 1.0$ and the Mach number at $T_{t,p}/T_{t,s} = 4.0$ increase with NPR but even at an NPR of 3.0 (the highest NPR attainable for the case $T_{t,p}/T_{t,s} = 1.0$), the Mach number at $T_{t,p}/T_{t,s} = 4.0$ is only 4.1% lower than the Mach number at $T_{t,p}/T_{t,s} = 1.0$. (All differences between values are presented as percentages of the quantity at the higher stagnation temperature or molecular weight ratio. They are presented in this manner because these would be the quantities of interest.)

Figures 2-9 and 2-10 present plots of pumping ratios and corrected mass flow ratios versus NPR for three temperature ratios. Correcting the mass flow ratio by the temperature ratio has the effect of collapsing the pumping ratios to one curve. At an NPR of 3.0, the difference between the corrected mass flow for $T_{t,p}/T_{t,s} = 1.0$ and the corrected mass flow for $T_{t,p}/T_{t,s} = 3.0$ is 17.3%. Figures 2-11 and 2-12 show that changing the molecular weight ratio in the same proportions as the stagnation

temperature ratio has the same effect on corrected mass flow ratio and gross thrust coefficient.

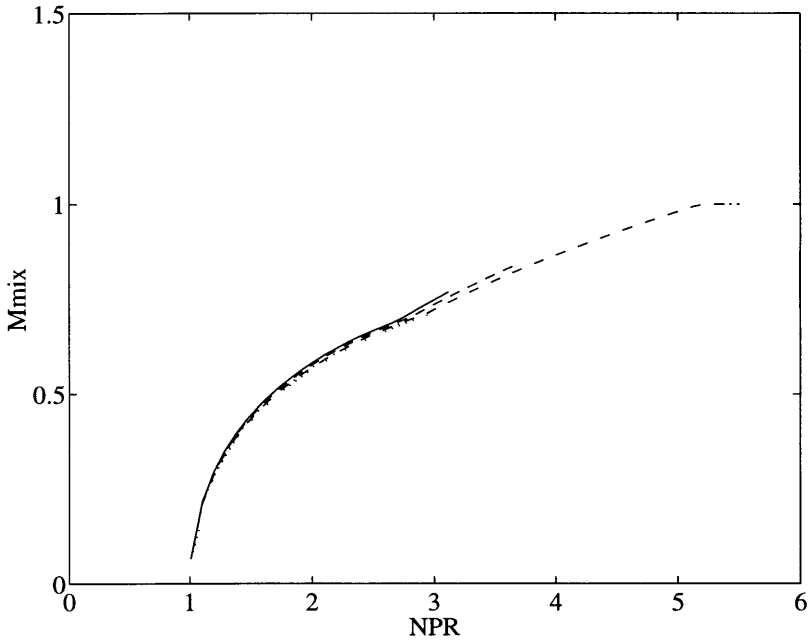

Figure 2-8: Mixed out exit Mach numbers as calculated from compressible control volume analysis, SNPR=1.0, Mp=supersonic, $\frac{A_s}{A_p} = 3.0$; —— $\frac{T_{t,p}}{T_{t,s}} = 1.0$; – – – – $\frac{T_{t,p}}{T_{t,s}} = 2.0$; – · – · $\frac{T_{t,p}}{T_{t,s}} = 3.0$; · · · · $\frac{T_{t,p}}{T_{t,s}} = 4.0$

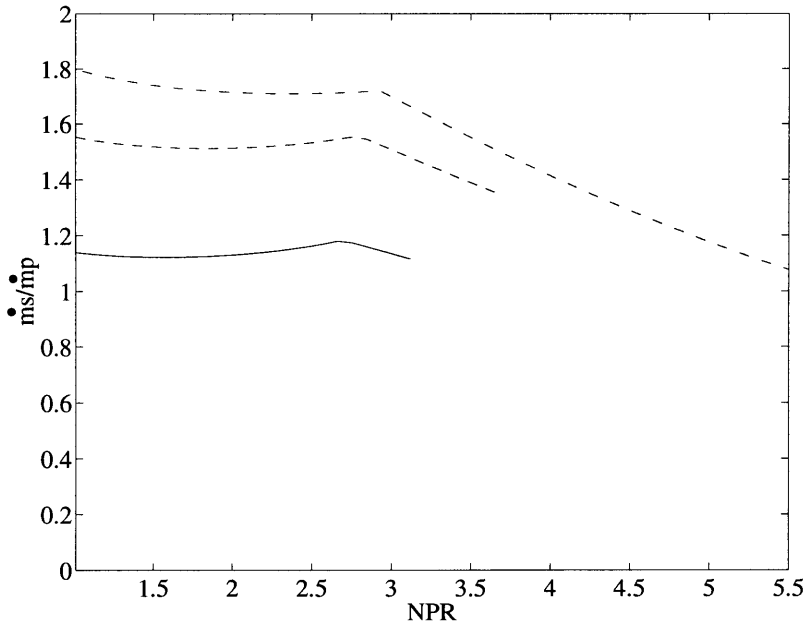

Figure 2-9: Mass flow ratios for flows with non-uniform stagnation temperature profiles as calculated from compressible, SNPR=1.0, Mp=supersonic, $\frac{A_s}{A_p} = 3.0$; —— $T_{t,p}/T_{t,s} = 1.0$, $- - -T_{t,p}/T_{t,s} = 2.0$, $- \cdot -T_{t,p}/T_{t,s} = 3.0$

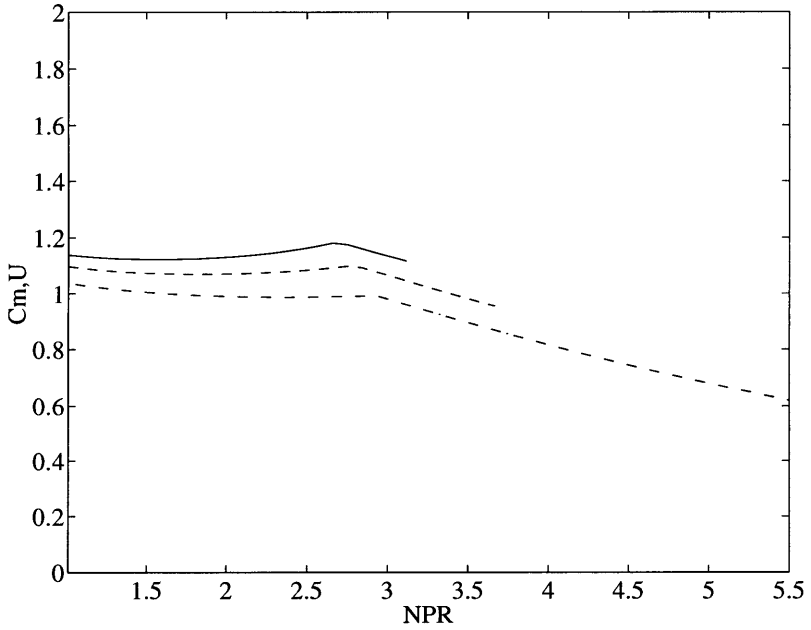

Figure 2-10: Corrected mass flow ratios for flows with non-uniform stagnation temperature profiles as calculated from compressible, SNPR=1.0, Mp=supersonic, $\frac{A_s}{A_p} = 3.0$; —— $T_{t,p}/T_{t,s} = 1.0$, $- - -T_{t,p}/T_{t,s} = 2.0$, $- \cdot -T_{t,p}/T_{t,s} = 3.0$

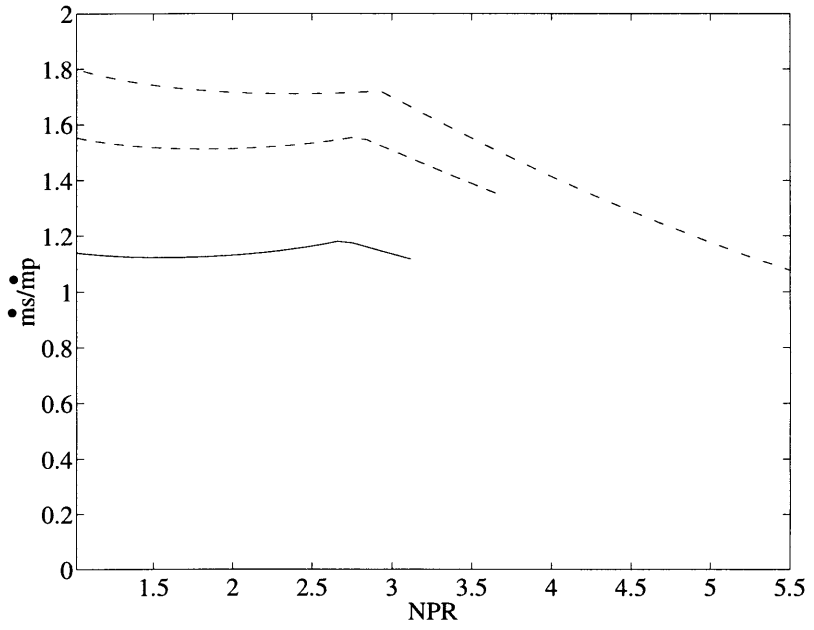

Figure 2-11: Mass flow ratios for flows with non-uniform molecular weight profiles as calculated from compressible, SNPR=1.0, Mp=supersonic, $\frac{A_s}{A_p} = 3.0$; —— $R_p/R_s = 1.0$, $- - -R_p/R_s = 2.0$, $- \cdot -R_p/R_s = 3.0$

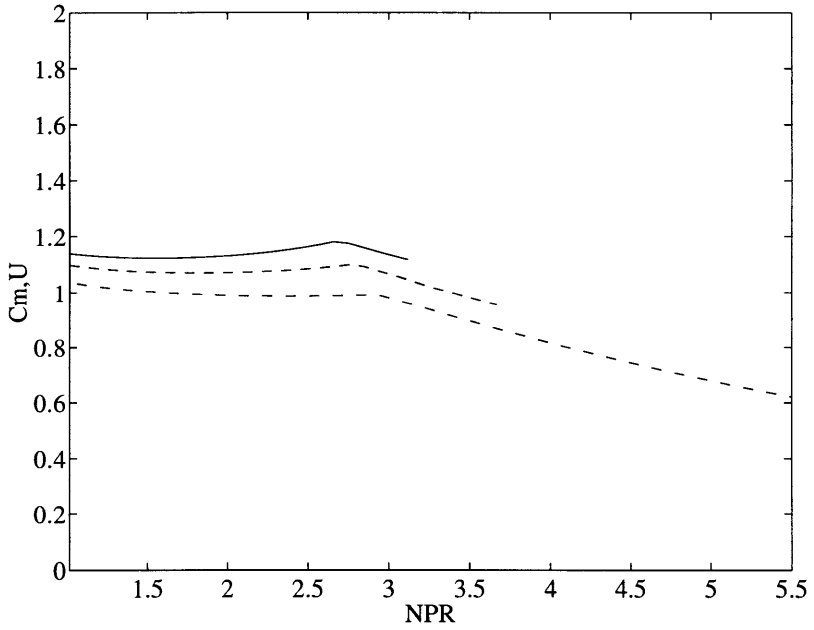

Figure 2-12: Corrected mass flow ratios for flows with non-uniform molecular weight profiles as calculated from compressible, SNPR=1.0, Mp=supersonic, $\frac{A_s}{A_p} = 3.0$; —— $R_p/R_s = 1.0$, $- - -R_p/R_s = 2.0$, $- \cdot -R_p/R_s = 3.0$

In all of the previous derivations, the ratio of specific heats was assumed to stay constant as the molecular weights and stagnation temperatures were varied. Results

in Figures 2-13, 2-14, and 2-15 justify this assumption. In these figures the exit stagnation pressures, and Mach numbers are plotted against NPR. Three combinations of stagnation temperature ratio and ratio of specific heats are presented. The values chosen for the ratios of specific heats represent values estimated at ambient conditions and at engine operating conditions. Changing in the hot case ratio of specific heats from 1.4 to 1.33 resulted in essentially the same exit stagnation pressures and exit Mach numbers. This translates into changes of the uncorrected mass flows that can be neglected(Figure 2-15).

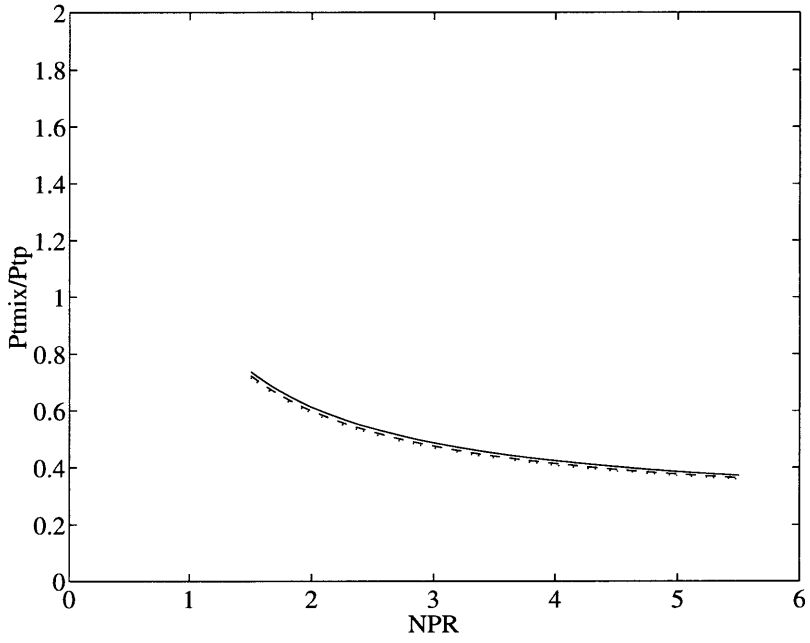

(a) Stagnation pressure curves

Figure 2-13: Effects of varying both the stagnation temperature ratio and the primary ratio of specific heats on exit stagnaiton pressure, SNPR=1.0, Mp=supersonic, $\frac{A_s}{A_p} = 3.0$; —— $\frac{T_{t,p}}{T_{t,s}} = 1.0, \gamma_p = 1.4$; $- - -\frac{T_{t,p}}{T_{t,s}} = 4.0, \gamma_p = 1.4$; $\cdots \frac{T_{t,p}}{T_{t,s}} = 4.0, \gamma_p = 1.33$

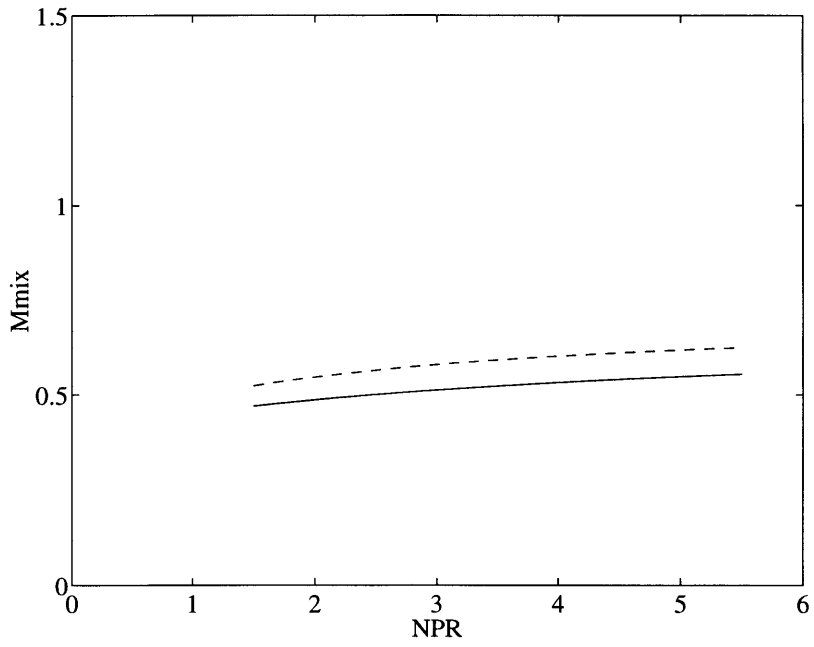

Figure 2-14: Effects of varying both the stagnation temperature ratio and the primary ratio of specific heats on exit Mach number, SNPR=1.0, Mp=supersonic, $\frac{A_s}{A_p} = 3.0$;—— $\frac{T_{t,p}}{T_{t,s}} = 1.0, \gamma_p = 1.4$; $- - -\frac{T_{t,p}}{T_{t,s}} = 4.0, \gamma_p = 1.4$; $\cdots \frac{T_{t,p}}{T_{t,s}} = 4.0, \gamma_p = 1.33$

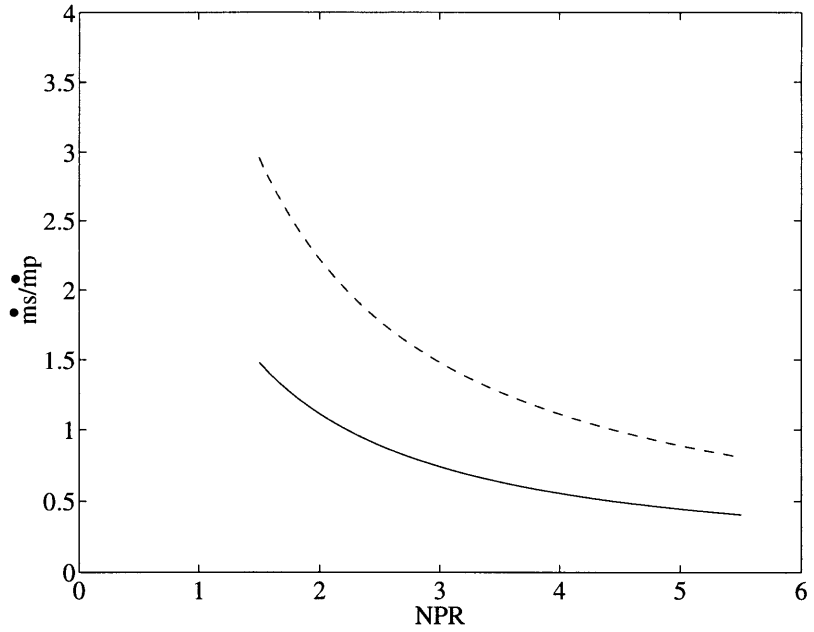

Figure 2-15: Effects of varying both the stagnation temperature ratio and the primary ratio of specific heats on mass flow, SNPR=1.0, Mp=supersonic, $\frac{A_s}{A_p} = 3.0$; —— $\frac{T_{t,p}}{T_{t,s}} = 1.0, \gamma_p = 1.4$; $- - -\frac{T_{t,p}}{T_{t,s}} = 4.0, \gamma_p = 1.4$; $\cdots \frac{T_{t,p}}{T_{t,s}} = 4.0, \gamma_p = 1.33$

2.4 Summary

The approximate similarity principle has been extended to flows of different gas compositions (i.e. different molecular weights). A similarity parameter that combined the effects of heat transfer and molecular weight change was introduced. It was shown that incompressible mixing flows with the same values of similarity parameter ratio undergo the same changes in stagnation pressure and Mach number. This occurs regardless of the combination of stagnation temperature ratio and molecular weight ratio used to achieve the similarity parameter ratio. It was demonstrated that heat transfer and molecular weight change counteract the effect of viscous forces on stagnation pressure in the high Mach number flow regimes associated with supersonic mixer-ejector. Finally, it was demonstrated that supersonic mixer-ejector performance (i.e. mass flow ratios) could be scaled with temperature and thus aerodynamic performance can be deduced from results obtained at room temperature.

Chapter 3

Applicability of the Approximate Similarity Principle to Supersonic Mixer Ejectors

3.1 Introduction

Data from the Boeing Single Lobe Tests, the Gen 1.5 Parametric Tests, and the tests of Gen 1.5 mixers at the NATR facility will now be examined in light of the approximate similarity principle. First, results from supersonic mixer-ejector tests will be examined for stagnation pressure and Mach number similarity. These tests were performed at stagnation temperatures ranging from 1.0 to 3.0. It will be shown that stagnation pressure and Mach number profiles measured at the exit of a supersonic mixer-ejector are similar regardless of the stagnation temperatures of the primary and entrained flows. It will also be shown that the aerodynamic performance of HSCT mixer-ejectors can be scaled with stagnation temperature. Second, results from experiments that involve the mixing of different gases will be employed to demonstrate the applicability of the similarity principle to the mixing of flows of different composition.

3.2 HSCT Test Results

A number of tests of supersonic mixer-ejectors [2, 8, 13] have been performed at engine operating conditions and at room temperature with the same geometries. The stagnation temperature and stagnation pressure of the primary flow could be varied. The primary flow was bounded on two sides by secondary flows of constant stagnation temperauture. The stagnation pressure of the secondary flow could be varied. Except for the Boeing Single Lobe tests which used a simple convergent-divergent nozzle, all of the tests used a lobed mixer of either a convoluted plate or forced mixer type to enhance mixing. Descriptions of the HSCT tests presented within this work can be found in Appendix B.

3.2.1 Stagnation Pressure and Mach Number Similarity in Supersonic Mixer-Ejectors

The measurements from the tests performed at the NATR Facility [13] at the Lewis Research Center will be used to assess if the stagnation pressure and Mach number similarity. Tests performed at NPR=3.4 are presented here for consideration. Stagnation pressure and stagnation temperature rakes were located at the exit of the mixing duct. These rakes were translated across the exit plane and measurements were taken at .25 inch intervals. From these surveys, two rake positions were chosen for investigation. Figures 3-1 and 3-2 show these positions relative to the mixer geometries. The first position corresponds to the center of a primary lobe while the second corresponds to the center of a secondary lobe.

The geometries of the two mixers were different. The first difference is that one is a forced mixer while the other is a convoluted plate. The second difference is that the upper and lower secondary lobes of the convoluted plate mixer are not separated by primary flow while they are in the forced mixer. This explains why the convoluted plate mixer produces two crested profiles and the forced mixer produces three crested profiles (see Figures 3-3 through 3-8).

Stagnation temperature, stagnation pressure, and Mach number distributions for

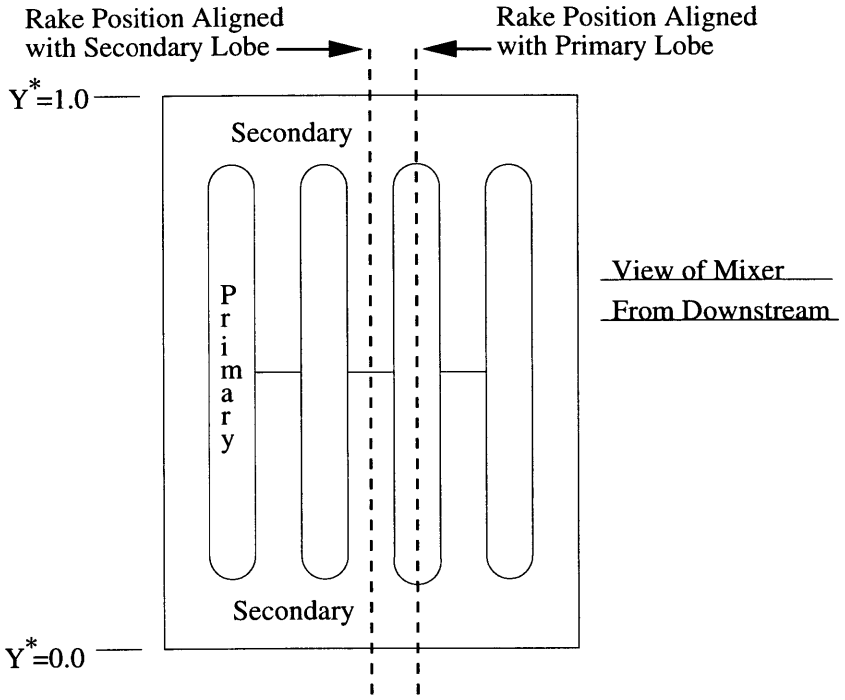

Figure 3-1: Exit condition profile locations for the Gen 1.5 convoluted plate (axial) mixer.

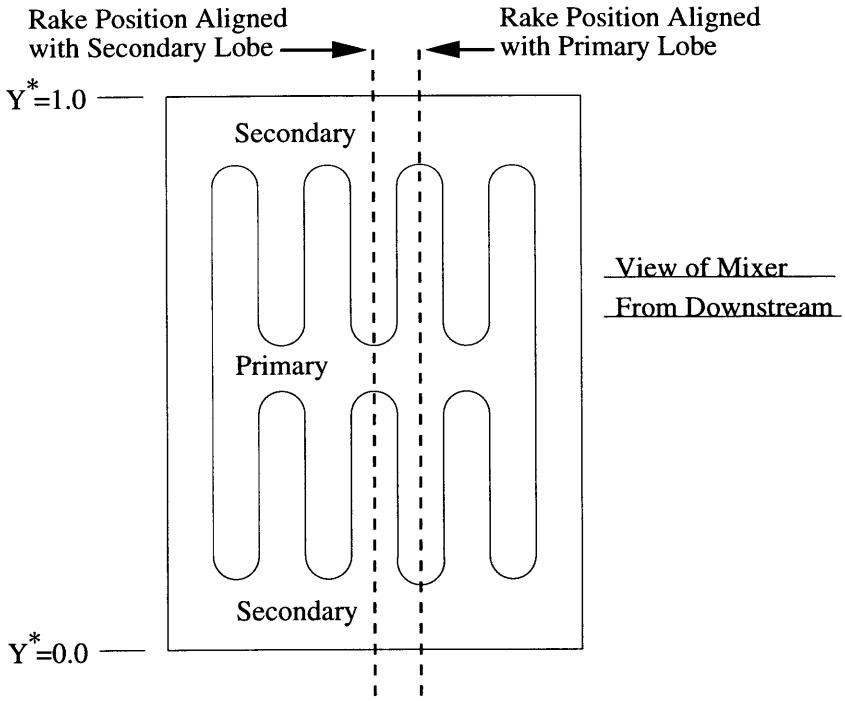

Figure 3-2: Exit condition profile locations for the Gen 1.5 forced (vortical) mixer.

tests of the convoluted plate and the forced mixer are given in Figures 3-3 through 3-8. Results are plotted for three initial primary to secondary stream stagnation temperature ratios, $T_{t,p}/T_{t,s} = 1.0$, 2.0, and 3.0.

Profiles of the exit stagnation temperature normalized by the ambient stagnation temperature for the convoluted plate are shown in figure 3-3. Profiles for $T_{t,p}/T_{t,s} = 2.0$ and $T_{t,p}/T_{t,s} = 3.0$ indicate that significant mixing has taken place. The peak values of the temperature profiles are much less at the mixing duct inlet (refer to Figure 1-1 for definitions of the dicussed locations).

Figure 3-4 shows the profiles of the exit stagnation pressure normalized by the stagnation pressure of the primary stream. The profiles of the nonhomenthalpic cases ($T_{t,p}/T_{t,s} \neq 1.0$) are similar to the homenthalpic case ($T_{t,p}/T_{t,s} = 1.0$). The exit Mach number profiles are given in Figure 3-5. These profiles also exhibit similarity between the homenthalpic case and the nonhomenthalpic cases. The profiles aligned with the primary lobe and those aligned with the secondary lobe show the same trends. These trends were also observed in the the profiles for the forced mixer. *This is the first time that stagnation pressure and Mach number similarity has been observed in supersonic mixing flows.*

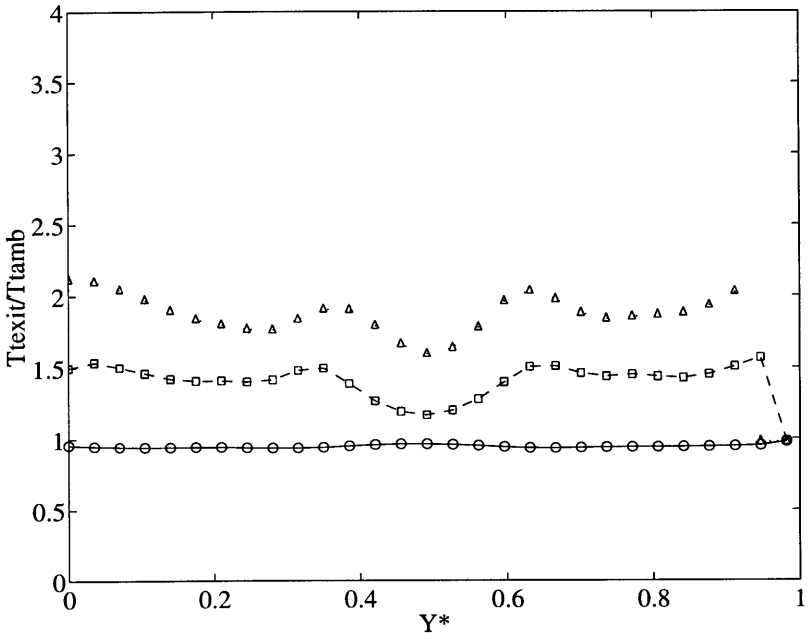

(a) Aligned with primary lobe

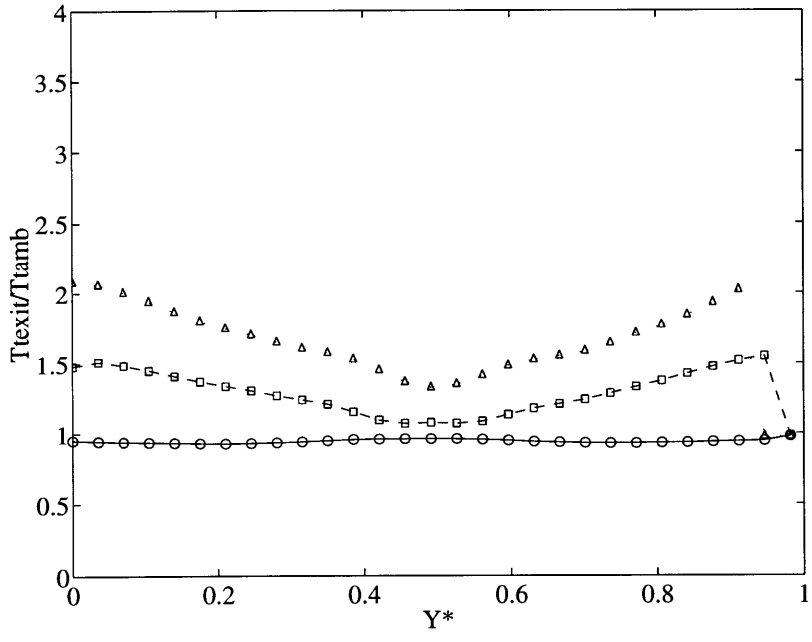

(b) Aligned with secondary lobe

Figure 3-3: Shroud exit stagnation temperature profiles from Gen 1.5 convoluted plate at NPR=3.4. ○ $\frac{T_{t,p}}{T_{t,s}} = 1.0$; □ $\frac{T_{t,p}}{T_{t,s}} = 2.0$; Δ $\frac{T_{t,p}}{T_{t,s}} = 3.0$

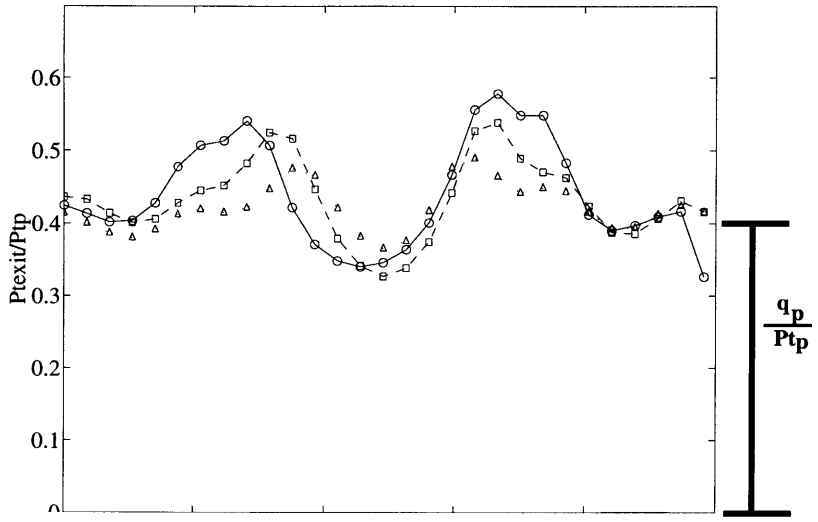

(a) Aligned with primary lobe

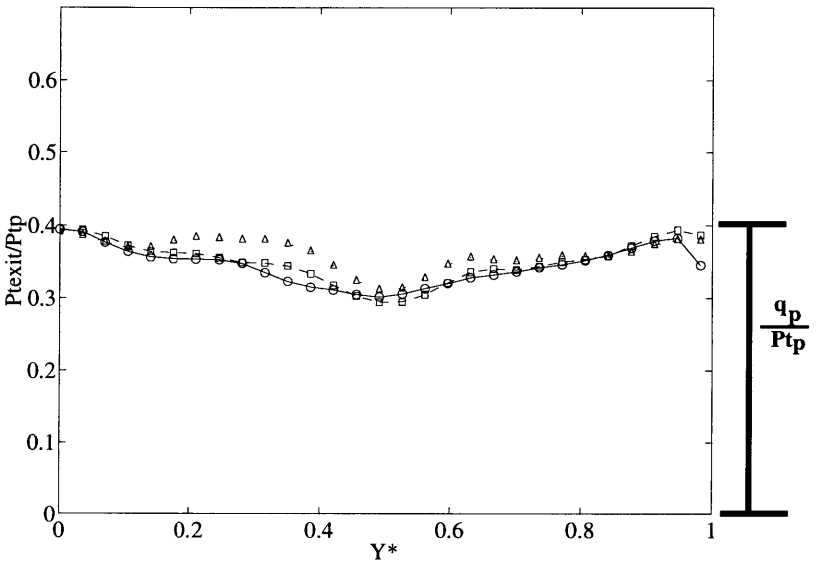

(b) Aligned with secondary lobe

Figure 3-4: Shroud exit stagnation pressure profiles from Gen 1.5 convoluted plate at NPR=3.4. $\bigcirc \frac{T_{t,p}}{T_{t,s}} = 1.0$; $\square \frac{T_{t,p}}{T_{t,s}} = 2.0$; $\triangle \frac{T_{t,p}}{T_{t,s}} = 3.0$

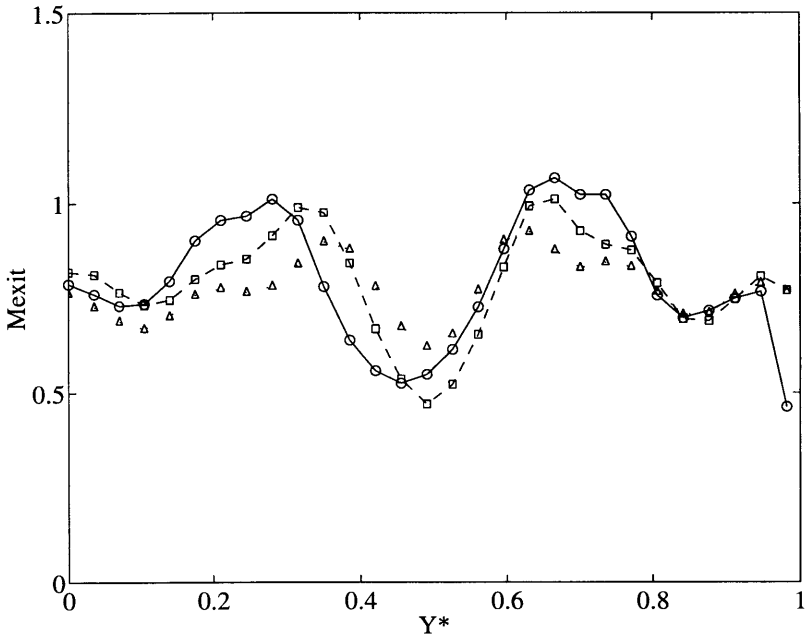

(a) Aligned with primary lobe

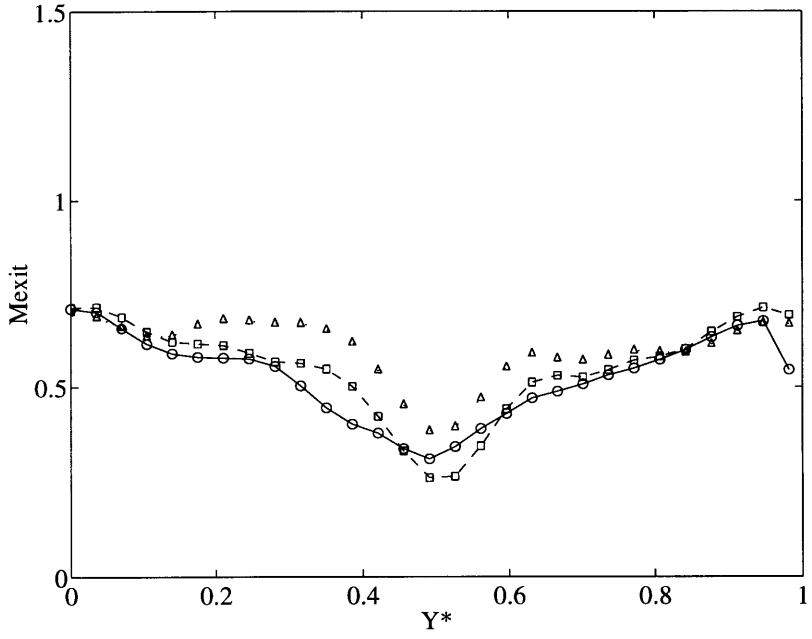

(b) Aligned with secondary lobe

Figure 3-5: Shroud exit Mach number profiles from Gen 1.5 convoluted plate at NPR=3.4. ○ $\frac{T_{t,p}}{T_{t,s}} = 1.0$; □ $\frac{T_{t,p}}{T_{t,s}} = 2.0$; △ $\frac{T_{t,p}}{T_{t,s}} = 3.0$

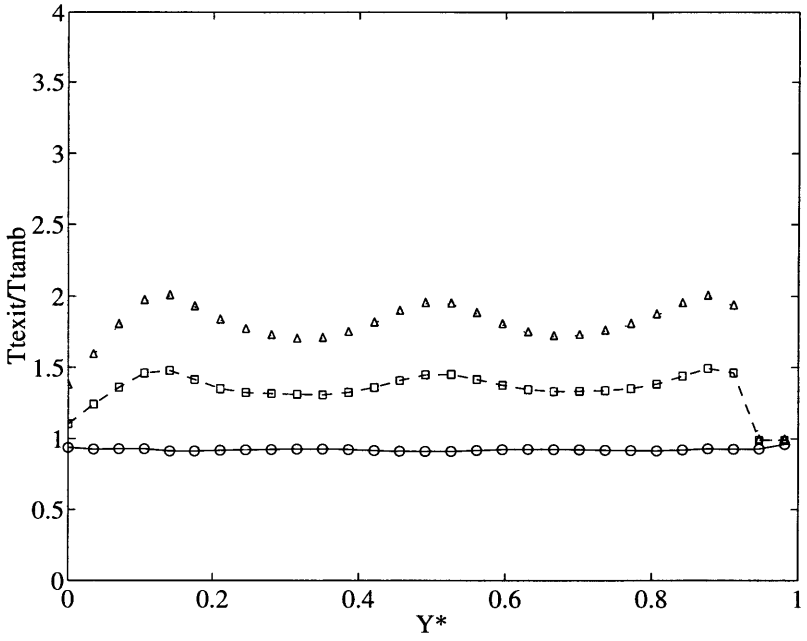

(a) Aligned with primary lobe

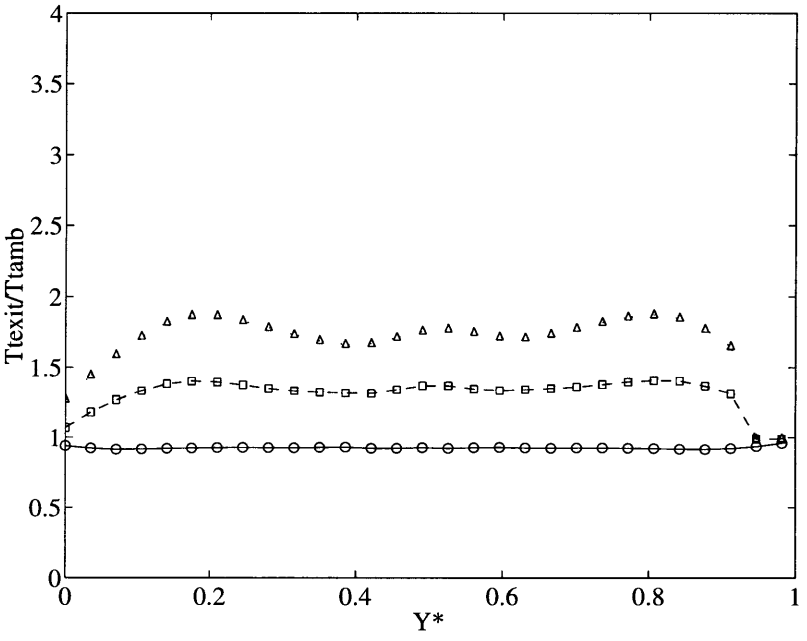

(b) Aligned with secondary lobe

Figure 3-6: Shroud exit stagnation temperature profiles from Gen 1.5 forced mixer at NPR=3.4. $\bigcirc \frac{T_{t,p}}{T_{t,s}} = 1.0$; $\square \frac{T_{t,p}}{T_{t,s}} = 2.0$; $\Delta \frac{T_{t,p}}{T_{t,s}} = 3.0$

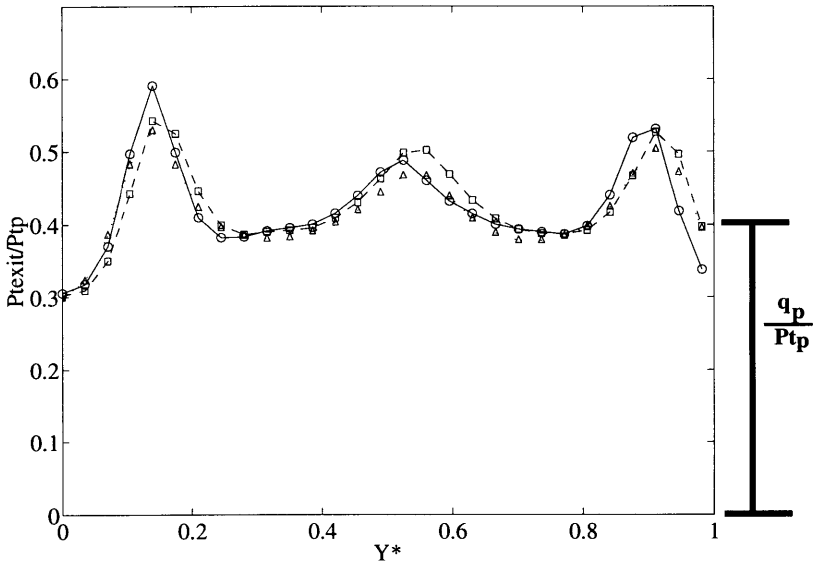

(a) Aligned with primary lobe

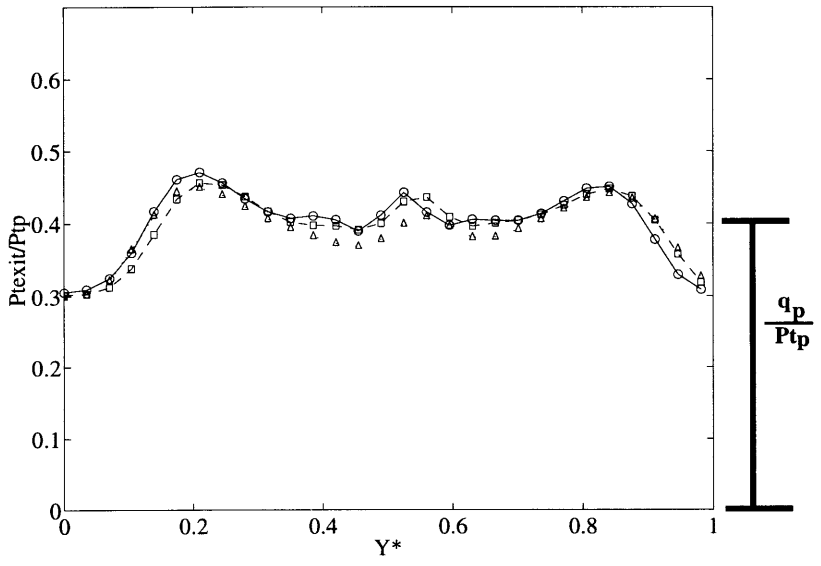

(b) Aligned with secondary lobe

Figure 3-7: Shroud exit stagnation pressure profiles from Gen 1.5 forced mixer at NPR=3.4. $\bigcirc \frac{T_{t,p}}{T_{t,s}} = 1.0$; $\square \frac{T_{t,p}}{T_{t,s}} = 2.0$; $\triangle \frac{T_{t,p}}{T_{t,s}} = 3.0$

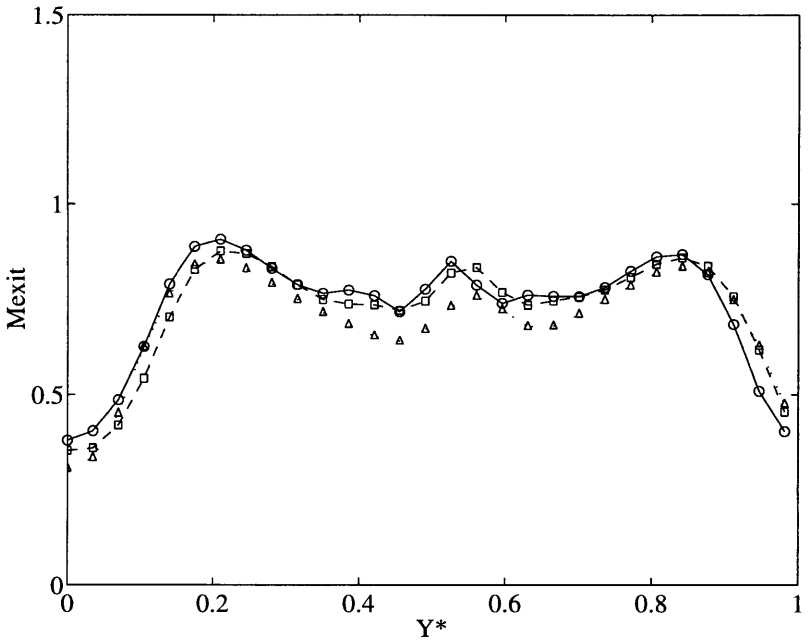

(a) Aligned with primary lobe

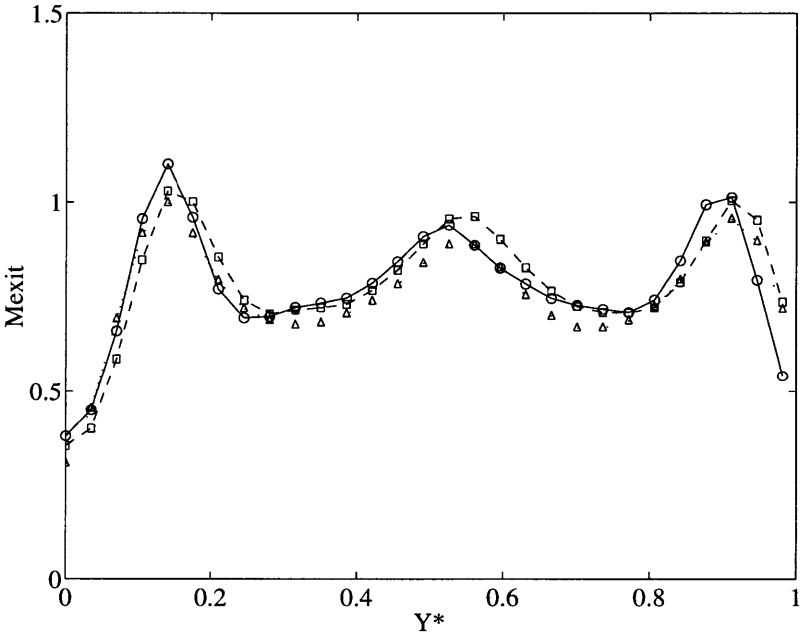

(b) Aligned with secondary lobe

Figure 3-8: Shroud exit Mach number profiles from Gen 1.5 forced mixer at NPR=3.4. ○ $\frac{T_{t,p}}{T_{t,s}} = 1.0$; □ $\frac{T_{t,p}}{T_{t,s}} = 2.0$; △ $\frac{T_{t,p}}{T_{t,s}} = 3.0$

3.2.2 Application of the Approximate Similarity Principle to HSCT Mixer-Ejector Aerodynamic Performance

The performance parameters considered are corrected mass flow ratio and gross thrust coefficient. The data presented here has been normalized in a manner that conforms to agreements between the author and the members of the HSCT Program. For the Boeing Single Lobe Tests, multiple runs were made at each test condition while in the Gen 1.5 Tests only one set of measurements were taken at each condition. In both tests, the stagnation temperature ratios between the streams was varied from 1 to greater than 2.5. The primary Mach numbers were supersonic (M_p =1.1 to 2.0) while the secondary Mach numbers were approximately 0.4 to 0.6. At these Mach numbers, the primary to secondary stream velocity ratio is approximately 2.0 for stagnation temperature ratios of 1.0 and 5.3 for stagnation temperature ratios of 2.5. With these temperature and velocity ratios, substantial heat transfer and momentum exchange is expected.

Figures 3-9 and 3-11 show that the mass flows are dependent on the temperature ratio. Correcting the mass flow ratios using the similarity parameter results in essentially a single curve (Figures 3-10 and 3-12). Scaling of the $T_{t,p}/T_{t,s} = 1.0$ case over predicts corrected mass flow ratios of the highest $T_{t,p}/T_{t,s}$ case by 16.2% to 10.5% for the Boeing Single Lobe Tests and 28.0% to 10.0% for the Gen 1.5 Tests. These errors can be split into two parts, random and systematic. The random error is observed in the spread of data points produced by identical conditions (see Figure 3-9). The random error is due to the limitations of the experimental insturmentation. The systematic error which scales with $\sqrt{T_{t,p}/T_{t,s}}+1/\sqrt{T_{t,s}/T_{t,p}}$ will be discussed in the next section. As in Chapter 2, differences between hot and cold quantities are presented as percentages of the hot quantity as it is the variable of interest in that flow situation.

The maximum error was 28.0% but for majority of the cases examined the errors are 10.0% or less. Without further reduction, the error in the scalings are too large for cold tests to replace hot testing entirely, but it can be used to determine trends. Hot tests would then be needed only for the assessment of final design concepts.

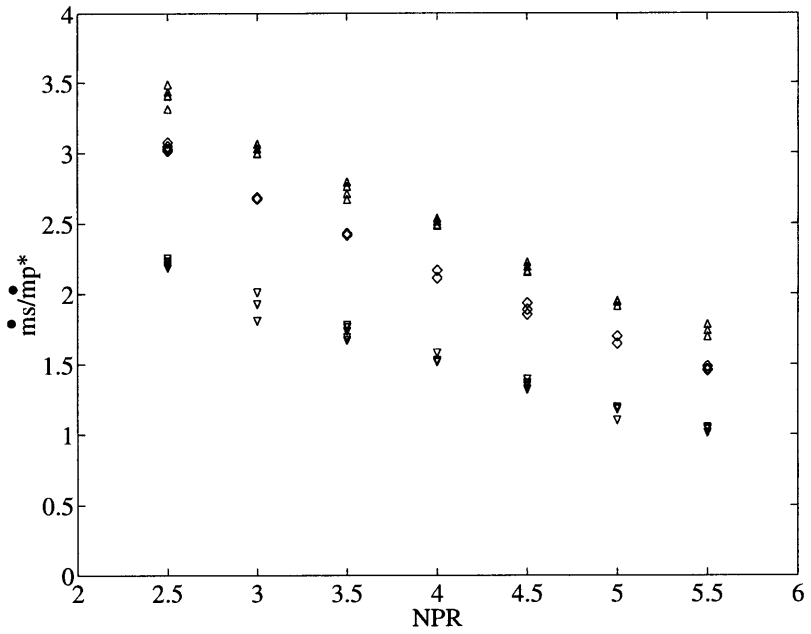

Figure 3-9: Mass flow ratios from Boeing Single Lobe Tests. $\nabla \frac{T_{t,p}}{T_{t,s}} = 1.0$; $\Diamond \frac{T_{t,p}}{T_{t,s}} = 2.4$; $\Delta \frac{T_{t,p}}{T_{t,s}} = 2.8$

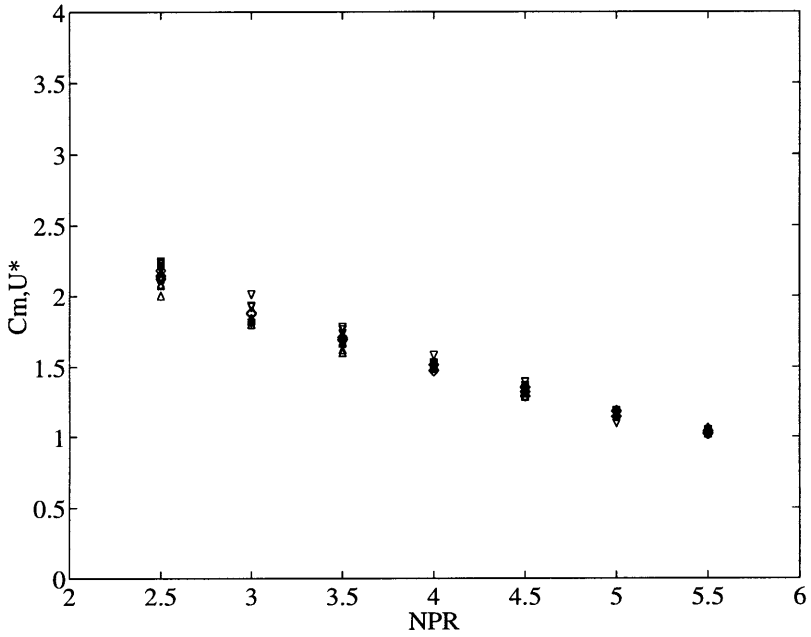

Figure 3-10: Corrected mass flow ratios from Boeing Single Lobe Tests. $\nabla \frac{T_{t,p}}{T_{t,s}} = 1.0$; $\Diamond \frac{T_{t,p}}{T_{t,s}} = 2.4$; $\Delta \frac{T_{t,p}}{T_{t,s}} = 2.8$

The gross thrust coefficients from the Boeing Single Lobe Tests and the Gen 1.5 Tests are given in Figures 3-13 and 3-14 respectively. The gross thrust coefficient

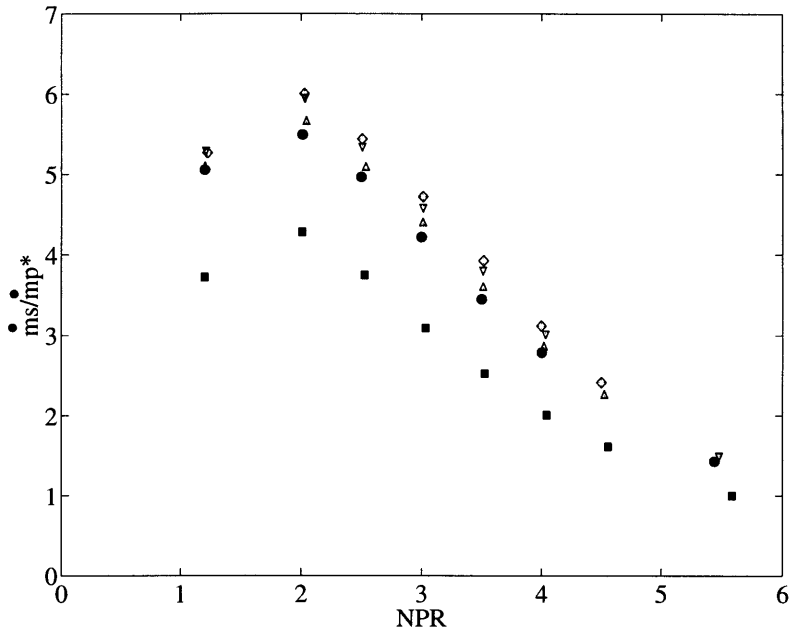

Figure 3-11: Mass flow ratios from Gen 1.5 Tests. ■ $\frac{T_{t,p}}{T_{t,s}} = 1.0$; • $\frac{T_{t,p}}{T_{t,s}} = 1.75$; ▲ $\frac{T_{t,p}}{T_{t,s}} = 2.1$; ▼ $\frac{T_{t,p}}{T_{t,s}} = 2.3$; ♦ $\frac{T_{t,p}}{T_{t,s}} = 2.6$

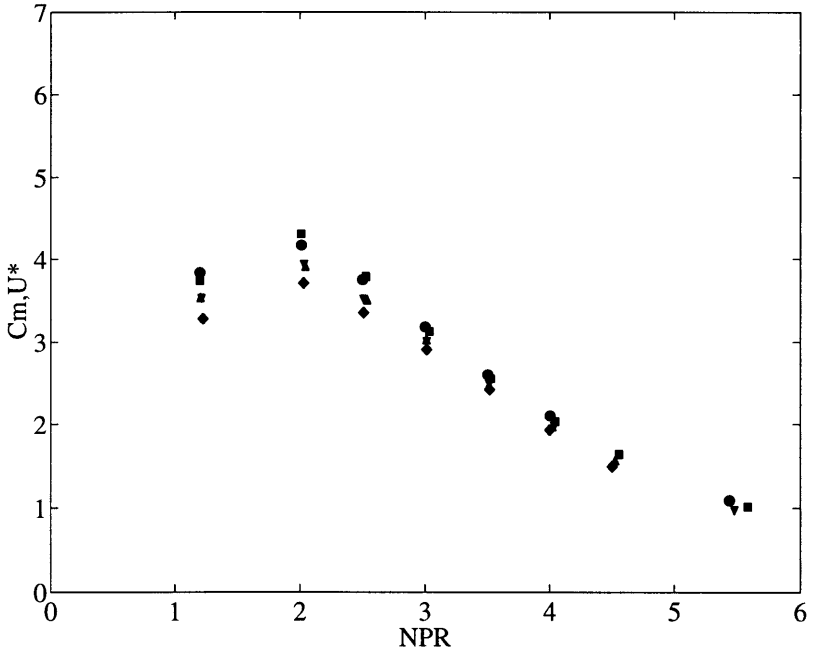

Figure 3-12: Corrected mass flow ratios from Gen 1.5 Tests. ■ $\frac{T_{t,p}}{T_{t,s}} = 1.0$; • $\frac{T_{t,p}}{T_{t,s}} = 1.75$; ▲ $\frac{T_{t,p}}{T_{t,s}} = 2.1$; ▼ $\frac{T_{t,p}}{T_{t,s}} = 2.3$; ♦ $\frac{T_{t,p}}{T_{t,s}} = 2.6$

exhibits little dependence on the stagnation temperature ratio. This behavior is expected because if the stagnation pressure and Mach numbers are similar the static pressures which determine the thrust must also be similar. In the Boeing Single Lobe Tests and the Gen 1.5 Tests, scaling of the homenthalpic (cold flow) case overpredicts the $T_{t,p}/T_{t,s} = 2.6$ case by 1.0% to 10.0%. For the majority of cases, the scaling overpredicts the nonhomenthalpic thrust performance by less than 5.0%. As with the corrected mass flow ratios, a portion of this error is systematic and scales with $\sqrt{T_{t,p}/T_{t,s}} + 1/\sqrt{T_{t,s}/T_{t,p}}$. In the next section, it will be shown that the error in the scaling can be reduced to less than 1.0% by accounting for this systematic error.

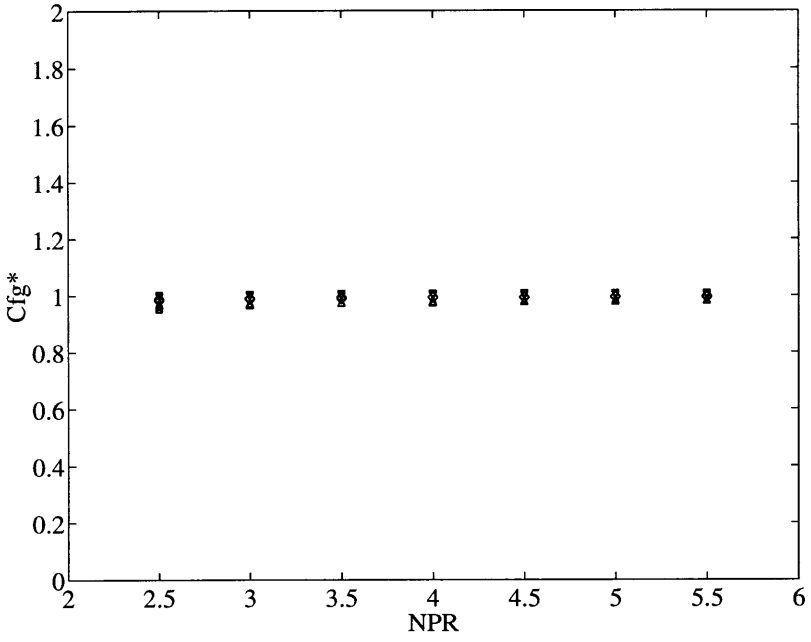

Figure 3-13: Gross thrust coefficients from Boeing Single Lobe Tests. $\nabla \frac{T_{t,p}}{T_{t,s}} = 1.0$; $\Diamond \frac{T_{t,p}}{T_{t,s}} = 2.4$; $\Delta \frac{T_{t,p}}{T_{t,s}} = 2.8$

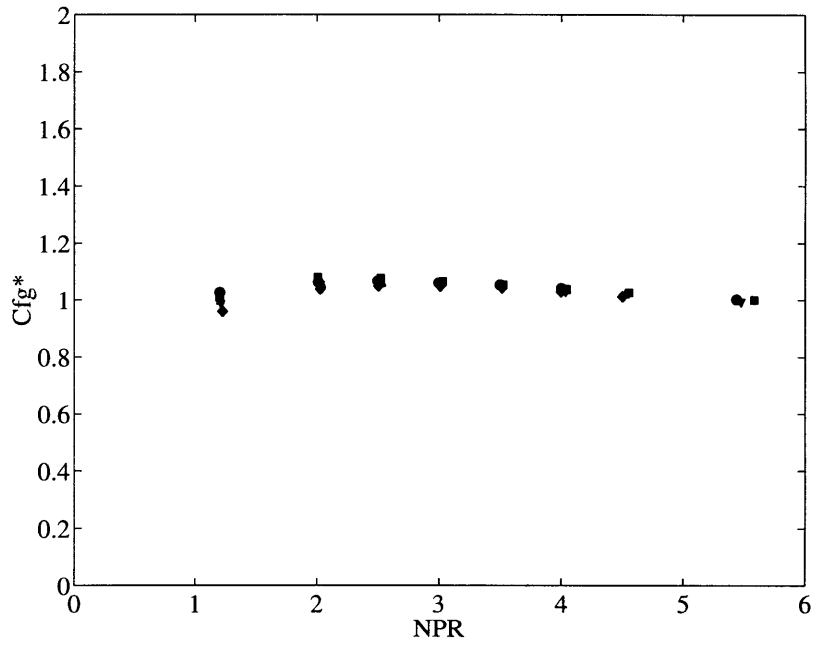

Figure 3-14: Gross thrust coefficients from Gen 1.5 Tests. ■ $\frac{T_{t,p}}{T_{t,s}} = 1.0$; • $\frac{T_{t,p}}{T_{t,s}} = 1.75$; ▲ $\frac{T_{t,p}}{T_{t,s}} = 2.1$; ▼ $\frac{T_{t,p}}{T_{t,s}} = 2.3$; ♦ $\frac{T_{t,p}}{T_{t,s}} = 2.6$

3.2.3 Identification of Systematic Error in Aerodynamic Performance Temperature Scaling

In Section 3.2.2, it was stated that cold tests generally overpredicted the values of hot test corrected mass flow ratio and gross thrust coefficient. This trend was also revealed in the results obtained from the incompressible and compressible control volumes (see Sections 2.2.2 and 2.3.2). Together, these results suggest that a portion of the error between the cold and hot test performance parameters is systematic and can be corrected for. This systematic difference between the perfomance parameters at different stagnation temperatures will be called the scaling error. Identification of this systematic error will be accomplished through the use of the incompressible control volume, the compressible control volume, and the data from the Boeing Single Lobe Tests.

To identify the systematic error, we examine the results from the incompressible control volume. The solution for $\sqrt{\frac{\rho_p}{\rho_s}}\left(\frac{\dot{m}_s}{\dot{m}_p}\right)$ comes from the following quadratic

equation.

$$\frac{\rho_s}{\rho_p}\left(\frac{\dot{m}_s}{\dot{m}_p}\right)^2\left[\left(\frac{A_p}{A_s}\right)^2+\left(\frac{A_2}{A_3}\right)^2\right]+\sqrt{\frac{\rho_p}{\rho_s}}\left(\frac{\dot{m}_s}{\dot{m}_p}\right)\left[1+\left(\frac{A_2}{A_3}\right)^2\right]\left[\sqrt{\frac{T_{t,p}}{T_{t,s}}}+\sqrt{\frac{T_{t,s}}{T_{t,p}}}\right]$$
$$+\left[\left(\frac{A_2}{A_3}\right)^2-1-2\left(\frac{A_s}{A_p}\right)\right]=0 \quad (3.1)$$

Only the coefficient associated with the first order term contains parameters that are not functions of the ejector geometry. Without the first order coefficient, the corrected mass flow would be independent of stagnation temperature ratio between the mixing streams. This suggests that the scaling error of the corrected mass flow ratios should scale with $\sqrt{T_{t,p}/T_{t,s}}+1/\sqrt{T_{t,s}/T_{t,p}}$. This quantity will be designated Θ. In Figure 3-15, the differences between cold case corrected mass flow ratios and hot case corrected mass flow ratios as calculated using the incompressible control volume analysis are plotted versus Θ.

In this figure, the value of Θ ranges from 2.0 to 2.5, corresponding to stagnation temperature ratios of 1.0 to 4.0. For all of the curves (which correspond to different area ratios) the scaling error relates to Θ linearly. Changing the geometry of the ejector has the effect of changing the slope of the error correlation, although the differences are small for the cases examined.

We will examine results from the compressible control volume and the HSCT mixer-ejector data for this relationship between the scaling error and Θ. Figure 3-16 shows the relationship between scaling error and Θ in the supersonic mixing regime for a geometry with $\frac{A_s}{A_p} = 3.0$. As in the incompressible regime, the scaling error is related linearly to Θ. The flow conditions correspond to those in HSCT representative supersonic mixer-ejectors, suggesting that this linear relationship between scaling error and Θ will also be present in the results from HSCT tests.

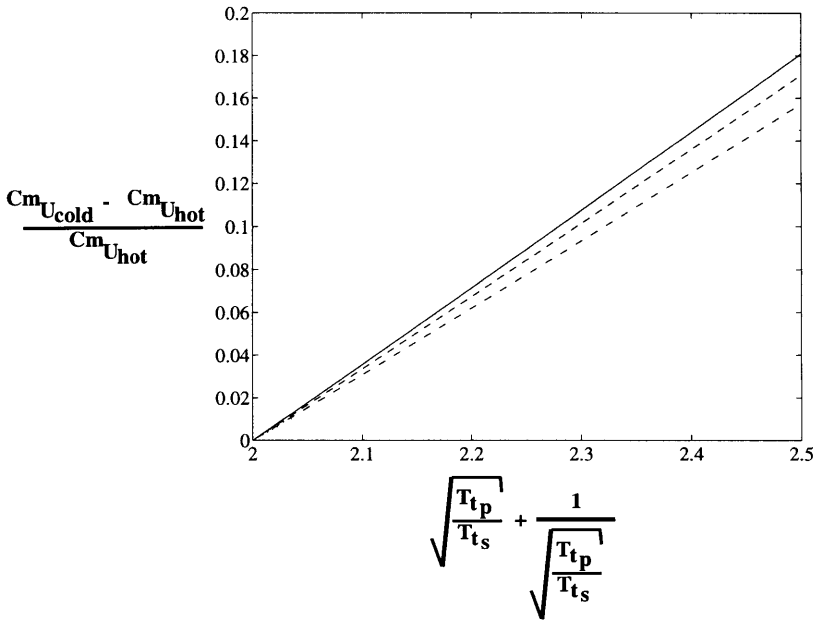

Figure 3-15: Prediction error versus $(\frac{T_{t,p}}{T_{t,s}} + 1/\frac{T_{t,p}}{T_{t,s}})$ calculated using the incompressible control volume, —— $\frac{A_s}{A_p} = 1.0$; – – – – $\frac{A_s}{A_p} = 2.0$; –·–·– $\frac{A_s}{A_p} = 3.0$; ···· $\frac{A_s}{A_p} = 4.0$.

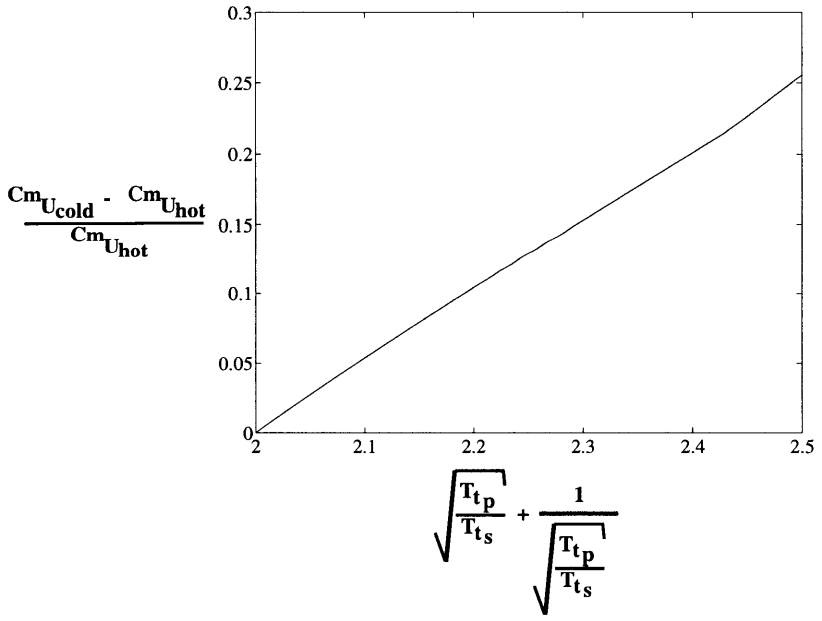

Figure 3-16: Prediction error versus $\frac{T_{t,p}}{T_{t,s}} + 1/\frac{T_{t,p}}{T_{t,s}}$ calculated with the compressible control volume.

In Figure 3-17, scaling errors of corrected mass flow ratio are presented for NPR's of 2.5 and 4.5. The straight lines are least squares fits to the two groups (i.e. NPR=2.5

and 4.5) of results. The data shows the same linear relationship between scaling error and Θ as was found in the analytical results. Changing the NPR changes the slope of the error correlation. The slope is reduced as the NPR is increased. This corresponds to the reduction of errors with NPR observed in results from both the Boeing Single Lobe Tests and the Gen 1.5 Tests.

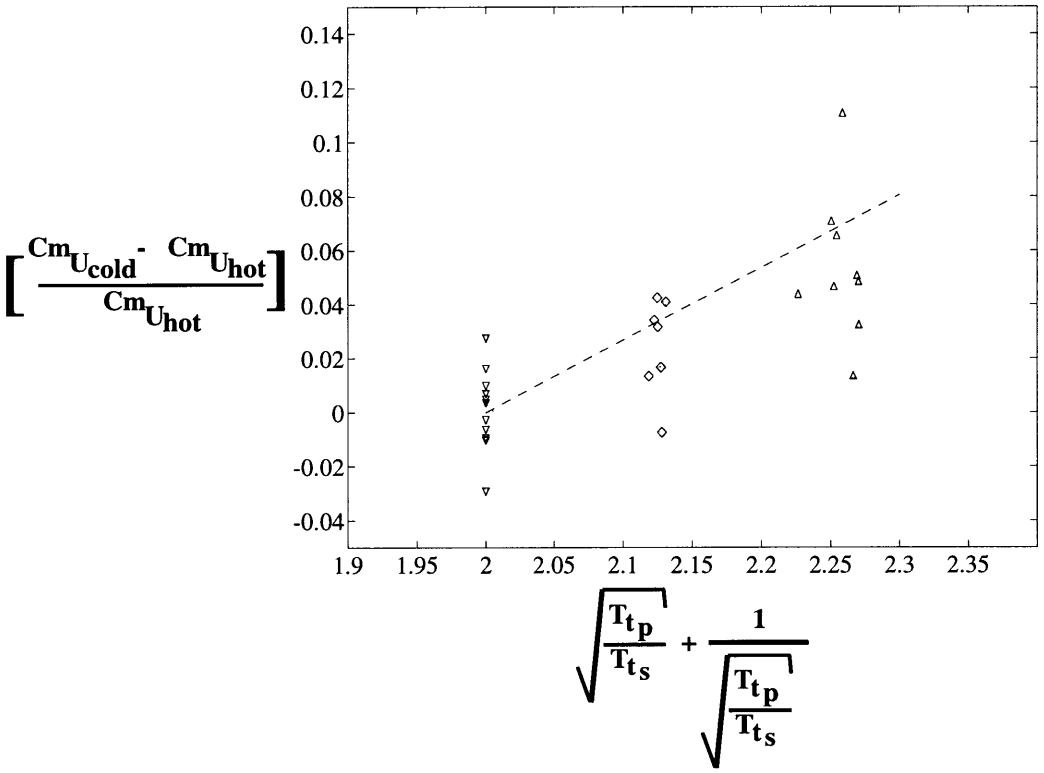

Figure 3-17: Differences between cold case corrected mass flow ratios and hot corrected mass flow ratio versus $\sqrt{\frac{T_{t,p}}{T_{t,s}}} + 1/\sqrt{\frac{T_{t,p}}{T_{t,s}}}$, $\nabla \frac{T_{t,p}}{T_{t,s}} = 1.0, NPR = 2.5$; $\Diamond \frac{T_{t,p}}{T_{t,s}} = 2.4, NPR = 2.5$; $\Delta \frac{T_{t,p}}{T_{t,s}} = 2.8, NPR = 2.5$; $\blacktriangledown \frac{T_{t,p}}{T_{t,s}} = 1.0, NPR = 4.5$; $\blacklozenge \frac{T_{t,p}}{T_{t,s}} = 2.4, NPR = 4.5$; $\blacktriangle \frac{T_{t,p}}{T_{t,s}} = 2.8, NPR = 4.5$; —— least squares fit to NPR=2.5; – – –– least squared fit to NPR=4.5 .

This information about the systematic error will now be used to further correct the data. The result of this correction on the NPR=2.5 data is presented in Figure 3-18. Only the random error associated with the test hardware and measurement insturmentation remains. From Figure 3-18, the random error of the test appears to be $\pm$ 2 to 3% of the hot test values.

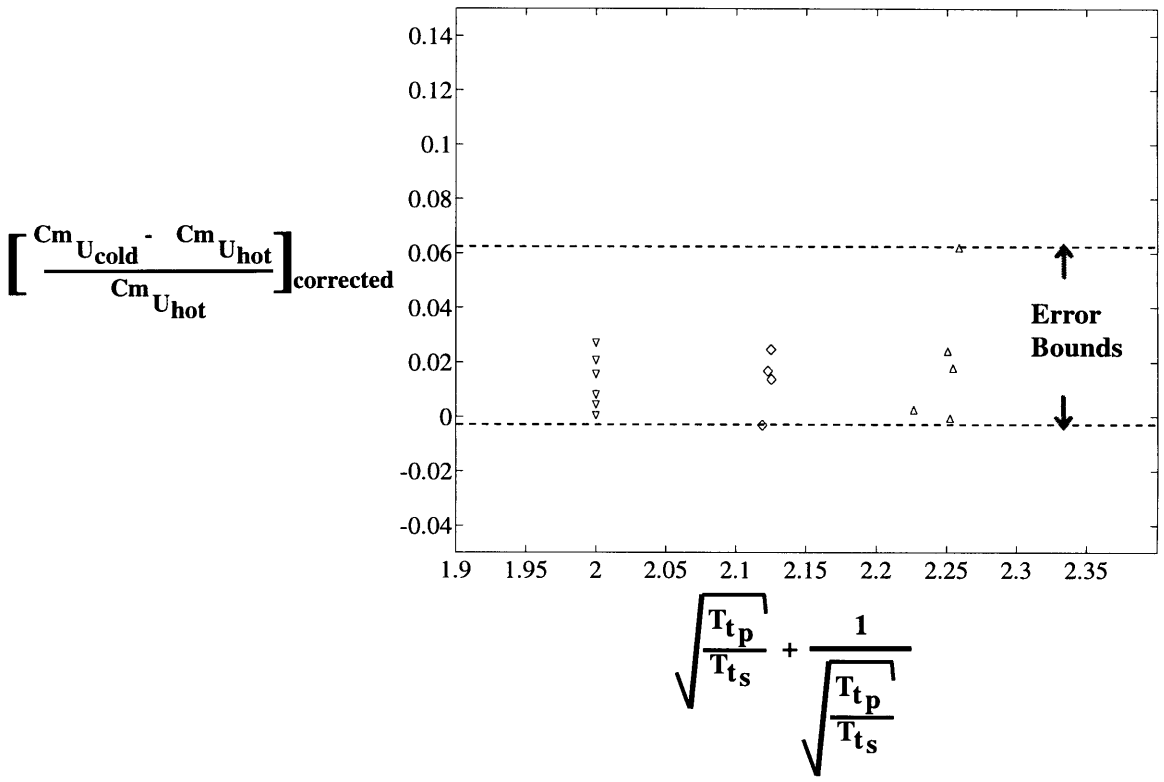

Figure 3-18: Differences between cold case corrected mass flow ratios and hot case corrected mass flow ratio versus $\frac{T_{t,p}}{T_{t,s}} + 1/\frac{T_{t,p}}{T_{t,s}}$ (corrected for systematic error), at NPR=2.5, $\nabla \frac{T_{t,p}}{T_{t,s}} = 1.0$; $\Diamond \frac{T_{t,p}}{T_{t,s}} = 2.4$; $\Delta \frac{T_{t,p}}{T_{t,s}} = 2.8$.

This correction can be reversed so that rather than reducing the hot case to its equivalent cold case value, room temperature test measurements can be used to predict hot case values. This assumes that the error correlation is known for the flow conditions that are being investigated. There are two ways in which the error correlation can be found without actually running a test at engine operating temperatures. The first method is to run a test at a temperature that is only slightly above ambient. A least squares fit can then be made to predict the error correlation. This method works because the relationship between scaling error and Θ is linear so only two points are required to define it. The other method is to use an accurate analytical model of the supersonic mixer-ejector flow. The Compound Flow Analysis currently being developed by Teeple [24] would be well suited to make this estimate. Thus, if the scaling error correlation is known, the hot case corrected mass flow can be predicted from cold case measurements with the an accuracy approaching that of

tests performed at engine operating temperatures.

Thus far, only the scaling error associated with the corrected mass flow ratio has been discussed. A systematic error is also present in the results for the gross thrust coefficient. Assuming low Mach numbers (i.e. $M^2 \ll 1$), the gross thrust coefficient can be expressed as [4]

$$Cfg = 1 + \left(\frac{M_s}{M_p}\right)\left[\left(\frac{\dot{m}_s}{\dot{m}_p}\right)\sqrt{\frac{T_{t,s}}{T_{t,p}}}\right] \tag{3.2}$$

This equation reveals that the gross thrust coefficient should have a scaling error similar to that of the corrected mass flow ratio. Figure 3-19 presents the error correlation for Boeing Single Lobe Tests performed at NPR's of 2.5 and 4.5. The values of Θ range from 2.0 to approximately 2.3. Unlike the scaling error for the corrected mass flow ratio this correlation is not a simple linear relationship. A second order polynomial was used in the least squares fit. Results from using the estimated scaling error to reduce the hot case values to their cold case equivalents are presented in Figure 3-20. The random error in the gross thrust coefficient measurements is 0.5 to 1.0 % of the hot case values.

Estimating the scaling error in the gross thrust coefficient is made difficult by the lack of a linear relationship between the scaling error and Θ. Therefore, a suitable method of determining the correlation for specific flow conditions would be an analytical model such as the Compound Flow Analysis [24]. This model has been shown to predict gross thrust coefficients for supersonic mixer-ejectors to within 1% to 2%. An accurate estimate would allow hot case values to be scaled from cold test measurements with the same accuracy as could be obtained from tests performed at engine operating temperatures.

A systematic use of the approximate similarity principle and the correlation for scaling error can be used to deduce hot test aerodynamic performance parameters from cold test results. The corrected mass flow ratios and the gross thrust coefficients determined through these methods can have the same accuracy as experimental results. This makes hot testing necessary only for the determination of acoustic per-

formance. The unsteady processes responsible for setting the acoustic performance of mixer-ejectors cannot be predicted through the use of the similarity principle.

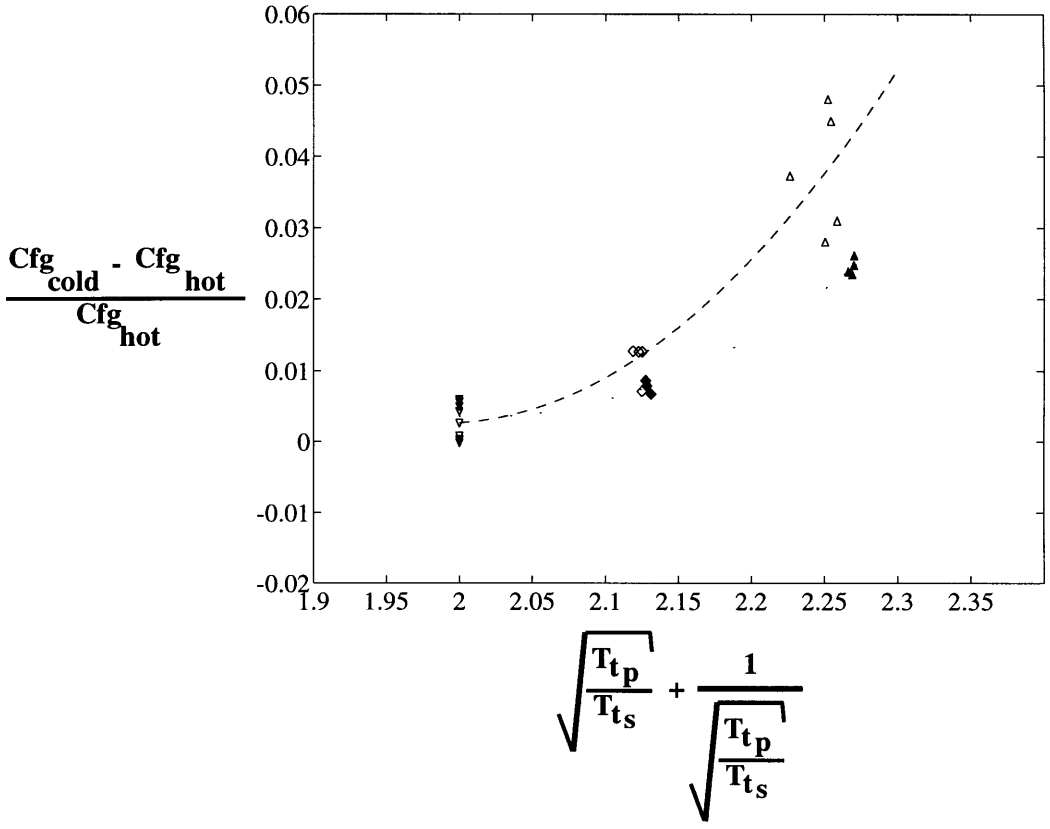

Figure 3-19: Differences between cold case gross thrust coefficient and hot case gross thrust coefficient versus $\frac{T_{t,p}}{T_{t,s}} + 1/\frac{T_{t,p}}{T_{t,s}}$, $\nabla \frac{T_{t,p}}{T_{t,s}} = 1.0, NPR = 2.5$; $\Diamond \frac{T_{t,p}}{T_{t,s}} = 2.4, NPR = 2.5$; Δ $\frac{T_{t,p}}{T_{t,s}} = 2.8, NPR = 2.5$; $\blacktriangledown \frac{T_{t,p}}{T_{t,s}} = 1.0, NPR = 4.5$; $\blacklozenge \frac{T_{t,p}}{T_{t,s}} = 2.4, NPR = 4.5$; $\blacktriangle \frac{T_{t,p}}{T_{t,s}} = 2.8, NPR = 4.5$; —— least squares fit to NPR=2.5; – – –– least squared fit to NPR=4.5.

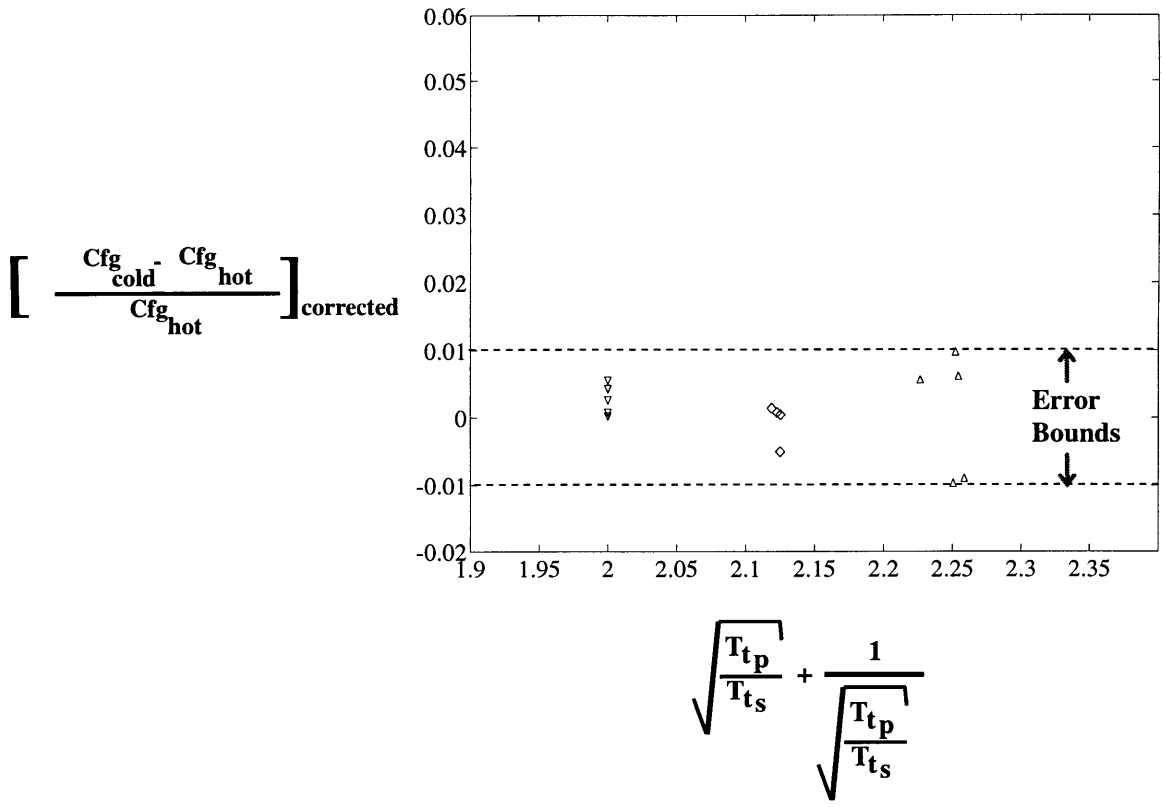

Figure 3-20: Differences between cold case gross thrust coefficient and hot case gross thrust coefficient versus $\frac{T_{t,p}}{T_{t,s}} + 1/\frac{T_{t,p}}{T_{t,s}}$ (corrected for systematic error) at NPR=2.5, $\nabla \frac{T_{t,p}}{T_{t,s}} = 1.0$; $\Diamond \frac{T_{t,p}}{T_{t,s}} = 2.4$; $\Delta\ \frac{T_{t,p}}{T_{t,s}} = 2.8$.

3.3 Results from Variable Molecular Weight Tests

The HSCT results do not provide a rigorous test of the molecular weight scaling that the approximate similarity principle suggests is possible because essentially all of the change occured in stagnation temperatures rather than molecular weight. (The combustion products made up only a small portion of the primary flow, and therefore, the molecular weight change was small.) To examine this aspect of the approximate similarity principle, mixing experiments utilizing streams of various gas combinations will be used [7, 15, 26].

These tests involved the mixing of streams of different composition but equal stagnation temperature. The experiments in references [7] and [15] were designed to measure the thicknesses of two dimensional and axisymmetric shear layers and the

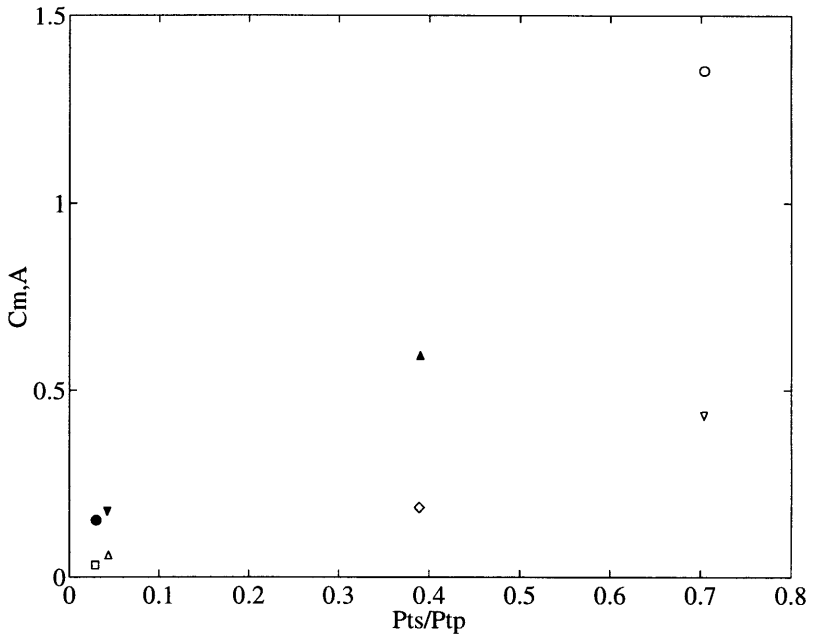

Figure 3-21: Mass flow ratios, $\bullet\frac{\mu_{M,s}}{\mu_{M,p}} = 9.98, \square\frac{\mu_{M,s}}{\mu_{M,p}} = 1.0, \circ\frac{\mu_{M,s}}{\mu_{M,p}} = 1.43, \triangledown\frac{\mu_{M,s}}{\mu_{M,p}} = 7.002$ Ref [15]; $\blacktriangledown\frac{\mu_{M,s}}{\mu_{M,p}} = 7.24, \vartriangle\frac{\mu_{M,s}}{\mu_{M,p}} = 0.725$ Ref [7]; $\blacktriangle\frac{\mu_{M,s}}{\mu_{M,p}} = 0.725, \Diamond\frac{\mu_{M,s}}{\mu_{M,p}} = 7.24$ Ref [26]

remaining experiment was designed to measure mixing. The Mach number ranges from low subsonic to supersonic values in each of the tests. The first set of data is from an experiment [15] that involved tailoring the area of the mixing duct to maintain a region of constant static pressure while the second [7] and third [26] pertains to the situation in constant area ducts. In all of these tests, the static pressures of the two streams were equal at the inlet to the mixing duct.

The mass flow ratios from eight experimental runs are plotted in Figure 3-21. These have been multiplied by the primary to secondary area ratio to allow clarity in data presentation. The mass flows are separated into four pairs, two from reference [15] and one each from references [7] and [26]. Each pair shares the same geometry, stagnation pressures, and Mach numbers but has different molecular weight ratios. The molecular weight ratio ranges from 0.725 to 9.98. The corrected mass flow ratios are shown in Figure 3-22. Each pair of mass flows collapsed into a single corrected mass flow, showing that the approximate similarity principle extends to flows of different composition and that the mass flow values of such flows can be

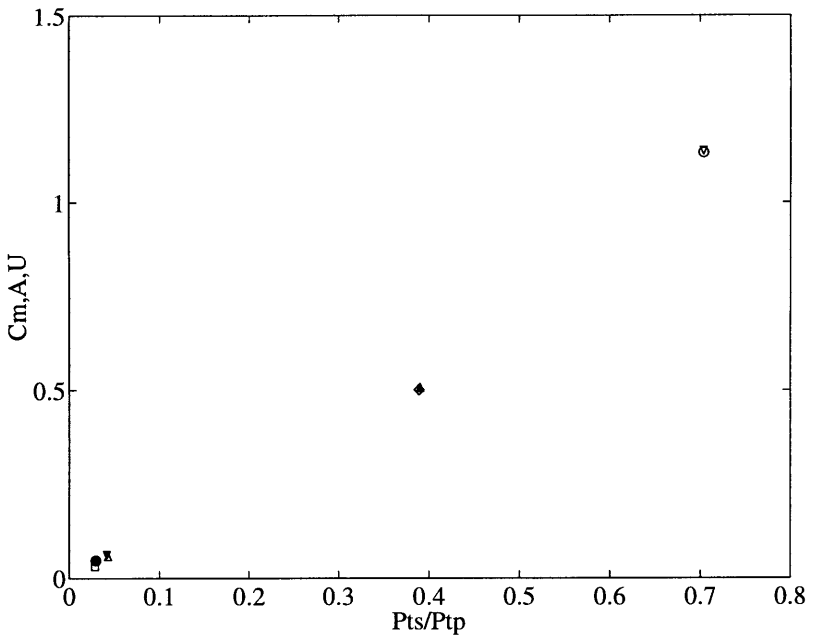

Figure 3-22: Molecular weight corrected mass flow ratios, $\bullet\frac{\mu_{M,s}}{\mu_{M,p}} = 9.98, \square\frac{\mu_{M,s}}{\mu_{M,p}} = 1.0, \circ\frac{\mu_{M,s}}{\mu_{M,p}} = 1.43, \nabla\frac{\mu_{M,s}}{\mu_{M,p}} = 7.002$ Ref [15]; $\blacktriangledown\frac{\mu_{M,s}}{\mu_{M,p}} = 7.24, \Delta\ \frac{\mu_{M,s}}{\mu_{M,p}} = 0.725$ Ref [7]; $\blacktriangle\frac{\mu_{M,s}}{\mu_{M,p}} = 0.725, \Diamond\frac{\mu_{M,s}}{\mu_{M,p}} = 7.240$ Ref [26]

scaled through the use of the similarity parameter.

The scaling error does not seem to affect molecular weight scaling in the same manner as it was shown to affect temperature scaling. The scaling error was shown to be significant for stagnation temperature ratios of 3.0 but for molecular weight ratios of of 9.98 it appears to be negligible. There is not enough appropriate data available for the mixing of gases of different composition to draw a conclusion on the magnitude of the scaling error associated with molecular weight scaling.

3.4 Summary

Supersonic mixer-ejector tests were examined in light of the approximate similarity principle. The exit stagnation pressures and exit Mach numbers were shown to be similar even though substantial amounts of heat transfer and momentum exchange were present in the mixing process. The similarity parameter introduced in Chapter 2 was used to scale the mass flow ratios from these tests. Scaling of tests in which the

stagnation temperatures of the streams were equal was shown to generally overpredict the mass flows measured at the highest temperature ratios by 10.0% or less. Gross thrust coefficients were generally overpredicted by 5.0% or less. By accounting for the systematic error in this scaling which correlates with $\sqrt{T_{t,p}/T_{t,s}}+1/\sqrt{T_{t,s}/T_{t,p}}$, it was shown that the predictions could attain the same accuracy as actual hot test results. This would make hot testing necessary for only acoustic performance determination. Finally, the approximate similarity principle was also shown to be applicable to mixing flows of different compositions.

Chapter 4

Summary and Conclusions

4.1 Summary

The applicability of the approximate similarity principle to supersonic mixer-ejector flows and to the mixing of different gases has been assessed. Control volume analyses, compressible flow influence coefficients and data obtained from the HSR Program and published literature were employed in this investigation. It was shown that the exchange of gases with different molecular weights affects stagnation pressure and Mach number in a manner analogous to that of heat transfer. For the first time, stagnation pressure and Mach number similarity was demonstrated in the mixing of different gases. The effects of heat transfer and molecular weight change were combined into a single similarity parameter. The mechanisms that lead to the approximate similarity principle were assessed in the supersonic mixing regime using control volume analyses and compressible flow influence coefficients (see Chapter 2). It was also shown that the competing effects of heat transfer, molecular weight change, and interstream forces result in stagnation pressure and Mach number similarity in that regime.

4.2 Conclusions

1. The applicability of the approximate similarity principle was extended to include the mixing of gases of different compositions. It was found that changes in

molecular weight effect stagnation pressure and Mach number in a manner analogous to heat transfer.

2. The approximate similarity principle was determined to be applicable to supersonic mixing flows. Exit stagnation pressures and exit Mach numbers resulting from supersonic mixing flows were found to be similar regardless of changes in stagnation temperature and composition.

3. The approximate similarity principle can be used to infer the performance of supersonic mixer-ejectors representative of the type being investigated in the HSR program. Mass flow ratios for hot tests can be obtained by multiplying the mass flow ratios obtained from a cold test by the square root of the primary to secondary similarity parameter ratio. The gross thrust coefficents do not change between hot and cold cases; thus cold test thrust performance can be used without alterations as a prediction of thrust performance for hot tests. The mass flow ratios are generally predicted within 10.0% and gross thrust coefficients can be predicted within 5.0%.

4. It was determined that the differences between hot case values of corrected mass flow ratios and gross thrust coefficients (noted in item 3 above) were due in part to a systematic error which was shown to scale with $\sqrt{T_{t,p}/T_{t,s}} + 1/\sqrt{T_{t,s}/T_{t,p}}$. Corrections for this scaling error allowed performance parameters to be obtained from cold tests with essentially the same accuracy as hot tests.

4.3 Recommendations

The current research was not able to address all of the questions associated with application of the approximate similarity principle to flow regimes of practical interest. Recommendations for future research are as follows:

1. Measurements of stagnation pressures and Mach numbers should be taken at various axial positions within the mixing duct of an HSCT style mixer-ejector to

determine the local applicability of the general approximate similarity principle. Measurements are only available for global quantities such as the mass flow ratio and for exit conditions. Internal measurements and the determination that the similarity principle is applicable locally would allow the prediction of internal pressure profiles which are important in thrust and structural load prediction.

2. Determination of the scaling error from flow conditions needs to be addressed. The goal of an investigation into the scaling error should be to develop a method for its determination without the use of additional tests or full flow models. Accurate prediction of this systematic error would make the similarity principle more useful by making it self-sufficient.

Bibliography

[1] "High-Speed Civil Transport Study". CR-4233, NASA, 1989. Prepared by Boeing Commercial Airplanes.

[2] ARNEY, L. D., AND LIDSTONE, G. L. "Volume I, Aero-Performance Test of the Single Lobe Supersonic Ejector Nozzle". CR number to be assigned upon end of restrictions, NASA, November 1994.

[3] ASAI, K. "Similarity Rule for Jet Temperature Effects on Transonic Back Pressure". *AIAA Journel, Vol. 33* (1994).

[4] BARANKIEWICZ, W. S., PERUSEK, G. P., AND IBRAHIM, M. "Use of an Approximate Similarity Principle for the Thermal Scaling of a Full-Scale Thrust Augmenting Ejectorv". AIAA paper 92-3792, 1992.

[5] BROADBENT, E. G. "Flows with Heat Addition". *Progress in Aerospace Sciences, Vol. 17*, No. 2 (1976), pp. 93–108.

[6] CLARK, L. T. "Application of Compound Compressible Flow Analysis to Supersonic Ejector-Mixer Performance Prediction". AIAA paper 95-0645, 1995.

[7] DUFFLOCQ, M., BENJAMIN, M. A., AND ROAN, V. P. "Comparison of the Initial Development of Shear Layers in Two-Dimensional and Axisymmetric Ejector Configurations". AIAA paper 93-2441, 1993.

[8] GAMBLE, E. J. "High Speed Civil Transport - Gen 1.5 Parametric Testing of Mixer/Ejector Nozzles". FTD 9435, United Technologies Pratt and Whitney, March 1995.

[9] GREITZER, E. M., PATERSON, R. W., AND TAN, C. S. "An Approximate Substitution Principle for Viscous Heat Conducting Flows". *Proceedings of the Royal Society of London, Vol. 401* (1985), pp. 163–193.

[10] HICKS, B. L. *Q. Appl. Math, Vol. 6* (1948), pp. 221–237.

[11] LORD, W. K., JONES, C. W., STERN, A. M., HEAD, V. L., AND KREJSA, E. A. "Mixer Ejector Nozzle for Jet Noise Suppression". AIAA paper 90-1909, 1990.

[12] MANNING, T. "Experimental Studies of Mixing Flows with Streamwise Vorticity". Master's thesis, Massachusetts Institute of Technology, 1991.

[13] MIZUKAMI, M. Personal Communication, 1995.

[14] MUNK, M., AND PRIM, R. "On the Multiplicity of Steady Gas Flows Having the Same Streamline Pattern". *Proceedings of the National Academy of Sciences, Vol. 33* (1947), pp. 137–141.

[15] PAPAMOUSCHOU, D., AND ROSHKO, A. "The Compressible Turbulent Shear Layer: An Experimental Study". *Journal of Fluid Mechanics, Vol. 197* (1988), pp. 453–477.

[16] PETERS, W. L. "A Comparison of Jet Temperature Effects on Afterbody Drag with those from Jet Molecular Weight and Nozzle Area Ratio Variations". AIAA paper 80-1161, 1980.

[17] PETERS, W. L. "A Simulation Technique for Jet Temperature Effects on Nozzle-Afterbody Drag at Transonic Mach Numbers". AIAA paper 85-1463, 1985.

[18] POWELL, A. "On the Generation of Noise by Turbulent Jets". ASME paper 59-AV-53, American Society of Mechanical Engineers, 1959.

[19] PRESZ, W. M., GOUSY, R., AND MORIN, B. "Forced Mixer Lobes in Ejector Designs". AIAA paper 86-1614, 1986.

[20] PRESZ, W. M., AND GREITZER, E. M. "A Useful Similarity Principle for Jet Engine Exhaust System Performance". AIAA paper 88-3001, 1988.

[21] QIU, Y. *A Study of Streamwise Vortex Enhanced Mixing in Lobed Mixer Devices.* PhD thesis, Massachusetts Institute of Technology, 1992.

[22] SEINER, J. M., AND KREJSA, E. A. "Supersonic Jet Noise and the High Speed Civil Transport". AIAA paper 89-2358, 1989.

[23] SHAPIRO, A. H. *The Dynamics and Thermodynamics of Compressible Fluid Flow*, vol. 1. New York: John Wiley and Sons, 1953.

[24] TEEPLE, B. S. "Optimization of the Mixer-Ejector System for the High Speed Civil Transport". PhD Thesis to be published in 1997.

[25] TEW, D. E. *Streamwise Vorticity Enhanced Compressible Mixing Downstream of Lobed Mixers.* PhD thesis, Massachusetts Institute of Technology, 1997.

[26] ZAKKAY, V., KRAUSE, E., AND WOO, S. D. L. "Turbulent Transport Properties for Axisymetric Heterogeneous Mixing". AIAA paper 64-99, 1964.

Appendix A

Constant Area Mixed-Out Two Flow Control Volume

In Chapter 2, a compressible control volume was used to investigate the similarity of stagnation pressure and Mach number in ejectors with variable stagnation temperature supersonic primary flows. This appendix contains the full derivation of the control volume and an explanation of how it was used to model the flow through an ejector. Figure A presents a schematic of the flow situation described in the control volume.

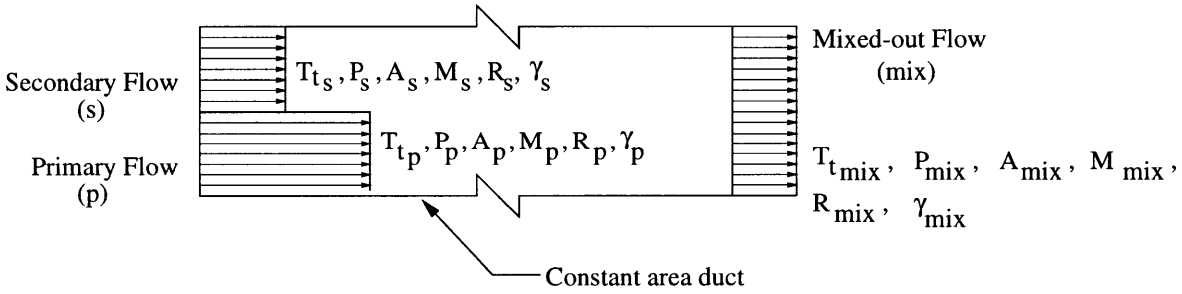

Figure A-1: Compressible control volume

In this derivation, the mass conservation, momentum, and energy equations as well as the equations of state will be combined and reduced into a quadratic equation in terms of the normalized mixed-out velocity, V_{mix}/V_p. Solving for this velocity ratio allows the derivation of the other mixed-out flow quantities. This derivation assumes that the flows entering and leaving the mixing duct are uniform, that the mixing duct

has a constant area, and that the flow exiting the mixing duct is completely mixed-out. Also, in this derivation, the molecular weights of the two entering streams may be different, hence, the ratios of specific heats and the gas constants can vary between streams.

We begin with the pertinent equations and definitions. The mass conservation equation, the momentum equation, and the energy equation are

$$\dot{m}_{mix} = \dot{m}_p + \dot{m}_s \tag{A.1}$$

$$\left(P + \rho V^2\right)_{mix} = \left(P + \rho V^2\right)_p A_p + \left(P + \rho V^2\right)_s A_s \tag{A.2}$$

and

$$C_{p,mix}\dot{m}_{mix}T_{t,mix} = C_{p,p}\dot{m}_p T_{t,p} + C_{p,s}\dot{m}_s T_{t,s} \tag{A.3}$$

respectively. The equations of state for the primary stream, secondary stream, and the mixed-out exiting flow are

$$P_p = \rho_p R_p T_p \tag{A.4}$$

$$P_s = \rho_s R_p T_s \tag{A.5}$$

and

$$P_{mix} = \rho_{mix} R_{mix} T_{mix} \tag{A.6}$$

Mass flow is defined as

$$\dot{m} = \rho V A \tag{A.7}$$

Because the mixing duct is of constant area, the normalized exit area can be defined as

$$\frac{A_{mix}}{A_p} = \left(\frac{A_s}{A_p} + 1\right) \tag{A.8}$$

The conservation, momentum, and energy equations will now be arranged so that the normalized mixed-out quantities are separated from and set equal to the quantities defined at the inlet. Both sides of the three equations will then be set equal to three variables, one for each equation. We wish to express the equation of mass conservation in terms of density, velocity, and area ratios. Therefore, after both sides of the relation have been divided by the primary mass flow, the definitions of mass flow and normalized mixing duct exit area are substituted into Equation A.1. This results in equation A.9.

$$\begin{aligned} \mathbf{A} &= \left(\frac{\rho_{mix}}{\rho_p}\right)\left(\frac{V_{mix}}{V_p}\right) \\ &= \frac{\left(\frac{\rho_s}{\rho_p}\right)\left(\frac{V_s}{V_p}\right)\left(\frac{A_s}{A_p}\right) + 1}{\left(\frac{A_s}{A_p} + 1\right)} \end{aligned} \tag{A.9}$$

Upon normalizing the momentum equation A.2 by ρV^2 and A_p we have

$$\begin{aligned} \left[\left(\frac{P_s}{P_p}\right)\frac{1}{\gamma_p M_p^2} + \left(\frac{\rho_s}{\rho_p}\right)\left(\frac{V_s}{V_p}\right)^2\right]\left(\frac{A_s}{A_p}\right) + \frac{1}{\gamma_p M_p^2} + 1 = \\ \left[\left(\frac{P_{mix}}{P_p}\right)\frac{1}{\gamma_p M_p^2} + \left(\frac{\rho_{mix}}{\rho_p}\right)\left(\frac{V_{mix}}{V_p}\right)^2\right]\left(\frac{A_s}{A_p} + 1\right) \end{aligned} \tag{A.10}$$

Note that the primary, secondary, and mixed-out exit static pressures can then be expressed as

$$\frac{P_p}{(\rho V^2)_p} = \frac{1}{\gamma_p M_P^2} \tag{A.11}$$

$$\frac{P_s}{(\rho V^2)_p} = \left(\frac{P_s}{P_p}\right)\frac{1}{\gamma_p M_P^2} \tag{A.12}$$

and

$$\frac{P_{mix}}{(\rho V^2)_p} = \left(\frac{P_{mix}}{P_p}\right)\frac{1}{\gamma_p M_P^2} \tag{A.13}$$

The momentum equation then takes the form

$$\begin{aligned}\mathbf{B} &= \left[\left(\frac{P_{mix}}{P_p}\right)\frac{1}{\gamma_p M_p^2} + \left(\frac{\rho_{mix}}{\rho_p}\right)\left(\frac{V_{mix}}{V_p}\right)^2\right] \\ &= \frac{1}{\left(\frac{A_s}{A_p}+1\right)}\left\{\left[\left(\frac{P_s}{P_p}\right)\frac{1}{\gamma_p M_p^2} + \left(\frac{\rho_s}{\rho_p}\right)\left(\frac{V_s}{V_p}\right)^2\right]\left(\frac{A_s}{A_p}\right) + \frac{1}{\gamma_p M_p^2} + 1\right\}\end{aligned} \tag{A.14}$$

Finally, the energy equation must be changed into the desired form. First, divide equation A.3 by $\dot{m}_p$, $C_{p,p}$, and $T_{t,p}$. This results in

$$\frac{C_{p,mix}T_{t,mix}}{C_{p,p}T_{t,p}} = \frac{\left[1 + \left(\frac{\dot{m}_s}{\dot{m}_p}\right)\left(\frac{T_{t,s}}{T_{t,p}}\right)\left(\frac{C_{p,s}}{C_{p,p}}\right)\right]}{1 + \left(\frac{\dot{m}_s}{\dot{m}_p}\right)} \tag{A.15}$$

Using the definition of mass flow and specific heat at constant pressure, this becomes

$$\frac{C_{p,mix}T_{t,mix}}{C_{p,p}T_{t,p}} = \frac{\left[1 + \left(\frac{\rho_s}{\rho_p}\right)\left(\frac{V_s}{V_p}\right)\left(\frac{A_s}{A_p}\right)\left(\frac{T_{t,s}}{T_{t,p}}\right)\left(\frac{\gamma_s}{\gamma_p}\right)\left(\frac{R_s}{R_p}\right)\left(\frac{\gamma_s-1}{\gamma_p-1}\right)\right]}{\left[1 + \left(\frac{\rho_s}{\rho_p}\right)\left(\frac{V_s}{V_p}\right)\left(\frac{A_s}{A_p}\right)\right]} \tag{A.16}$$

Using

$$\begin{aligned}C_pT_t &= C_pT + \frac{V^2}{2} \\ &= \left(\frac{\gamma}{\gamma-1}P + \frac{\rho V^2}{2}\right)\frac{1}{\rho}\end{aligned} \tag{A.17}$$

and dividing both the nominator and the denominator of the left hand side of Equa-

tion A.16 by $\rho_p V_p^2$ results in the following expression.

$$\frac{C_{p,mix}T_{t,mix}}{C_{p,p}T_{t,p}} = \left[\frac{\frac{\gamma_{mix}}{\gamma_{mix}-1}\left(\frac{P_{mix}}{P_p}\right)\frac{1}{\gamma_p M_p^2} + \frac{1}{2}\left(\frac{\rho_{mix}}{\rho_p}\right)\left(\frac{V_{mix}}{V_p}\right)^2}{\left(\frac{\gamma_p}{\gamma_p-1}\frac{1}{\gamma_p M_p^2} + \frac{1}{2}\right)}\right]\frac{\rho_p}{\rho_{mix}} \tag{A.18}$$

Combining equations A.16 and A.18 results in the equation A.19.

$$\begin{aligned}\mathbf{C} &= \left[\frac{\gamma_{mix}}{\gamma_{mix}-1}\left(\frac{P_{mix}}{P_p}\right)\frac{1}{\gamma_p M_P^2}\left(\frac{\rho_p}{\rho_{mix}}\right) + \frac{1}{2}\left(\frac{V_{mix}}{V_p}\right)^2\right] \\ &= \left(\frac{1}{\gamma_p - 1}\frac{1}{M_P^2} + \frac{1}{2}\right)\frac{\left[1 + \left(\frac{\rho_s}{\rho_p}\right)\left(\frac{V_s}{V_p}\right)\left(\frac{A_s}{A_p}\right)\left(\frac{T_{t,s}}{T_{t,p}}\right)\left(\frac{\gamma_s}{\gamma_p}\right)\left(\frac{R_s}{R_p}\right)\left(\frac{\gamma_p-1}{\gamma_s-1}\right)\right]}{\left[1 + \left(\frac{\rho_s}{\rho_p}\right)\left(\frac{V_s}{V_p}\right)\left(\frac{A_s}{A_p}\right)\right]}\end{aligned} \tag{A.19}$$

A quadratic equation in terms of the normalized mixed-out velocity ,V_{mix}/V_p, will now be formed. Rearranging equation A.9 gives

$$\left(\frac{\rho_{mix}}{\rho_p}\right) = \frac{\mathbf{A}}{\left(\frac{V_{mix}}{V_p}\right)} \tag{A.20}$$

Substituting this result into equation A.14 gives

$$\mathbf{B} = \left(\frac{P_{mix}}{P_p}\right)\frac{1}{\gamma_p M_p^2} + \mathbf{A}\left(\frac{V_{mix}}{V_p}\right) \tag{A.21}$$

Substituting both equations A.20 and A.21 into equation A.19 creates the following quadratic equation.

$$\frac{\gamma_{mix}+1}{2(1-\gamma_{mix})}\left(\frac{V_{mix}}{V_p}\right)^2 + \left(\frac{\gamma_{mix}}{\gamma_{mix}-1}\right)\frac{\mathbf{A}}{\mathbf{B}}\left(\frac{V_{mix}}{V_p}\right) - \mathbf{C} = 0 \tag{A.22}$$

In order to solve this equation, the value of the mixed-out ratio of specific heats is

assumed to be

$$\begin{aligned}\gamma_{mix} &= \frac{\dot{m}_s\gamma_s + \dot{m}_p\gamma_p}{(\dot{m}_s + \dot{m}_p)} \\ &= \frac{\left[\left(\frac{\rho_s}{\rho_p}\right)\left(\frac{V_s}{V_p}\right)\left(\frac{A_s}{A_p}\right)\gamma_s + \gamma_p\right]}{\left[\left(\frac{\rho_s}{\rho_p}\right)\left(\frac{V_s}{V_p}\right)\left(\frac{A_s}{A_p}\right) + 1\right]}\end{aligned} \tag{A.23}$$

With a solution for the normalized mixed-out velocity, the other mixed-out exit quantities can be found. The normalized mixed-out static pressure, P_{mix}/P_p, can be defined by substituting V_{mix}/V_p into equation A.21, which upon rearranging yields

$$\left(\frac{P_{mix}}{P_p}\right) = \gamma_p M_P^2\left[\mathbf{AB}\left(\frac{V_{mix}}{V_p}\right)\right] \tag{A.24}$$

Likewise, a expression fo the normalized mixed-out density, ρ_{mix}/ρ_p, can be obtained by substituting V_{mix}/V_p into Equation A.20. M_{mix} is obtained through the following equation.

$$\begin{aligned}M_{mix} &= \frac{1}{M_p}\left(\frac{V_{mix}}{V_p}\right)\sqrt{\frac{\gamma_p R_p T_p}{\gamma_{mix} R_{mix} T_{mix}}} \\ &= \left(\frac{V_{mix}}{V_p}\right)\sqrt{\gamma_p M_p^2 \frac{P_p}{P_{mix}}\left(\frac{\rho_{mix}}{\rho_p}\right)\frac{1}{\gamma_m ix}}\end{aligned} \tag{A.25}$$

Finally, $C_{p,mix}/C_{p,p}$ and the normalized mixed-out stagnation temperature, $T_{t,mix}/T_{t,p}$, are found through the use of equations A.26 and A.27, respectively.

$$\frac{C_{p,mix}}{C_{p,p}} = \left(\frac{\gamma_{mix}}{\gamma_p}\right)\left(\frac{R_{mix}}{R_p}\right)\frac{\gamma_p - 1}{\gamma_{mix}} \tag{A.26}$$

$$\frac{T_{t,mix}}{T_{t,p}} = \frac{\gamma_p}{\gamma_{mix}}\frac{R_p}{R_{mix}}\left(\frac{\gamma_{mix} - 1}{\gamma_p - 1}\right)\frac{\left[1 + \left(\frac{\rho_s}{\rho_p}\right)\left(\frac{V_s}{V_p}\right)\left(\frac{A_s}{A_p}\right)\left(\frac{T_{t,s}}{T_{t,p}}\right)\left(\frac{\gamma_s}{\gamma_p}\right)\left(\frac{R_s}{R_p}\right)\left(\frac{\gamma_p - 1}{\gamma_s - 1}\right)\right]}{\left[1 + \left(\frac{\rho_s}{\rho_p}\right)\left(\frac{V_s}{V_p}\right)\left(\frac{A_s}{A_p}\right)\right]} \tag{A.27}$$

For flows in an ejector system, the mixed-out exit static pressure must be equal to the ambient static pressure when the exiting flow is subsonic. The secondary and primary stagnation pressures, stagnation temperatures, gas constants, and ratios of specific heats along with the primary stream Mach number are specified as they would be in an ejector experiment. The secondary Mach number starts at an initial guess and is then iterated upon using the bisection method until the pressures at the exit of the mixing duct assumes the ambient value. Because of this requirement, some sets of inlet conditions fail to produce a solution. In an actual ejector, all possible sets of flow conditions will result in a flow, but many of these flows violate the assumptions that govern the model (e.g. the solution is not fully mixed or the flow is not subsonic at the mixng duct exit).

Appendix B

Description of Available Data

B.1 Boeing Single Lobe Parametric Tests

The Boeing Single Lobe Tests [2],[6] were designed to provide a geometry that is representative of the current HSCT mixer-ejector design philosophy. The parameters that were varied included stagnation temperature ratio, NPR, SNPR, and length of the mixing duct. Other parameters such as lobe angle, primary Mach number, penetration, and mixing duct area ratio (MAR) were fixed by the design of the facility and therefore their influence was not assessed in this series of tests. Figure B-1 shows that the test geometry was representative of a single lobe of a multi-lobe mixer/ejector. The two dimensional primary jet was located between two secondary flows. The primary width to height ratio was 4.8. Both the secondary streams and the primary stream were of the same width, so that the secondary width to primary height ratio is the same as the primary width to height ratio. The secondary height to primary height ratio was 1.9 while the secondary to primary area ratio was 3.8. The primary nozzle had a exit to throat area ratio greater than one which assured a supersonic design Mach number. The baseline ratio of mixing duct length to primary jet height was 41.4. Figure B-2 shows a schematic of the test geometry.

The facility was designed to allow temperatures and pressures representative of actual aircraft design conditions. Two pressurized airflows, one for the primary stream and one for both secondary streams, were ducted directly into the test section. The

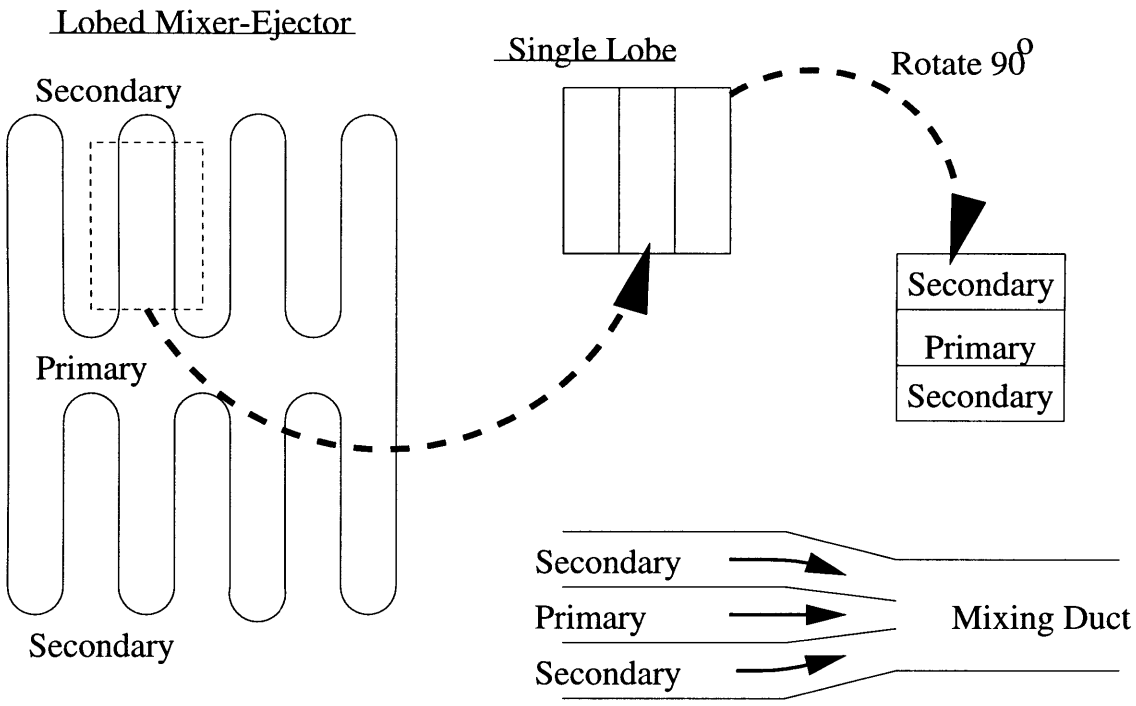

Figure B-1: Single Lobe test concept [6]

range of NPR and SNPR examined ranged from 1.5 to 5.5 and 1.0 to 1.6 respectively. A propane burner located upstream of the primary nozzle allowed the primary to secondary stagnation temperature ratio to be varied between 1.0 and 3.3.

Measurements taken in the tests include mass flows, thrust, flow visualization, and flow velocities. The mass flow readings were taken by flow venturis located between the test section and the airflow control system. In the case of the primary stream, the flow venturi is located upstream of the propane burner. Thrust measurements were made possible by placing the model on a thrust stand. Flow visualization was achieved through the use of a focused Schlieren System that allowed individual flow planes to be imaged. Flow velocities were obtained by seeding the primary flow with particles of titanium dioxide and using Laser Doppler Velocimetry (LDV).

B.2 Gen 1.5 Parametric Tests

The Gen 1.5 Parametric Tests [8] were performed to incorporate critical design parameters into a single series of tests so that trends in performance could be determined.

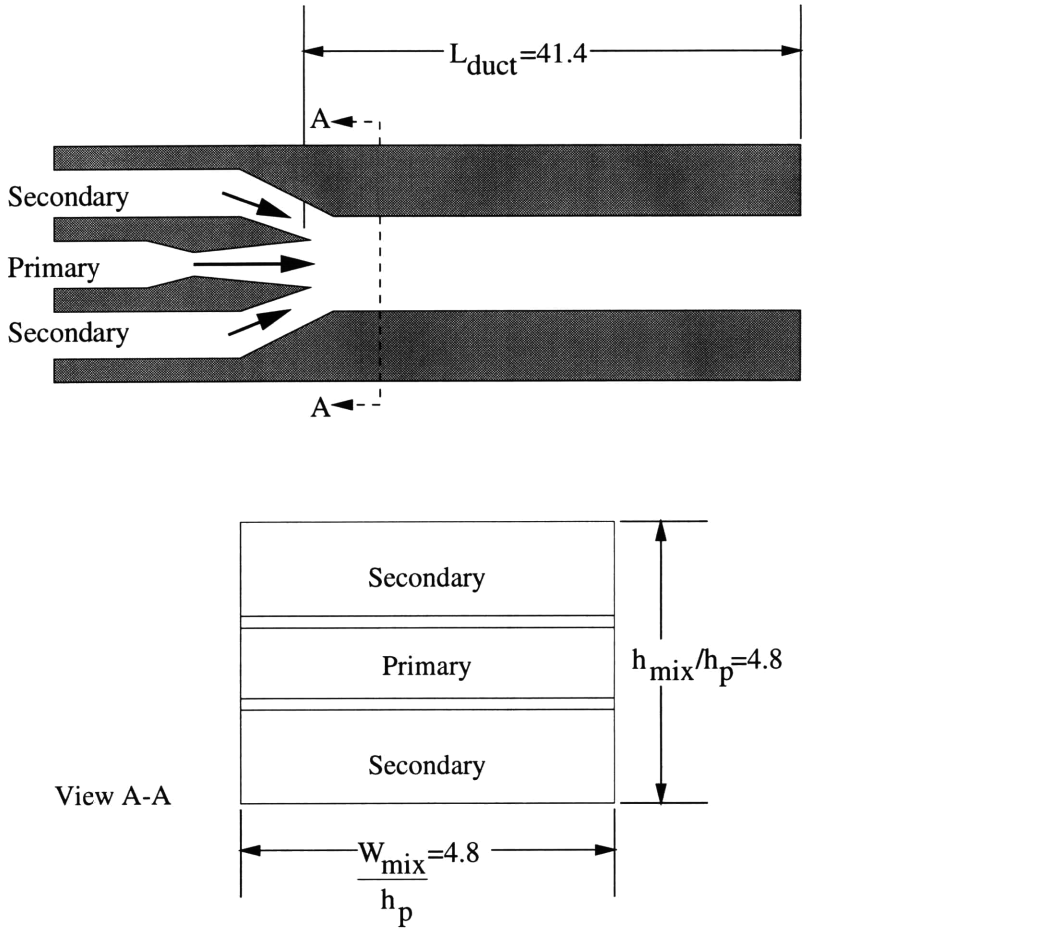

Figure B-2: Boeing Single Lobe test model [6]

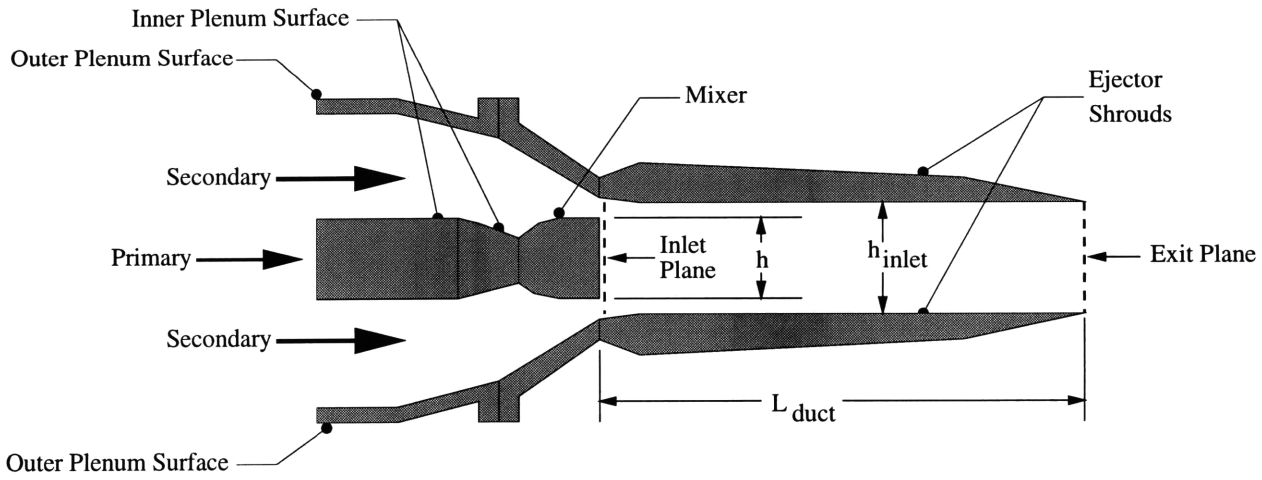

Figure B-3: Gen 1.5 test model

Previous testing had been done on individually designed mixers that had no common point of reference. The tested parameters can be placed into two catagories, mixing duct and mixer parameters. The mixing duct parameters are suppressor area ratio (SAR), mixing duct area ratio (MAR), shroud length, and penetration, while the mixer parameters are chute expansion ratio (CER), mixer length, number of lobes, and lobe shaping. A schematic of the test model is shown in Figure B-3.

These tests were performed in the Large Dual Flow Rig at the Boeing Nozzle Test Facility (NTF) which can simulate the exit conditions of proposed HSCT engines. Primary and secondary flows were supplied by a common pressurized source. This allowed the value of NPR and SNPR to range from 1.5 to 5.5 and from 0.6 to 1.2, respectively. A propane burner in the primary stream allowed the stagnation temperature ratio to range from 1.0 to 2.8.

Both the test facility and the test hardware were equiped with instrumentation. Mass flow measurements were taken using flow venturis located in both the secondary and primary streams. The model was mounted on a 3-component thrust balance allowing the axial and side forces produced by the model to be recorded. Static pressure measurements were collected using wall static taps located on both upper mixing shroud and the primary and secondary sides of the mixer. Secondary stagnation pressures near the mixing duct inlet were recorded by two pressure rakes, one on the crest of a mixer lobe pointed upstream and the other attached to the upper plenum.

B.3 Gen 1.5 Mixers Tested at NATR Facility (LeRC)

The testing of Gen 1.5 Mixers at the NATR Facility [13] had two objectives. The first was to obtain parametric information as in the Gen 1.5 Tests. The second was to provide data that would help determine if the approximate similarity principle was applicable to supersonic mixer-ejectors. To accomplish these objectives, runs were performed at values of NPR ranging from 2.5 to 4.5 for stagnation temperature ratios from 1.0 to 3.0 The secondary stream was entrained from the ambient air and not ducted to the test section from a pressurized source. Hence, the SNPR for all of the

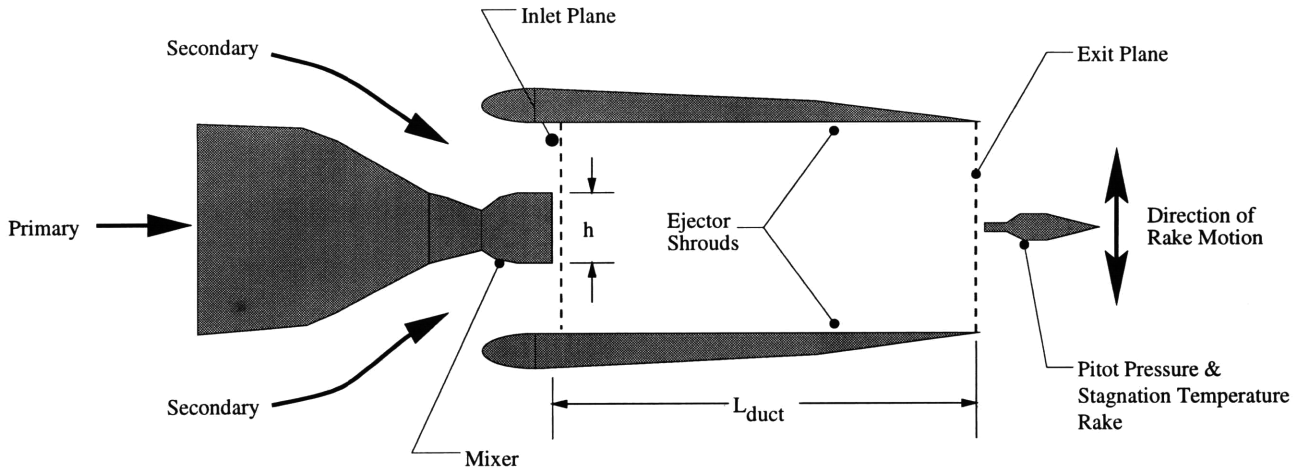

Figure B-4: NATR test model

tests was 1.0. A schematic of the test model is shown in figure B-4. Both the SAR's and the MAR's of the model were changed during the course of the testing. The CER of the model was greater than one to assure a supersonic design primary Mach number.

Only the test model was oufitted with instrumentation. Wall static pressure taps were located on the shroud and aligned with a primary lobe and a secondary lobe. Stagnation temperature and pressure rakes at the exit of the shroud were translated across the exit plane to provide profiles of the exit conditions. Thrust measurements, secondary mass flow measurements, and primary mass flow readings are not available.

Appendix C

Governing Equations of the Approximate Munk and Prim Similarity Principle at Low Mach Numbers

In Chapter 2, the effect of molecular weight change on stagnation pressure and Mach number was determined through the use of the equations of motion for a steady flow of a perfect gas at Mach numbers M, such that $M^2 \ll 1$. This appendix contains the full derivation which was merely summarized in Chapter 2. In this derivation, it is assumed that the temperature of the flow can change through heat transfer (i.e. $dT_t \neq 0$), that the mass averaged molecular weight can change(i.e. $d\mu_M \neq 0$), and that momentum can be added or taken away from the flow through shear forces. It is also assumed that the ratio of specific heats remains constant even though the mass averaged molecular weight is changing. This assumption can be made because, as was shown in Section 2.3.2, the effects of variable ratio of specific heats on stagnation pressure and Mach number similarity are negligible.

The equations of motion for this flow situation are

$$\vec{\nabla} \cdot (\rho \vec{V}) = 0 \tag{C.1}$$

$$\vec{\omega} \times \vec{V} = -\frac{1}{\rho}\vec{\nabla}P - \vec{\nabla}\frac{V^2}{2} + \frac{\vec{f}_{viscous}}{\rho} \tag{C.2}$$

where $\vec{\omega}$ is the vorticity vector ($\vec{\omega} = \vec{\nabla} \times \vec{V}$). It is assumed that heat transfer and molecular weight changes can only occur through turbulent processes.

To express the equations of motion in terms of Mach number and stagnation pressure, the definition of the Mach number vector, $\vec{M} = \vec{V}/a$, where a is the local speed of sound and the approximation for the equation of state for low numbers

$$\bar{\rho}\bar{R}\bar{T} = \rho RT + O(M^2) \tag{C.3}$$

where $\bar{\rho}$, $\bar{T}$, and $\bar{R}$ are reference values of density, temperature, and gas constant are substituted into the equations of motion. This approximation for the equation of state (see Reference [5]) can be justified by considering a binomial expansion of

$$\frac{P_t}{P} = \left(1 + \frac{\gamma - 1}{2}M^2\right)^{\frac{\gamma}{\gamma-1}} = 1 + \frac{\gamma}{2}M^2 + \frac{\gamma}{8}M^4 + \cdots \tag{C.4}$$

The stagnation pressure is considered the reference pressure

$$P_t = \bar{P} = \bar{\rho}\bar{R}\bar{T} \tag{C.5}$$

and the static pressure is

$$P = \rho RT \tag{C.6}$$

Therefore, the product of the local quantities, ρ, R, and T, differ from the product of the reference quantities, $\bar{\rho}$, $\bar{R}$, and $\bar{T}$, by $O(M^2)$ in the same manner as the static pressure differs from the stagnation pressure. Note that the relationship between the stagnation temperature and the static temperature can also be expressed as

$$T_t = T + O(M^2)$$

hence to the order of M^2 it does not matter whether the local Mach number is defined with the static or stagnation temperature.

The mass conservation equation needs to be expressed in terms of the Mach number. By substituting the definition of the Mach number vector into the equation and using the vector identity

$$\vec{\nabla} \cdot (\phi \vec{X}) = (\vec{\nabla}\phi) \cdot \vec{X} + \phi(\vec{\nabla} \cdot \vec{X}) \tag{C.7}$$

where ϕ is a scalar quantity and $\vec{X}$ is a vector quantity, the conservation equation takes the form

$$\vec{\nabla} \cdot \vec{M} = -\vec{M} \cdot \frac{\vec{\nabla}(\rho\sqrt{\gamma RT})}{(\rho\sqrt{\gamma RT})} \tag{C.8}$$

After applying the assumption that the ratio of specific heats is constant, it can then be be expressed as

$$\vec{\nabla} \cdot \vec{M} = -\vec{M} \cdot \frac{\vec{\nabla}\left(\frac{\rho RT}{\sqrt{RT}}\right)}{\left(\frac{\rho RT}{\sqrt{RT}}\right)} \tag{C.9}$$

Because $\bar{\rho}\bar{R}\bar{T} \approx \rho RT$ and the gas constant is defined as

$$R = \frac{\Re}{\mu_M} \tag{C.10}$$

where $\Re$ is the universal gas constant and μ_M is the molecular weight, the expression becomes

$$\vec{\nabla} \cdot \vec{M} = -\vec{M} \cdot \frac{\vec{\nabla}(\frac{\mu_M}{T})}{(\frac{\mu_M}{T})} \tag{C.11}$$

The final form of the equation shows the relationship between the Mach number field

and the changes in temperature and molecular weight.

$$\vec{\nabla} \cdot \vec{M} = -\vec{M} \cdot \frac{\vec{\nabla}\mu_M}{2\mu_M} + \vec{M} \cdot \frac{\vec{\nabla}T}{2T} \tag{C.12}$$

The momentum equation must also be expressed in terms of the stagnation pressure and the Mach number. Using vector identities and the definition of the Mach number vector, it can be shown that

$$\vec{\nabla} \times \vec{V} = a\vec{\nabla} \times \vec{M} + \vec{\nabla}a \times \vec{M} \tag{C.13}$$

and

$$\vec{\omega} \times \vec{V} = \left(\vec{\nabla} \times \vec{V}\right) \times \vec{V} = a^2\left(\vec{\omega}_m \times \vec{M}\right) - M^2\vec{\omega}\frac{a^2}{2} + a\vec{M}\left(\vec{M} \cdot \vec{\nabla}a\right) \tag{C.14}$$

where the quantity $\vec{\omega}_m$ is defined as

$$\vec{\omega}_m = \vec{\nabla} \times \vec{M} \tag{C.15}$$

Substituting these relationships into Equation C.2 results in

$$\vec{\omega}_m \times \vec{M} = \frac{M^2}{a^2}\vec{\nabla}\frac{a^2}{2} - \vec{M}\left(\vec{M} \cdot \vec{\nabla}\ln a\right) - \frac{1}{\rho a^2}\vec{\nabla}P - \frac{1}{a^2}\vec{\nabla}\frac{V^2}{2} + \frac{\vec{f}_{viscous}}{\rho a^2} \tag{C.16}$$

With

$$\frac{1}{a^2}\vec{\nabla}\frac{V^2}{2} = \vec{\nabla}\frac{M^2}{2} + \frac{M^2}{a^2}\vec{\nabla}\frac{a^2}{2} \tag{C.17}$$

the following is obtained

$$\vec{\omega}_m \times \vec{M} = -\vec{M}\left(\vec{M} \cdot \vec{\nabla}\ln a\right) - \frac{1}{\rho a^2}\vec{\nabla}P - \vec{\nabla}\frac{M^2}{2} + \frac{\vec{f}_{viscous}}{\rho a^2} \tag{C.18}$$

The momentum equation will be seperated into three parts that will be evaluated

seperately and then recombined. The three terms are

$$\vec{M} \cdot \vec{\nabla} \ln a \tag{C.19}$$

$$-\frac{1}{\rho a^2}\vec{\nabla}P - \vec{\nabla}\frac{M^2}{2} \tag{C.20}$$

and

$$\frac{\vec{f}_{viscous}}{\rho a^2} \tag{C.21}$$

After substituting the definition of the speed of sound into the natural logarithm of the first term, it takes the form

$$\ln a = \ln \sqrt{\frac{\gamma \Re T}{\mu_M}} \tag{C.22}$$

Taking the gradient of both sides of expression results in

$$\vec{\nabla} \ln a = -\frac{\vec{\nabla}\mu_M}{2\mu_M} + \frac{\vec{\nabla}T}{2T} \tag{C.23}$$

Hence, the first term of the momentum equation can be expressed as

$$\vec{M} \cdot \vec{\nabla} \ln a = -\vec{M} \cdot \frac{\vec{\nabla}\mu_M}{2\mu_M} + \vec{M} \cdot \frac{\vec{\nabla}T}{2T} \tag{C.24}$$

The second term (Equation C.20) can be expressed as

$$\frac{1}{\rho a^2}\vec{\nabla}P + \vec{\nabla}\frac{M^2}{2} = \frac{\vec{\nabla}P_t}{\bar{\rho}\bar{a}^2} + O(M^2) \tag{C.25}$$

through the use of the following substitutions

$$\rho a^2 \vec{\nabla}\frac{M^2}{2} = P\vec{\nabla}\frac{\gamma M^2}{2} \tag{C.26}$$

$$\vec{\nabla}P_t = \vec{\nabla}P + P\vec{\nabla}\frac{\gamma M^2}{2} + \frac{\gamma M^2}{2}\vec{\nabla}P + O(M^4) \tag{C.27}$$

and

$$\frac{\bar{\rho}\bar{R}\bar{T}}{\rho RT} = \frac{\bar{\rho}\bar{a}^2}{\rho a^2} = 1 + \frac{\gamma M^2}{2} + \frac{\gamma M^4}{8} + \cdots \tag{C.28}$$

Finally, the last term (Equation C.21) can be expanded to

$$\frac{\vec{f}_{viscous}}{\rho a^2} = \frac{\vec{f}_{viscous}}{\bar{\rho}\bar{a}^2}\left(1 + \frac{\gamma M^2}{2} + \frac{\gamma M^4}{8} + \cdots\right) \tag{C.29}$$

or

$$\frac{\vec{f}_{viscous}}{\rho a^2} = \frac{\vec{f}_{viscous}}{\bar{\rho}\bar{a}^2} + O(M^4) \tag{C.30}$$

since $\vec{f}_{viscous}$ is of order M^2.

Substituting Equations C.24, C.25, and C.30 back into the momentum equation (Equation C.18) results in

$$\vec{\omega}_m \times \vec{M} = \left(-\vec{M} \cdot \frac{\vec{\nabla}\mu_M}{2\mu_M} + \vec{M} \cdot \frac{\vec{\nabla}T}{2T}\right) - \frac{\vec{\nabla}P_t}{\bar{\rho}\bar{a}^2} + \frac{\vec{f}_{viscous}}{\bar{\rho}\bar{a}^2} + O(M^4) \tag{C.31}$$

This can then be reorganized into the result that was presented in Chapter 2

$$\vec{M} \times \vec{\omega}_m = \frac{\vec{\nabla}P_t}{\bar{\rho}\bar{a}^2} + \frac{aM}{\bar{\rho}\bar{a}^2}\left[\left(\frac{\vec{M}}{M}\right)\left(\frac{\bar{\rho}\bar{a}^2}{a}\right)\left(-\vec{M} \cdot \frac{\vec{\nabla}\mu_M}{2\mu_M} + \vec{M} \cdot \frac{\vec{\nabla}T}{2T}\right) - \frac{\vec{f}_{viscous}}{V}\right] + O(M^4) \tag{C.32}$$

Appendix D

Derivation of the Similarity Parameter Influence Coefficient for Stagnation Pressure

In this appendix, the influence coefficients for the similarity parameter, stagnation temperature, molecular weight, and interstream shear forces will be derived in terms of P_t, $\mathcal{U}$, T_t, μ_M, γ, and M using the assumption that the ratio of specific heats is constant. This is a valid assumption effect of the variable ratios of specific heats on stagnation pressure and Mach number similarity is negligible as was shown in Chapter 3.

Use of the First and Second Laws of Thermodynamics gives

$$Tds = dh - \frac{1}{\rho}dP \tag{D.1}$$

Assuming that molecular weight varies and the ratio of specific heats is kept constant, enthalpy can be expressed as follows.

$$dh = d(C_pT) = \frac{\gamma\Re}{\gamma - 1}d(\frac{T}{\mu_M}) \tag{D.2}$$

Substituting equation D.2 into D.1

$$Tds = \frac{\gamma\Re}{\gamma - 1} d(\frac{T}{\mu_M}) - \frac{1}{\rho} dP \tag{D.3}$$

and dividing both sides of the equation by RT, it takes the following form

$$\frac{Tds}{\Re(\frac{T}{\mu_M})} = \frac{\gamma}{\gamma - 1} \frac{d(\frac{T}{\mu_M})}{(\frac{T}{\mu_M})} - \frac{dP}{P} \tag{D.4}$$

The above equation needs to be expressed in terms of the stagnation conditions. If γ is constant, the stagnation temperature maybe expressed as

$$T_t = T\left(1 + \frac{\gamma - 1}{2} M^2\right) \tag{D.5}$$

This becomes an expression for the similarity parameter once both sides are divided by molecular weight.

$$\mathcal{U} = (\frac{T_t}{\mu_M}) = (\frac{T}{\mu_M})\left(1 + \frac{\gamma - 1}{2} M^2\right) \tag{D.6}$$

Taking the logarithms and differentiating, we find

$$\frac{d\mathcal{U}}{\mathcal{U}} = \frac{(\frac{T}{\mu_M})}{(\frac{T}{\mu_M})} + \frac{\frac{\gamma-1}{2} M^2}{\left(1 + \frac{\gamma-1}{2} M^2\right)} \frac{dM^2}{M^2} \tag{D.7}$$

Similarlily, the differential form of the stagnation pressure relation can be expressed as

$$\frac{dP_t}{P_t} = \frac{dP}{P} + \frac{\frac{\gamma M^2}{2}}{\left(1 + \frac{\gamma-1}{2} M^2\right)} \frac{dM^2}{M^2} \tag{D.8}$$

Finally, these relations for the stagnation conditions are substituted into D.4 to give

$$\frac{Tds}{\Re(\frac{T}{\mu_M})} = \frac{\gamma}{\gamma-1}\frac{d\mathcal{U}}{\mathcal{U}} - \frac{dP_t}{P_t} \tag{D.9}$$

The second law can be expressed as follows

$$\begin{aligned} Tds &= d'q_{rev} \\ &= d\Big(C_pT_t\Big) \\ &= \frac{\gamma\Re}{\gamma-1}d\Big(\frac{T_t}{\mu_M}\Big) \end{aligned} \tag{D.10}$$

Combining and rearranging equations D.9 and D.10 results in

$$\frac{\gamma}{\gamma-1}\frac{d(\frac{T_t}{\mu_M})}{(\frac{T}{\mu_M})} = \frac{\gamma}{\gamma-1}\frac{d\mathcal{U}}{\mathcal{U}} - \frac{dP_t}{P_t} \tag{D.11}$$

This can be expanded to

$$\frac{\gamma}{\gamma-1}\frac{(\frac{T_t}{\mu_M})}{(\frac{T}{\mu_M})}\frac{d(\frac{T_t}{\mu_M})}{(\frac{T_t}{\mu_M})} = \frac{\gamma}{\gamma-1}\frac{d\mathcal{U}}{\mathcal{U}} - \frac{dP_t}{P_t} \tag{D.12}$$

which simplifies to

$$\frac{\gamma}{\gamma-1}\Big(\frac{T_t}{T}-1\Big)\frac{d\mathcal{U}}{mU} = -\frac{dP_t}{P_t} \tag{D.13}$$

Finally, by applying the isentropic relation for stagnation temperature, the influence coefficient for the similarity parameter is found.

$$\frac{dP_t}{P_t} = -\frac{\gamma M^2}{2}\frac{d\mathcal{U}}{\mathcal{U}} \tag{D.14}$$

This equation can be separated into its components by integrating, seperating the numerator and denominator of the natural logarithm term, and finally taking the derivative. The resulting equation contains the influence coefficients of both the stagnation temperature and the molecular weight.

$$\frac{dP_t}{P_t} = -\frac{\gamma M^2}{2}\frac{dT_t}{T_t} + \frac{\gamma M^2}{2}\frac{d\mu_M}{\mu_M} \tag{D.15}$$

5516-68